Multiple Model Adaptive Control with Blending in State Space

by

Alex Lövi

A thesis
presented to the University of Waterloo
in fulfillment of the
thesis requirement for the degree of
Doctor of Philosophy
in
Electrical and Computer Engineering

Waterloo, Ontario, Canada, 2025

© Alex Lövi 2025

Examining Committee Membership

The following served on the Examining Committee for this thesis. The decision of the Examining Committee is by majority vote.

External Examiner:	Gang Tao Professor, Dept. of Electrical and Computer Engineering, University of Virginia
Supervisors:	Barış Fidan Professor, Dept. of Mechanical and Mechatronics Engineering, University of Waterloo
	Christopher Nielsen Professor, Dept. of Electrical and Computer Engineering, University of Waterloo
Internal Members:	Daniel E. Davison Associate Professor, Dept. of Electrical and Computer Engineering, University of Waterloo
	Stephen L. Smith Professor, Dept. of Electrical and Computer Engineering, University of Waterloo
Internal-External Member:	Nasser Lashgarian Azad Professor, Dept. of Systems Design Engineering, University of Waterloo

Author's Declaration

I hereby declare that I am the sole author of this thesis. This is a true copy of the thesis, including any required final revisions, as accepted by my examiners.

I understand that my thesis may be made electronically available to the public.

Abstract

Adaptive Control (AC) provides a systematic framework for handling uncertainty in linear and non-linear systems. Single-model adaptive schemes such as Model Reference Adaptive Control (MRAC) and Adaptive Pole Placement Control (APPC) face inherent limitations when applied to systems with large parametric uncertainty, such as slow convergence rates and limited noise robustness. This has motivated researchers to investigate multiple-model strategies that employ several candidate plants to represent different regions of the operating space.

In this thesis, we develop Multiple-Model Adaptive Control (MMAC) methodologies based on the blending of signals from multiple fixed models. We consider uncertain plants with known, compact, convex polytopic uncertainty. Our starting point is the design of a Multiple-Model Parameter Identification (MMPI) scheme that quickly and robustly identifies the uncertain plant parameters. In combination with a Model Reference Control (MRC) framework, this leads to a Multiple-Model Reference Adaptive Control (MMRAC) with blending for Linear, Time-Invariant (LTI), non-square (different number of inputs and outputs), multi-input systems, with full-state feedback. Under an exact matching condition, the parameter estimates are used to design a control input such that the plant states asymptotically track the reference signal generated by a state-space reference model. A procedure is provided to select the corner models based solely on the polytopic uncertainty. The proposed MMRAC guarantees the boundedness of all closed-loop signals and the asymptotic convergence of the state-tracking error to zero. Statistical analysis demonstrate improved tracking speed and robustness to noise compared with single-model approaches.

The combination of MMPI with pole-placement techniques, allowed us to develop Multiple-Model Adaptive Pole Placement Control (MMAPPC) for LTI, square (same number of inputs and outputs), multivariable systems with full-state feedback, and for with LTI, Single-Input, Single-Output (SISO) systems via an intermediate state estimation step. The resulting controller again ensures the boundedness of all closed-loop signals, while also asymptotically placing the closed-loop eigenvalues at designer-specified locations. Statistical analysis shows a clear increase in robustness to noise relative to single-model schemes. These improvements were validated in the context of motion control of lateral vehicle dynamics, where multiple-model schemes consistently outperformed single-model approaches, including cases with slowly time-varying unknown parameters.

Acknowledgements

This PhD consisted of five intense and fruitful years. The road was challenging and I could not have done it alone. Friends, family, and supervisors played a key role in this personal achievement.

First, and foremost, my supervisors deserve great praise. In 2021, Prof. Drs. Fidan and Nielsen, Baris and Chris, took a gamble and allowed me to join their research group. For the past five years, they have given me tools and guidance that have allowed me to complete our research and most importantly to enjoy the process. They have taken care of me not just as a PhD student, pushing me and letting me get great results, but also as a person, giving me space to learn from my mistakes and adapt (no pun intended) into who I am today. For all your efforts and support, I am forever in your debt. I hope we continue to do research together and thank you for allowing me to take on this challenge.

I want to thank my family for going through life with me and, in particular, for these last years, where I needed them most. Thank you Mom, Dad, Juan, Pablo, and Ana for everything you do and for being my family. Thank you to my beautiful nieces and nephews, who fill me with so much happiness.

Life has provided me with many friends and now I have found an excuse to thank them. Thank you Shaundell for endless talks, walks, meals, drinks, and great memories during the past years. Thank you Rollen for challenging my ideas and having fun doing research with me. Thank you Lucas, Juan, and Ash for so many great memories and discussions. Thank you to Hanspal, Indrani and everyone at the Bhakti house for all our years together. A special thanks to the Goldmans, Propps, and Erlichs for their warm welcome into their families. Thanks to all my friends from Argentina who are very present despite the long distance!

Finally, I would like to thank the committee members, whose questions and comments allowed us to improve the final version of this thesis.

Dedication

To my Dad, a friend and example in life.

Table of Contents

Examining Committee ii

Author's Declaration iii

Abstract iv

Acknowledgements v

Dedication vi

List of Figures x

List of Tables xiii

List of Abbreviations xiv

1 Introduction 1

1.1 Problem Domain and Motivation 1

1.2 Contributions of this Thesis 4

1.3 Organization and Notation 5

2 Literature Review and Theoretical Background 8

2.1 Historical Background of Adaptive Control 8

2.2 Switching Control . . . 11
2.3 Blending Control . . . 14
2.4 Theoretical Background . . . 16
2.4.1 Parametric Models . . . 17
2.4.2 Persistence of Excitation . . . 17
2.4.3 Barbalat's Lemma . . . 18
2.4.4 Parameter Identification: Gradient Algorithm . . . 18
2.4.5 Parameter Identification: Parameter Projection . . . 19
2.4.6 Model Reference Adaptive Control . . . 19
2.4.7 Adaptive State Estimation . . . 21
2.4.8 Adaptive Pole Placement Control . . . 22

3 Multiple-Model Parameter Identification (MMPI) 25
3.1 State-Feedback MMPI . . . 26
3.1.1 Simulation Example . . . 32
3.2 Output-Feedback MMPI . . . 35
3.3 State Estimation of Output-Feedback Systems using Multiple Models . . . 41
3.3.1 Simulation Example . . . 44

4 Multiple Model Reference Adaptive Control (MMRAC) with Blending 51
4.1 MMRAC in State Space . . . 51
4.1.1 Corner Model Selection . . . 53
4.1.2 Control Design . . . 57
4.1.3 Stability Analysis . . . 59
4.1.4 Simulation Example . . . 61
4.2 Application of MMRAC to Motion Control of Lateral Vehicle Dynamics . . . 70

5 Multiple-Model Adaptive Pole Placement Control (MMAPPC) with Blending **77**

5.1 State-Feedback MMAPPC of Square MIMO Systems 77

5.1.1 Control Design 78

5.1.2 Stability Analysis 80

5.2 Application of MMAPPC with State Feedback to the Motion Control of Lateral Vehicle Dynamics 82

5.3 Output-Feedback MMAPPC of SISO Systems 84

5.3.1 Control Design 86

5.3.2 Stability Analysis 87

5.3.3 Simulation Example 89

6 Conclusions **97**

6.1 Summary 97

6.2 Open Problems and Future Research 98

6.2.1 Extension to Discrete-Time Systems 98

6.2.2 Persistence of Excitation Considerations 99

6.2.3 Combining Switching and Blending Techniques 100

6.2.4 Extension of MMAPPC to General MIMO Systems 100

6.2.5 Extension to a Class of Nonlinear Systems 100

References **101**

List of Figures

1.1 Illustration of the polytopic uncertainty for $N = 5$. 3

1.2 High-level illustration of the MMPI framework that can be connected to different controllers. 4

3.1 Time evolution of the uncertain constant matrices A_p and B_p. 33

3.2 Time evolution of the weight vector $\hat{w}$. 33

3.3 Time evolution of the states of the system. Note they are bounded. 34

3.4 Time evolution of the state estimates without and with uncertain dynamics and measurement noise, on the left and right, respectively. 47

3.5 Time evolution of $\hat{\Theta}_p$ without and with uncertain dynamics and measurement noise, on the left and right, respectively. 47

3.6 Time evolution of $\|\hat{x}_p - x_p\|$ without and with uncertain dynamics and measurement noise, on the left and right, respectively. 48

3.7 Amplification of the noise in each state in open-loop. 48

3.8 Statistical analysis for open-loop state estimation using multiple models. . 49

4.1 Graphic illustration of the projection process to select corner models. . . . 56

4.2 Block diagram of the proposed MMRAC. 58

4.3 On the left: Time evolution of the states of the system and the reference model for MRAC and MMRAC. On the right: Control effort for MRAC and MMRAC. 61

4.4 Euclidean norm of the tracking error for MMRAC and a single-model MRAC. 62

4.5 Semilog plot for the norm 2 of the tracking errors, and the linear regressions (LR) for MMRAC and a single-model. 62
4.6 Evolution of the estimates $\hat{w}(t)$. 62
4.7 Time evolution of the estimates of A_p and B_p. 63
4.8 Simulations with measurement noise. On the left: Time evolution of the states of the system and the reference model for MRAC and MMRAC. On the right: Control effort for MRAC and MMRAC. 63
4.9 Euclidean norm of the tracking error for MMRAC and a single-model MRAC with measurement noise. 64
4.10 Evolution of the estimates $\hat{w}(t)$ with measurement noise. 64
4.11 Time evolution of the estimates of A_p and B_p with measurement noise. . . 64
4.12 Compilation of Whisker plots of the ∞-norm of the tracking error (top), slopes of the linear regression (middle), and control efforts (bottom). . . . 65
4.13 Free-body diagram for lateral vehicle dynamics using a bicycle model. . . . 71
4.14 $r(t)$ for the reference model. 74
4.15 Constant $\eta = \begin{bmatrix} 1 & 1 & 1 \end{bmatrix}^\top$. On the left: Time evolution of the states of the system and the reference model for MRAC and MMRAC. On the right: Control effort for MRAC and MMRAC. 74
4.16 Time-variation of $\eta(t)$. 75
4.17 The vector $\eta(t)$ changes as shown in Figure 4.16. On the left: Time evolution of the states of the system and the reference model for MRAC and MMRAC. On the right: Control effort for MRAC and MMRAC. 75

5.1 Block diagram of the proposed state-feedback MMAPPC. 80
5.2 States of the system for different control techniques assuming $\eta = \eta(t)$. . . 83
5.3 Control effort of the different control techniques assuming $\eta = \eta(t)$. . . . 83
5.4 Time evolution of the weight vector $\hat{w}(t)$ when $\eta = \eta(t)$. 84
5.5 Block diagram of the proposed output-feedback MMAPPC. 87
5.6 Time evolution of x_p and $\hat{x}_p$ for multiple models without measurement noise. On the left we present a single-model approach, and on the right a multiple-model approach. 91

5.7 Time evolution of x_p and $\hat{x}_p$ for multiple models with measurement noise. On the left we present a single-model approach, and on the right a multiple-model approach. 91

5.8 Amplification of the noise in each state in closed loop. 92

5.9 Compilation of Whisker plots of the 2-norm of the closed-loop parameter estimation (top) and state estimation (bottom). 95

5.10 Compilation of Whisker plots of the 2-norm of the closed-loop state regulation (top), control effort (middle) and noise amplification (bottom). 96

List of Tables

3.1 Summary of results of the statistical analysis in open-loop. 50

4.1 Summary of results of the statistical analysis. 66
4.2 Values used to run simulations. 73

5.1 Summary of results of the statistical analysis in open-loop. 93
5.2 Summary of results of the statistical analysis in closed-loop. 94

List of Abbreviations

AC Adaptive Control iv, 5, 8, 16

APPC Adaptive Pole Placement Control iv, 5, 11, 98

LTI Linear, Time-Invariant iv, 1, 8, 26, 51, 77, 97

MIMO Multiple-Input, Multiple-Output 11, 26, 51, 77, 97

MMAC Multiple-Model Adaptive Control iv, 3, 8, 10, 100

MMAPPC Multiple-Model Adaptive Pole Placement Control iv, 3, 16, 77, 78, 80, 86, 87, 98, 100

MMPI Multiple-Model Parameter Identification iv, 3, 15, 25, 51, 77, 78, 97

MMRAC Multiple-Model Reference Adaptive Control iv, 3, 4, 15, 16, 51, 52, 57, 59, 97, 98

MMSE Multiple-Model State Estimation 4, 25, 41, 77

MRAC Model Reference Adaptive Control iv, 3, 9, 51, 68, 99

MRC Model Reference Control iv, 3, 57, 97

PE Persistently Exciting 17, 18, 21, 34, 38, 46, 60, 81, 99

PPC Pole Placement Control 6, 97

SISO Single-Input, Single-Output iv, 3, 12, 35, 87, 100

Chapter 1

Introduction

1.1 Problem Domain and Motivation

The foundation of modern control theory is based on Linear, Time-Invariant (LTI) systems whose applications extend across all areas of engineering, including aerospace, robotics, automotive, chemical, and electrical systems. Control of LTI systems provides a mathematically rigorous and tractable framework for modeling, analyzing, and designing controllers that guarantee a particular dynamic behavior of physical processes. Despite their apparent simplicity, LTI systems capture the essential dynamics of a wide range of engineering problems and serve as a local approximation to more complex nonlinear systems. In practical settings, however, the exact parameters of a dynamical system are rarely known with complete certainty. Parametric uncertainty is an unavoidable feature of physical-world systems, arising due to modeling approximations, inherent variability in physical components, degradation and wear over time, external environmental influences, measurement errors during the system identification process, among others. If the true parameters of an uncertain system deviate *much* from the assumed ones, a controller that was designed using the nominal model may fail to deliver the desired performance or result in an unstable closed-loop. In this thesis, the primary focus is to design feedback controllers that stabilize uncertain LTI systems, achieve a desired performance specification, and are robust to measurement and process noise.

The type of problems that we focus on in this thesis are as follows: Consider the LTI

plant

$$\dot{x}_p(t) = A_p x_p(t) + B_p u(t),\ x_p(0) = x_{p0},\ t \geq 0,$$
$$y_p(t) = C_p x_p(t),$$

where $A_p \in \mathbb{R}^{n\times n}$, $B_p \in \mathbb{R}^{n\times m}$ are uncertain constant matrices and $C_p \in \mathbb{R}^{q\times n}$ is a *known* output matrix. The signals $x_p(t) \in \mathbb{R}^n$, $u(t) \in \mathbb{R}^m$, and $y_p(t) \in \mathbb{R}^q$ are the state vector, control input, and output of the system, respectively. A key assumption in this work is that we have certain knowledge of the parametric uncertainty of the matrices A_p and B_p, that is, they lie inside a *known*, compact, convex polytope of uncertainty; we will refer to this type of uncertainty as polytopic uncertainty in this work.

Any compact convex polytope has a finite number N of extreme points. For every extreme point $\begin{bmatrix} A_i & B_i \end{bmatrix}$ of this polytope, we can define the dynamics of a fixed model, also referred to as a corner model:

$$\dot{x}_i(t) = A_i x_i(t) + B_i u(t),\ x_i(0) = x_{p0},\ t \geq 0,$$
$$y_i(t) = C_p x_i(t),$$

where $A_i \in \mathbb{R}^{n\times n}$, $B_i \in \mathbb{R}^{n\times m}$ are known constant matrices, for every $i \in \{1, \cdots, N\}$. The signals $x_i(t) \in \mathbb{R}^n$, $u(t) \in \mathbb{R}^m$, and $y_i(t) \in \mathbb{R}^q$ are the state vector, control input, and output of the corner models, respectively.

The control objective is to design the signal u so that the dynamics of the closed-loop system behaves as specified by the control engineer using the information of the polytope of uncertainty. The information of all convex models is very relevant, since we can write the unknown matrices A_p and B_p as a convex combination of all A_i and B_i, i.e., there exists a non-empty set

$$\mathcal{W} = \left\{ w \in [0,1]^N : \begin{bmatrix} A_p & B_p \end{bmatrix} = \sum_{i=1}^{N} w_i \begin{bmatrix} A_i & B_i \end{bmatrix}, \sum_{i=1}^{N} w_i = 1 \right\}.$$

The problem of identifying the unknown system matrices A_p and B_p is equivalent to identifying an estimate $\hat{w}$ of a vector w $\in \mathcal{W}$. Figure 1.1 depicts an example of the polytopic uncertainty we consider in this work, for the case of $N = 5$; note that the plant is inside the convex hull of uncertainty.

A key benefit and motivation to blend the information obtained from multiple models is that all simulations in the literature show that the tracking speed, parameter identification speed, and state-estimation speed are at least one order of magnitude faster than

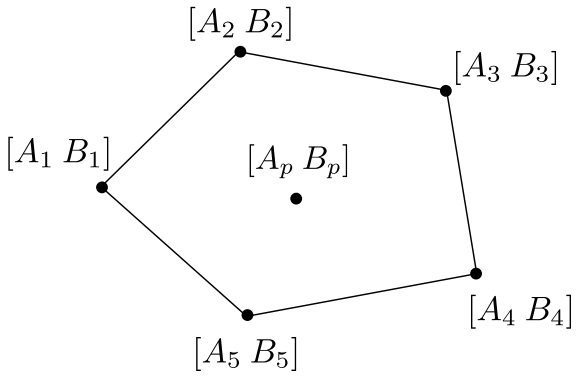


Figure 1.1: Illustration of the polytopic uncertainty for $N = 5$.

any single-model approach. Although no formal proofs guarantee this result, it has been conjectured to be the case by leading experts in the field (see [61]). Another important advantage of Multiple-Model Adaptive Control (MMAC) with blending is that during the implementation of our controllers, we do not need to run or simulate each corner model, but instead we can *greatly* decrease the number of differential equations that need to be solved.

The problem stated in this section is really broad and allows for multiple approaches. Taking into account the matrix C_p, we can differentiate between two large families of problems; state-feedback problems when C_p is the identity matrix and output-feedback problems when $C_p \in \mathbb{R}^{q\times n}$ is arbitrary. In both cases, our approach was to apply the certainty equivalence principle and develop a Multiple-Model Parameter Identification (MMPI) that provided rapid convergence of the estimated parameters to the uncertain true parameters, and was robust to noise. Once the parameters are identified, different possibilities open to use the true states or estimated states to achieve particular closed-loop behaviors.

The first problem we tackle in this thesis is the use of multiple models in a Model Reference Control (MRC) setting. We combined MMPI with Model Reference Adaptive Control (MRAC) to obtain a Multiple-Model Reference Adaptive Control (MMRAC) control scheme using the true states of the system as feedback. A second problem was developing multiple-model controllers for regulation, referred to as Multiple-Model Adaptive Pole Placement Control (MMAPPC), which place the poles of the closed-loop of the plant at the desired locations. We initially solved this problem for the case of state-feedback of square multivariable uncertain systems, and extended it to the case of Single-Input, Single-Output (SISO) systems via a state-estimation step. In Figure 1.2 we present a

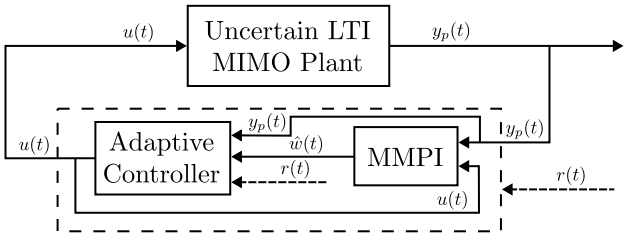


Figure 1.2: High-level illustration of the MMPI framework that can be connected to different controllers.

high-level illustration of the MMPI framework. Note that depending on C_p, the controller will change to satisfy either the MMRAC problem scheme or the MMAPPC problem with state-feedback or output-feedback with a state estimator.

1.2 Contributions of this Thesis

We outline our contributions of this thesis in the following list.

- Provided rigorous mathematical proofs for a MMPI scheme using a gradient adaptive law. The systems under consideration are non-square, i.e., the number of inputs is less than the number of states, multi-input, LTI with polytopic uncertainty, and the full states of the plant are available for feedback. Note that this result can also be applied to square systems. We extended this result for SISO, LTI systems with the same notion of uncertainty, and only the output was available for feedback. This parameter identification scheme was used to develop a Multiple-Model State Estimation (MMSE) with blending. The stability and boundedness of signals has been studied and the effectiveness validated via simulations. They show the effectiveness of these approaches and the increase in robustness to noise and the improvements in the convergence speed of the error signals to zero. In addition, simulations show that the MMPI scheme can also be applied for linear systems with uncertain parameters that are slowly time-varying. The MMPI approaches can easily be combined with any model-based control scheme.

- We combine the MMPI scheme with a MRAC framework to develop a MMRAC scheme for non-square, multi-input, LTI systems with polytopic uncertainty, and the full states of the plant are available for feedback; note that the results also hold for square systems. For each corner model, we compute two offline gains that are used

to generate a control input based on multiple models. The control input with MMPI guarantees that the states x_p of the uncertain plant perfectly asymptotically track the states generated by a *known* reference model with a *known*, bounded and piecewise continuous reference input signal, under the assumption of persistence of excitation. Moreover, all closed-loop signals remain bounded. A complete stability analysis is provided alongside a set of simulations. Statistical analysis shows that the proposed approach improves noise robustness and significantly decreases the convergence speed of the MMRAC scheme compared to single-model approaches.

- We combine the MMPI scheme with a Adaptive Pole Placement Control (APPC) framework to develop a MMAPPC scheme for square, multi-input, LTI systems with polytopic uncertainty, and the full states of the plant are available for feedback. For each corner model, we compute one offline gain that is used to generate a control input based on multiple models. The control input with MMPI guarantees that the states x_p converge to zero and that all signals of the closed-loop remain bounded, under the assumption of persistence of excitation. A complete stability analysis is provided alongside a set of simulations. We extend this result to the case of SISO, LTI systems with polytopic uncertainty, with a MMSE intermediate step. For the latter case, we do not require persistence of excitation to guarantee our results. Statistical analysis shows how the proposed MMAPPC approach improves the robustness to noise and regulates the states faster compared to a single-model approach.

- The MMRAC and MMAPPC are tested on the interesting engineering problem of motion control of lateral vehicle dynamics. Our approaches outperform the performance of single-model approaches, most notably in the case of slowly time-varying parameters, for similar control efforts. Combining these results with the statistical analyzes for MMRAC and MMAPPC suggests that the use of multiple models can be used to improve the performance of automobile systems and could potentially decrease the number of accidents on the road.

1.3 Organization and Notation

Chapter 2 deals with the literature review of Adaptive Control (AC) and part of the mathematical foundation in AC. First, we provide a historical summary of the origins of AC, the drawbacks, and how MMAC presented a novel approach to overcome the limitations of single-model approaches. We cover the main MMAC approaches consisting of switching control and blending control and justify the use of blending for this thesis. As background

information, we include a set definitions and common results in AC that are used multiple times throughout the thesis.

In Chapter 3, we present the formal problem formulation of online MMPI with blending for LTI, non-square, multi-input systems with state-feedback, and for LTI, SISO systems with a state estimator. The key assumption of polytopic uncertainty is made and justified. Under these constraints, parameter projection is properly defined and can bound the region where the minimization problem is defined. Lastly, we present simulations of the effectiveness of the MMPI scheme and robustness analysis for the MMPI solution with state estimation.

We dedicate Chapter 4 to combine the MMPI scheme in a MRAC framework to develop a MMRAC scheme. Complete stability proofs are provided, as well as the necessary conditions to guarantee a perfect tracking of plant states x_p to the states generated by a reference model that is considered ideal or nominal. A procedural algorithm is given for the selection of the corner models that satisfy all the assumptions for this problem formulation. We present simulations of the effectiveness of the MMRAC scheme and robustness analysis. The last part of the chapter applies MMRAC to the motion control of lateral vehicle dynamics.

In Chapter 5, we combine MMPI with a Pole Placement Control (PPC) framework to create a MMAPPC scheme. Firstly, we formulate and provide stability proofs for square, multi-input, LTI systems with polytopic uncertainty, and the full states of the plant are available for feedback. Second, we formulate and provide stability proofs for SISO, LTI systems with polytopic uncertainty, with a MMSE intermediate step. Third, we present simulations of the effectiveness of the MMAPPC scheme and robustness analysis. We finish the chapter with an application of MMAPPC to the motion control of lateral vehicle dynamics.

Finally, we devote Chapter 6 to discussing the conclusions of this work. We mention some limitations to the current theory and a brief list of open problems that time did not allow us to cover, but would greatly improve the applicability of our results more widely.

Notation

If $S \subseteq \mathbb{R}^n$, then $\operatorname{conv}(S)$ denotes the closed convex hull of S, the interior of S is written $\operatorname{int}(S)$. Let $\|\cdot\|$ denote the 2-norm of both vectors and matrices, and let $\|\cdot\|_\infty$ denote the infinity norm of vectors. The kernel of a matrix A is denoted by $\operatorname{Ker} A$. Given two matrices $Q, R \in \mathbb{R}^{n\times n}$, we write $Q \succeq R$ if $Q - R$ is positive semidefinite. For two signals f_1 and f_2 we write $f_1 \equiv f_2$, if there exist α, $\beta > 0$ such that for all $t \geq 0$, $\|f_1(t) - f_2(t)\| \leq \beta e^{-\alpha t}$.

Furthermore, if $e_f = f_1 - f_2$ satisfies $\dot{e}_f(t) = -\alpha e_f(t)$, then we write $f_1 \overset{\alpha}{=} f_2$. If $x \in \mathbb{R}^N$, then x_i denotes the i-th component, and $\bar{x} = (x_1, \cdots, x_{N-1}) \in \mathbb{R}^{N-1}$. Two polynomials are strongly coprime if there exists a positive constant $\varepsilon > 0$ such that the distance between their roots is greater than ε. The matrix pairs $(A(t), b(t))$ and $\left(A(t), c^\top\right)$ are strongly controllable and strongly observable, respectively, if there exists $\varepsilon > 0$, such that for every t, the polynomials $\det(s\mathbb{I} - A(t))$ and $c^\top \mathrm{adj}(s\mathbb{I} - A(t))b(t)$ are strongly coprime. If $A \in \mathbb{R}^{n\times n}$, then $\sigma(A)$ denotes the n roots of its characteristic polynomial.

Chapter 2

Literature Review and Theoretical Background

This chapter provides a review of the literature of Adaptive Control (AC). A brief historical summary motivates the use of multiple models based on the shortcomings of single-model approaches. Then, we study multiple-model approaches, where we analyze the history of switching control and blending control, and the evolution of recent advances in Multiple-Model Adaptive Control (MMAC). Finally, this chapter reviews several fundamental concepts and results that will be used throughout the thesis. The aim is not to provide exhaustive proofs, which can be found in standard references [27, 77], but rather to present the key statements and intuition behind each result to establish a common foundation for the developments in later chapters.

2.1 Historical Background of Adaptive Control

The origins of adaptive control are closely tied to the aerospace industry of the 1950s, when the first high-performance aircraft and guided missiles began to operate in flight regimes that could not be stabilized reliably with fixed-gain controllers. Autopilot failures were frequent: a set of gains that worked well at low altitude and moderate speed often led to instability at higher altitudes or at different speeds. This problem highlighted the fundamental weakness of Linear, Time-Invariant (LTI) controllers in the presence of parameter variations [27, 77].

The basic principle of adaptive control was to automatically tune controller parameters in real time to compensate for these variations. One of the first schemes was the *MIT rule*,

derived from the idea of adjusting controller parameters in the direction of the negative gradient of a cost function. If $y(t)$ is the plant output and $y_m(t)$ the reference model output, the error is defined as $e(t) = y(t) - y_m(t)$. The adaptation law was chosen as $\dot{\theta}(t) = -\gamma \dfrac{\partial e(t)}{\partial \theta} e(t)$, where θ is the adaptive parameter and $\gamma > 0$ a learning rate. Although conceptually simple, the MIT rule lacked rigorous stability guarantees and could diverge in the presence of disturbances or a modeling mismatch [45].

This motivated the development of Lyapunov-based adaptive control. Lyapunov's direct method allowed researchers to construct adaptation laws that guaranteed global stability under certain assumptions. For example, given a candidate Lyapunov function,

$$V(e, \tilde{\theta}) = \frac{1}{2} e^2 + \frac{1}{2\gamma} \tilde{\theta}^\top \tilde{\theta},$$

where $\tilde{\theta}$ is the parameter estimation error, one can derive adaptation laws that ensure $\dot{V}(t) \leq 0$, proving the boundedness of all signals. Typically, an application of the invariance principle is used to show the convergence of the tracking error to zero.

Despite these advances, early adaptive controllers suffered from several practical limitations, such as slow convergence rates, high sensitivity to noise, and restrictive assumptions. As a result, many early adaptive autopilot prototypes did not deliver the expected reliability. These difficulties motivated alternative strategies, and researchers continued to refine adaptive methods into more practical forms.

Model Reference Adaptive Control (MRAC) became the canonical framework for adaptive control in the 1960s and 1970s. The idea is that given an uncertain plant with known structure

$$\begin{aligned} \dot{x}_p(t) &= A_p(\theta_p) x_p(t) + B_p(\theta_p) u(t),\ x_p(0) = x_{p0},\ t \geq 0, \\ y_p(t) &= C_p x_p(t), \end{aligned}$$

and a stable reference model

$$\begin{aligned} \dot{x}_r(t) &= A_r x_r(t) + B_r r(t),\ x_r(0) = x_{r0}, \\ y_r(t) &= C_r x_r(t), \end{aligned}$$

where r is a bounded command input, the adaptive controller adjusts the estimated parameter $\hat{\theta}_p(t)$ so that the closed-loop system drives the error $e(t) = y_p(t) - y_r(t)$ to zero [77]. A standard MRAC controller has the form

$$\begin{aligned} u(t) &= \hat{\theta}_p^\top(t) \phi_p(t), \\ \dot{\hat{\theta}}_p(t) &= -\Gamma \phi_p(t) e^\top(t) P B_p, \end{aligned}$$

where $\phi_p(t)$ is a regressor vector of measurable signals, such as the plant states or the filtered inputs, P is a positive definite matrix solving a Lyapunov equation for the reference model and Γ is a gain matrix. It can be shown that this controller keeps all signals bounded and that $e(t)$ asymptotically converges to zero under persistence of excitation.

Over the years, MRAC has been improved with robustness modifications. The σ-modification [80, 28] adds a damping term to prevent parameter drift:

$$\dot{\hat{\theta}}_p(t) = -\Gamma \phi_p(t) e^\top(t) P B_p - \sigma \hat{\theta}_p(t).$$

The σ-modification scales the adaptation based on the magnitude of the tracking error to improve the robustness of the noise. Despite its rigorous foundation, MRAC is not without weaknesses. Adaptation may be slow for large uncertainties, noise robustness is limited, and the choice of an appropriate reference model can be non-trivial in complex systems. These limitations led to parallel developments in gain scheduling and MMAC.

Gain scheduling was developed in parallel with MRAC as a more pragmatic method, particularly well suited to aerospace applications [25, 47, 46, 54]. The central idea is to design linear controllers at a set of operating points (for example, steady flight conditions characterized by altitude and Mach number) and then interpolate controller gains based on measurable scheduling variables [31]. Mathematically, the controller is written as

$$u(t) = K(\rho(t)) x_p(t),$$

where $\rho(t)$ is the scheduling variable, such as air speed or load condition. At each frozen operating point $\rho = \rho_i$, the gain $K(\rho_i)$ is designed to stabilize the corresponding linearized plant model. The interpolated controller then attempts to stabilize the full nonlinear system as $\rho(t)$ varies [70].

Gain scheduling has enjoyed widespread industrial success. Modern flight control systems, gas turbines, and chemical plants often rely on scheduling strategies due to their transparency and ease of certification [8, 9, 65, 93]. The frozen-time stability analysis generally assumes that $\rho(t)$ varies slowly.

Several refinements have been introduced [71], including linear, parameter-varying control [69, 68, 72, 62], which casts gain scheduling into a convex optimization framework with guaranteed stability under parameter variations. However, classical gain scheduling remains essentially an interpolation method [74].

From a theoretical perspective, gain scheduling can be viewed as a precursor to MMAC. The interpolation of gains across operating points [73] resembles the blending of multiple controllers, while the selection of appropriate gains for each region resembles switching

strategies. This perspective motivated researchers to develop MMAC as a more rigorous extension of scheduling ideas.

Pole placement control originated in the 1960s, as state-space methods gained prominence in modern control theory, providing a systematic way to assign the closed-loop poles of a linear system to desired locations in the complex plane. Given a controllable pair (A_p, B_p), the controller designer could select a feedback gain matrix K such that the eigenvalues of $A_p - B_pK$ match a chosen set [66], directly shaping the closed-loop dynamics. The approach was strongly influenced by the increasing availability of digital computers, which made state-space methods practical for real engineering problems [30, 35].

One of the main strengths of pole placement is its generality. As long as the system is controllable, arbitrary closed-loop poles can be assigned. This provides great flexibility in tuning the response speed, the damping ratio, and the oscillatory behavior [86]. Furthermore, the method naturally extends to Multiple-Input, Multiple-Output (MIMO) systems [1], offering systematic procedures to the most common classical control design problems. When combined with observers [43] or Kalman filters [35], pole placement also became the foundation of modern output-feedback control and optimal control.

Although pole placement provides a systematic way to assign closed-loop dynamics, its effectiveness can be limited when the system model is uncertain. In such cases, Adaptive Pole Placement Control (APPC) techniques have been developed [29] to adjust controller gains online, ensuring that stability and desired transient performance are preserved despite parameter variations or modeling errors. However, APPC alone may suffer from limitations, such as slow adaptation, poor robustness margins, or sensitivity to noise [85]. To address these issues, multiple-model approaches have been proposed in which a set of candidate models and controllers is maintained in parallel. By blending or switching among these models, the closed-loop system can achieve improved robustness, faster adaptation, and better overall performance in the presence of uncertainty.

2.2 Switching Control

Multiple-model switching techniques emerged as a structured approach to dealing with large uncertainties by maintaining a set of candidate models $\{M_1, M_2, \cdots, M_N\}$, each representing a possible plant behavior. For each model M_i, a corresponding controller K_i is predesigned. Then, a switching logic [22, 21, 23, 19] selects which controller to apply based on the observed plant signals. A typical switching rule involves computing an identification error for each candidate model $e_i(t) = y(t) - y_i(t)$, where $y_i(t)$ is the output

predicted by the model M_i. The identification error is used to compute a cost function $J_i(e_i(t))$, commonly calculated as

$$J_i(t) = \|e_i(t)\|^2 \text{ [57]},$$
$$J_i(t) = \int_0^t \|e_i(\tau)\|^2 \mathrm{d}\tau \text{ [21]},$$
$$J_i(t) = \alpha\|e_i(t)\|^2 + \beta \int_0^t \|e_i(\tau)\|^2 \mathrm{d}\tau,\ \alpha > 0,\ \beta > 0 \text{ [3]},$$
$$J_i(t) = \alpha\|e_i(t)\|^2 + \beta \int_0^t e^{-\lambda(t-\tau)}\|e_i(\tau)\|^2 \mathrm{d}\tau,\ \alpha > 0,\ \beta > 0,\ \lambda > 0 \text{ [20]},$$

which is then used by a decision maker, known as a *supervisor* or *monitor* [50, 51, 20, 5, 81], to select the best model as the one that minimizes $J_i(e_i(t))$ at time t, i.e., the supervisor produces a signal $\sigma(t) \in \mathbb{N}$ that selects the controller. The set of controllers was invariant in time [48, 53, 83, 50]. As time advanced, the researchers developed the switching and tuning technique [55, 56], where the models could switch and adapt as more information about the system was obtained.

Initially, instability problems occurred due to frequent switching; different techniques have been developed to counteract this issue. A dwell-time condition [36]: once a controller is selected, it must remain active for at least $\tau_D > 0$ seconds before another switch is allowed. A limitation of this approach is that in τ_D seconds the system may deteriorate to an unacceptable level before the next switching is allowed. A solution for this problem is the implementation of a hysteresis condition [20]: once a controller is selected, it cannot change until $\tau_D > 0$ seconds have passed, or the error has increased above a particular threshold.

Under suitable conditions, MMAC with switching can guarantee different levels of stability and boundedness of signals for distinct classes of systems. For LTI, Single-Input, Single-Output (SISO) systems, we can find the majority of results; in [22], they guarantee boundedness of all signals for the case of bounded noise, bounded disturbances, and unmodeled dynamics, obtaining bounded output tracking, under an assumption on the initial state of the system. In [50, 51], a *supervisor* is developed that is able to select a controller from a family of candidate controllers that achieves perfect tracking of a constant reference input and rejection of bounded constant disturbances. The robustness of this result is proven for the case of bounded measurement noise, where the tracking error of the input remains bounded. For implementation purposes, given an infinite uncertainty set [4] shows how to obtain a finite set of models such that at least one of the elements of the finite set corresponding to the controllers is able to satisfactorily control each plant in

the uncertainty set. A collection of most of the early results in switching control techniques can be found in [36], including global uniformly asymptotic stability conditions of switched systems under arbitrary or restricted switching.

Natural extensions of these results appeared for other classes of systems. In [13], a robust adaptive multivariate switching control algorithm is presented for MIMO, LTI systems that uses very little *a priori* knowledge of the plant and achieves closed-loop stability and bounded tracking and regulation of a reference signal and a disturbance signal, respectively. For stochastic problems, [12] combines cautious randomized control and switching control to provide robustness in finite time and asymptotically stable. For nonlinear and time-varying systems, [44] provides conditions for global uniform asymptotic stability, given that the system is measurable and the state functions satisfy Carathéodory conditions. These techniques have also been combined with a MRAC framework in [50, 51, 76, 32, 55] and with APPC in [67].

In recent years, switching control has tackled problems related to event-triggered switching of uncertain nonlinear systems in [89], constructing multiple Lyapunov functions to solve tracking control problems of multiple agents in [84]. Results that guarantee integral input-to-state stability were developed in [38]. For discrete-time switched systems, switching control has provided a solution to develop interval observers [24] with notions of optimality [92].

Even with these stability guarantees, switching introduces some challenges. First, one of the fixed models is **required** to be sufficiently close to the original plant, and the corresponding number N of fixed models may be large or grow exponentially with the dimension of the uncertainty parameter vector [59]. Second, transients at the switching instant can be abrupt, leading to undesirable oscillations or stress on the actuators. Finally, models that are not the best match for the plant at time t do not contribute to the estimation of unknown parameters. These limitations motivated the development of blending strategies, where the outputs of multiple controllers are combined continuously rather than being switched discretely. The contrast between switching and blending is fundamental. Switching methods are attractive due to their conceptual simplicity [52], but introduce discontinuities in the control signal that can cause undesirable transients or even instability if switching is too frequent and are computationally demanding when implemented. In contrast, blending mitigates the risk of abrupt changes in closed-loop dynamics, lowers the computational demand, uses the information of all models to better estimate the parameters at all times, and for the case of very large parametric uncertainty, blending can decrease the number of models used.

2.3 Blending Control

Multiple-model techniques with blending are a modern control architecture that tries to use multiple models in a way that mitigates each of the limitations experienced in the multiple-model switching control framework [59]. Consider an uncertain system M with input u and output y_p, and let the N candidate models $\{M_1, M_2, \cdots, M_N\}$ represent possible plant behaviors. For an input u, each model M_i will have a corresponding output vector y_i. A fundamental assumption for MMAC with blending is the existence of a vector $w \in [0,1]^N$, such that $\sum_{i=1}^{N} w_i = 1$, and the output $y_p(t)$ can be written as a convex combination of the output of all candidate models $y_i(t)$ as

$$y_p(t) = \sum_{i=1}^{N} w_i y_i(t).$$

If the vector w is known, then all the usual control techniques can be applied given that the usual matching, controllability, or observability conditions are met. In the uncertain case, the problem of identifying the plant M is equivalent to identifying the vector w. This modern control architecture creates a control input that is continuous in time, which removes the abrupt transient behavior that switching control can exhibit. In addition, it is not required for any of the models M_i to be close to the original model. Instead, a convex combination condition is introduced; we show in Section 4.1.1 that this assumption is automatically satisfied for most common parametric system identification processes. Moreover, for a given system with a known, compact, convex polytope of uncertainty, if the size of the polytope is scaled up by a large factor, then the number of models needed in the blending approach would not change, but grow exponentially fast with the scaling factor. Finally, all models are used during the adaptation of the parameter identification.

One of the first results in blending control is based on the notion of gain scheduling. When gain scheduling controllers interpolate between two fixed controllers, it can be interpreted both as a switching control technique and as a blending technique. By measuring the state and identifying that is within a particular region, two controllers are chosen out of all possible controllers (switching behavior). To avoid abrupt transitions, one possible solution is to interpolate the controllers (blending behavior). This allowed [34] to improve the performance of SISO, LTI systems with uncertainty, provide stability, and robustness to noise using a blending approach of two controllers at a time. The uncertainty set is known and discretized into smaller overlapping sets. For each set a stabilizing controller is designed; considering the state of the system, a single controller is selected for the non-overlapping regions, and an interpolated version of two controllers is chosen in

the overlapping regions. This foundational work provides formal stability and robustness proofs, showing that blending control can be used with guarantees.

The theoretical challenge in blending lies in guaranteeing stability and performance for the combination of controllers. Unlike switching, where stability can often be deduced from dwell-time or multiple Lyapunov function arguments [37, 36, 50, 19], blending introduces coupling between controllers that requires a more delicate analysis. Early works focused on SISO, LTI systems [34], where a robust performance specification can be met exponentially fast in the presence of unmodeled dynamics, noise, and disturbances. The regulation error is shown to be in the same order as the mean square value of these exogenous signals. Under persistence of excitation of the input, the parameter estimates converge to their true values.

A natural extension to LTI, single-input, state-feedback systems was presented in [60, 17]. In these works, a Multiple-Model Reference Adaptive Control (MMRAC) scheme, called second-order adaptation, is designed that achieves exponentially fast state tracking and perfect parameter identification under the condition of persistence of excitation. The main limitation of this approach is that the matrix pair $\begin{bmatrix} A_p & B_p \end{bmatrix}$ is in canonical controllable form, i.e., only the matrix A_p allows for uncertainty and that the number of identification models is not arbitrary; for a state vector x_p with n entries, $n+1$ adaptive models are selected, making it very difficult to obtain the set of corner models. This class of systems was extended to the use of N arbitrary models in [2], allowing for an easier implementation of the approach, although no corner model selection procedure was proposed.

More recently, an extension to LTI, MIMO systems was presented in our work published in [42]. In that article, we developed an Multiple-Model Parameter Identification (MMPI) schemed that combined with a MRAC framework achieves perfect state tracking. A procedure to select corner models that can be used for most system identification processes is presented, and robustness properties are studied via statistical analysis. These results are presented in Chapters 3 and 4. The first extension of second-order adaptation to a class of nonlinear systems started in a brief paper [90], where this approach is used in combination with back-stepping adaptive control to achieve output tracking of a system in parametric-strict-feedback form. Later results presented in [94] extended to general discrete-time nonlinear systems with parametric uncertainty, given that the uncertain parameters are inside of a *known*, compact, convex polytope of uncertainty and the nonlinearity is zero-order bounded. Under this assumptions, the output is able to perfectly track a desired output and guarantee boundedness of all closed-loop signals.

In experimental studies, the use of blending control has decreased overshoot, settling time, steady-state error [63, 15], was used to design fault tolerant controllers [11] for drone

applications, and has been applied as an output-feedback solution to the control of dielectric electroactive polymer actuators [7]. Other applications include multiple model estimation of power systems models [49], development of an adaptive controller for partially-observed boolean dynamical systems [26], distributed state estimation using a network of local sensors [82], and motion control of lateral vehicle dynamics [40, 91].

An important application of multiple-model methods has been the integration with MRAC and APPC. Classical MRAC provides rigorous guarantees but suffers from transient oscillations, slow adaptation, and structural restrictions. Most of the MMRAC developed are for switched systems, as seen in [88, 75], but suffer the same limitations of switched systems. In [58, 60, 17, 42, 40], we find solutions to MMRAC using a blending approach that have smooth control signals. When it comes to pole placement, in [91] an optimal Multiple-Model Adaptive Pole Placement Control (MMAPPC) with blending is developed that guarantees state regulation and boundedness of all closed-loop signals. A similar result for non-optimal pole-placement is presented in [41], where motion control of lateral vehicle dynamics is studied.

This brief review of the literature suggests that MMAC with blending provides a promising path to overcome the shortcomings of classical AC and also address the shortcomings of switching control. However, several key gaps remain. First, existing schemes are often tailored to specific system classes such as canonical, square, or scalar systems, limiting their generality. Second, theoretical guarantees of stability and convergence are frequently incomplete, particularly for blending-based designs. Third, the assumption of persistence of excitation is required to achieve perfect asymptotic convergence of the parameter to the true values. Finally, it is interesting to note that for some problems, switching control is inherently better suited to design controllers: (i) when the uncertainty is very small, (ii) when there are abrupt changes in dynamics, switching control can adapt faster than the blending approach. Some cases where blending approaches perform better include: (i) uncertain and cyclic slowly-time varying parameters can cause cyclic transient behaviors from the switching approach, and (ii) very large parametric uncertainty. Both approaches can have designs that guarantee robustness to noise.

2.4 Theoretical Background

We combine a series of common definitions and results here.

2.4.1 Parametric Models

Consider a SISO, LTI system described by the n-th order differential equation:

$$y_p^{(n)} + a_{n-1}y_p^{(n-1)} + \cdots + a_1\dot{y}_p + a_0 y_p = b_m u^{(m)} + \cdots + b_1\dot{u} + b_0 u. \tag{2.1}$$

Assume that y_p, $u \in \mathbb{R}$ are the output and the input, respectively. Considering that all parameters $a_0, \cdots, a_{n-1}$, $b_0, \cdots, b_m$ are unknown, we can define the uncertainty vector as

$$\theta_p = \begin{bmatrix} b_m & \cdots & b_0 & a_{n-1} & \cdots & a_0 \end{bmatrix}^\top \tag{2.2}$$

and rewrite the differential equation as

$$y_p^{(n)} = \theta_p^\top \begin{bmatrix} u^{(m)} & \cdots & u & -y_p^{(n-1)} & \cdots & -y_p \end{bmatrix}^\top \in \mathbb{R}^{n+m+1}.$$

Filtering both sides by $\dfrac{1}{\Lambda(s)}$, where $\Lambda(s)$ is a monic Hurwitz polynomial, we obtain the parametric model

$$z_p = \theta_p^\top \phi_p, \tag{2.3}$$

where

$$\begin{aligned} z_p &= \frac{1}{\Lambda(s)} y_p^{(n)} = \frac{s}{\Lambda(s)} y_p, \\ \phi_p &= \left[\frac{s^m}{\Lambda(s)} u \quad \cdots \quad \frac{1}{\Lambda(s)} u \quad -\frac{s^{n-1}}{\Lambda(s)} y_p \quad \cdots \quad -\frac{1}{\Lambda(s)} y_p \right]^\top. \end{aligned}$$

Note that z_p and y_p differ only by a signal that decays exponentially fast, that is, $y_p \overset{\alpha}{=} z_p$.

2.4.2 Persistence of Excitation

A signal $\Phi : [0, \infty) \to \mathbb{R}^k$ is Persistently Exciting (PE), if there exist $\alpha_{\Phi 1}$, $\alpha_{\Phi 2}$, $T_\Phi > 0$ such that for every $t \geq 0$

$$\alpha_{\Phi 1}\mathbb{I} \preceq \int_t^{t+T_\Phi} \Phi(\tau)\Phi^\top(\tau)\mathrm{d}\tau \preceq \alpha_{\Phi 2}\mathbb{I}. \tag{2.4}$$

Since $\Phi\Phi^\top$ is always positive semidefinite, the persistence of excitation condition requires that the integral over any interval of time length T_Φ be a positive definite matrix. The notion of a signal being PE gives an idea of how much information it carries. PE signals will allow us to completely excite the system and to asymptotically identify the uncertain parameters, as we will see in future chapters.

2.4.3 Barbalat's Lemma

In adaptive control analysis, a central objective is to establish the asymptotic convergence of the error signals to zero as time goes to infinity. This property typically follows from demonstrating that the error signal is square-integrable with a bounded derivative, a result formalized by Barbalat's lemma [27].

Lemma 2.1 (Barbalat's Lemma). *For a function $f : [0, \infty) \to \mathbb{R}$, if f, $\dot{f} \in \mathcal{L}_\infty$ and $f \in \mathcal{L}_p$, for some $p \in [1, \infty)$, then $\lim_{t\to\infty} f(t) = 0$.*

2.4.4 Parameter Identification: Gradient Algorithm

Consider the parametric model (2.3) and define its estimate $\hat{z}_p$, generated by the estimation model $\hat{z}_p = \hat{\theta}_p^\top \phi_p$, where $\hat{\theta}_p$ is the time estimate of θ_p. We can construct the estimation error as

$$\varepsilon_p = \frac{z_p - \hat{z}_p}{m_s^2} = \frac{z_p - \hat{\theta}_p^\top \phi_p}{m_s^2},$$

where $m_s^2 \geq 1$ is a normalization signal designed to bound ϕ_p from above. If we define a cost function $J(\hat{\theta}_p)$ as

$$J(\hat{\theta}_p) = \frac{\varepsilon_p^2 m_s^2}{2} = \frac{(z_p - \hat{\theta}_p^\top \phi_p)^2}{2m_s^2},$$

the gradient algorithm takes the form

$$\dot{\hat{\theta}}_p = -\Gamma \nabla J = \Gamma \varepsilon_p \phi_p, \tag{2.5}$$

where $\Gamma = \Gamma^\top \succ 0$ is a design matrix referred to as the *adaptive gain*.

Proposition 2.2 (See [27] (Theorem 3.6.1)). *The gradient algorithm (2.5) guarantees that:*

1. *ε_p, $\varepsilon_p m_s$, $\dot{\hat{\theta}}_p$ are bounded and square integrable, and $\hat{\theta}_p$ is bounded.*
2. *If $\dfrac{\phi_p}{m_s}$ is PE, then $\hat{\theta}_p$ converges to θ_p exponentially fast.*
3. *If the plant (2.1) has stable poles, no zero-pole cancellations, and u is sufficiently rich of order $n + m + 1$, i.e., it consists of at least $\dfrac{n+m+1}{2}$ distinct frequencies, then ϕ_p and $\dfrac{\phi_p}{m_s}$ are PE. Furthermore, $\|\hat{\theta} - \theta_p\|$, ε_p, $\varepsilon_p m_s$ and $\dot{\hat{\theta}}_p$ converge to zero exponentially fast.*

2.4.5 Parameter Identification: Parameter Projection

In many applications, we have some information about the bounds where $\theta_p \in \mathbb{R}^n$ is located, i.e., we know a convex subset of R^n that contains all the parameters. If this information is available, we want to restrict the estimation algorithm only to the region where the unknown parameters are located.

Considering the gradient algorithm and a convex set S given by

$$S = \left\{ \hat{\theta}_p \in \mathbb{R}^n : g(\hat{\theta}_p) \leq 0 \right\},$$

where $g : \mathbb{R}^n \to \mathbb{R}$ is a smooth function; we can transform the gradient algorithm from the previous subsection to

$$\dot{\hat{\theta}}_p = \Pr(-\Gamma \nabla J) = \begin{cases} -\Gamma \nabla J, & \text{if } \hat{\theta}_p \in S^0 \text{ or } \hat{\theta}_p \in \delta(S) \\ & \text{and } (\Gamma \nabla J)^\top \nabla g \leq 0, \\ -\Gamma \nabla J + & \Gamma \dfrac{\nabla g \nabla g^\top}{\nabla g^\top \Gamma \nabla g} \Gamma \nabla J, \text{ otherwise,} \end{cases} \tag{2.6}$$

where $\delta(S) = \left\{ \hat{\theta}_p \in \mathbb{R}^n : g(\hat{\theta}_p) = 0 \right\}$ and $S^0 = \left\{ \hat{\theta}_p \in \mathbb{R}^n : g(\hat{\theta}_p) < 0 \right\}$ denote the boundary and interior of S, respectively.

Proposition 2.3 (See [27] (Theorem 3.10.1))**.** *The gradient adaptive law (2.5), with projection modification (2.6) retains all properties that are established in the absence of projection. In addition, it guarantees that $\hat{\theta}_p(t) \in S$ for all $t \geq 0$, provided that $\hat{\theta}_p(0) \in S$ and $\theta_p \in S$.*

2.4.6 Model Reference Adaptive Control

Consider a MIMO, LTI system

$$\dot{x}_p(t) = A_p x_p(t) + B_p u(t),\ x_p(t) \in \mathbb{R}^n,\ u(t) \in \mathbb{R}^m,\ x_p(0) = x_{p0},\ t \geq 0, \tag{2.7}$$

where $A_p \in \mathbb{R}^{n \times n}$, $B_p \in \mathbb{R}^{n \times m}$ are unknown constant matrices, and the state vector $x_p(t)$ is available for feedback.

The control objective is to design $u(t)$ to ensure closed-loop stability and that the states of the system $x_p(t)$ asymptotically track the states of the following given reference model system:

$$\dot{x}_r(t) = A_r x_r(t) + B_r r(t),\ x_r(t) \in \mathbb{R}^n,\ r(t) \in \mathbb{R}^m,\ x_r(0) = x_{r0}, \tag{2.8}$$

where $A_r \in \mathbb{R}^{n\times n}$ is Hurwitz, $B_r \in \mathbb{R}^{n\times m}$, and $r(t)$ is a known, bounded, piecewise continuous signal. Even in the case of no uncertainty, we must make the following assumptions:

Assumption 2.1. *(i) There exist a constant matrix $K_1^* \in \mathbb{R}^{n\times m}$ and a non-singular constant matrix $K_2^* \in \mathbb{R}^{m\times m}$ such that*

$$\begin{aligned} A_p + B_p K^* &= A_r, \\ B_p L^* &= B_r. \end{aligned}$$

(ii) There is a known matrix $S \in \mathbb{R}^{m\times m}$ such that L^*S is symmetric and positive definite: $M_s = L^*S = (L^*S)^\top = S^\top L^{*\top} \succ 0$.

If the parameters A_p and B_p were known, the control law $u(t) = K^*x_p(t) + L^*r(t)$ would achieve exponential tracking of the states $x_r(t)$, i.e., the tracking error $e(t) = x_p(t) - x_r(t)$ would converge to zero exponentially fast.

When considering an uncertain setting, the parameters A_p and B_p are not known, and we use certain equivalence to obtain an adaptive version of the control law as

$$u(t) = \hat{K}(t)x(t) + \hat{L}(t)r(t), \tag{2.9}$$

where $\hat{K}(t)$ is the estimate of K^*, and $\hat{L}(t)$ is the estimate of L^*. We can define the update laws

$$\begin{aligned} \dot{\hat{K}}(t) &= -S^\top B_r^\top P e(t) x_p^\top(t), \ \hat{K}(0) = \hat{K}_0, \\ \dot{\hat{L}}(t) &= -S^\top B_r^\top P e(t) r^\top(t), \ \hat{L}(0) = \hat{L}_0, \end{aligned} \tag{2.10}$$

where S satisfies Assumption 2.1, $\hat{K}_0$ and $\hat{L}_0$ are arbitrary, and $P \in \mathbb{R}^{n\times n}$ is a constant matrix such that $P = P^\top \succ 0$ and solves $PA_r + A_r^\top P = -Q$ for some constant $Q \in \mathbb{R}^{n\times n}$ such that $Q = Q^\top \succ 0$.

Proposition 2.4. *Consider the uncertain system (2.7) and the reference model (2.8). Assume that Assumption 2.1 holds, then the MRAC scheme (2.9) and (2.10) guarantees that for any x_{r0} and bounded, piecewise continuous reference signal $r(t)$ all closed-loop signals are bounded and $e(t)$ asymptotically converges to zero.*

In order to identify the system, we can define estimates of A_p and B_p as $\hat{A}_p(t)$ and $\hat{B}_p(t)$ to obtain the following adaptive identification law:

$$\begin{aligned} \dot{\hat{A}}_p(t) &= -\Gamma_1 P e(t) x_p^\top(t), \ \hat{A}_p(0) = \hat{A}_{p0}, \\ \dot{\hat{B}}_p(t) &= -\Gamma_2 P e(t) r^\top(t), \ \hat{B}_p(0) = \hat{B}_{p0}, \end{aligned} \tag{2.11}$$

where $\hat{A}_{p0}$ and $\hat{B}_{p0}$ are arbitrary, $\Gamma_1 \in \mathbb{R}^{n\times n}$ and $\Gamma_2 \in \mathbb{R}^{n\times n}$ are constant, positive definite, symmetric matrices. If the control signal u is PE, then we have exponential convergence of the matrices estimates $\hat{A}_p$ and $\hat{B}_p$ to A_p and B_p, respectively. See [77] for the complete analysis.

2.4.7 Adaptive State Estimation

Consider the LTI, SISO plant

$$\begin{aligned} \dot{x}_p(t) &= A_p x_p(t) + b_p u(t),\ x_p(0) = x_{p0},\ t \geq 0, \\ y_p(t) &= c_p^\top x_p(t), \end{aligned} \tag{2.12}$$

where $A_p \in \mathbb{R}^{n\times n}$ and $b_p \in \mathbb{R}^n$ are unknown constant matrices, A_p is Hurwitz, $c_p \in \mathbb{R}^n$, $x_p(t) \in \mathbb{R}^n$ is the state vector, $u(t) \in \mathbb{R}$ is a known, bounded, piecewise continuous control signal. The matrix pair (A_p, b_p) is controllable and $(A_p, c_p^\top)$ is observable.

Assumption 2.2. *The systems considered in* (2.12) *are in canonical observable form, that is, they have the following structure*

$$\begin{aligned} A_p &= \left[\begin{array}{c|c} -a_p & \begin{matrix} \mathbb{I}_{n-1} \\ \hline 0 \end{matrix} \end{array}\right], \\ a_p &= \begin{bmatrix} a_{n-1} & a_{n-2} & \cdots & a_1 & a_0 \end{bmatrix}^\top \in \mathbb{R}^n, \\ b_p &= \begin{bmatrix} b_{n-1} & b_{n-2} & \cdots & b_1 & b_0 \end{bmatrix}^\top, \\ c_p &= \begin{bmatrix} 1 & 0 & \cdots & 0 \end{bmatrix}^\top. \end{aligned} \tag{2.13}$$

To perform online parameter identification, we redefine the uncertain vector (2.2) as

$$\theta_p \coloneqq \begin{bmatrix} b_p \\ a_p \end{bmatrix}. \tag{2.14}$$

In this setting, if u is PE, then the estimates $\hat{\theta}_p$ will converge to θ_p exponentially fast. Combining this with a Luenberger observer structure [43] we get the following adaptive Luenberger observer:

$$\begin{aligned} \dot{\hat{x}}_p(t) &= \hat{A}_p(t)\hat{x}_p(t) + \hat{b}_p(t)u(t) + K_o(t)(y_p(t) - \hat{y}_p(t)),\ \hat{x}_p(0) = \hat{x}_{p0}, \\ \hat{y}_p(t) &= c_p^\top \hat{x}_p(t), \end{aligned} \tag{2.15}$$

where $\hat{x}_p(t)$ is the estimate of $x_p(t)$,

$$\hat{A}_p(t) = \left[\begin{array}{c:c} -\hat{a}_p(t) & \mathbb{I}_{n-1} \\ \hline & 0 \end{array}\right],$$
$$K_o(t) = a^* - \hat{a}_p(t),$$

$\hat{a}_p(t)$ and $\hat{b}_p(t)$ are estimates of a_p and b_p, respectively, $a^* \in \mathbb{R}^n$ is chosen such that

$$A^* = \left[\begin{array}{c:c} -a^* & \mathbb{I}_{n-1} \\ \hline & 0 \end{array}\right]$$

is Hurwitz.

Proposition 2.5. *The adaptive observer described by (2.12), (2.14) and (2.15) with Assumption 2.2 guarantees that:*

(i) All signals are bounded.

(ii) If u is sufficiently rich of order $2n$, then the state observation error $\|x_p - \hat{x}_p\|$ and the parameter error $\|\hat{\theta}_p - \theta_p\|$ converge to zero exponentially fast.

2.4.8 Adaptive Pole Placement Control

The results in this subsection were developed in [29]. Consider a SISO, LTI system represented by the transfer function

$$y_p = G(s)u, \tag{2.16}$$

where $G(s) = \dfrac{Z(s)}{R(s)}$, $G(s)$ is proper, $R(s)$ is monic. The control objective is to design $u(t)$ such that the closed-loop poles are assigned to those of a known Hurwitz polynomial $A_c^*(s)$. In addition, we want to include a tracking objective, i.e., $y_p(t)$ has to asymptotically track a class of bounded reference signals $y_r(t)$ that satisfy

$$Q_r(s)y_r = 0,$$

where $Q_r(s)$ is a known internal model of $y_r(t)$, is a monic polynomial of degree q with all of its roots with non-positive real part, and no repeated roots in the imaginary axis.

To achieve this control objective, we make the following assumptions:

Assumption 2.3. *(i) $R(s)$ is a monic polynomial whose degree n is known.*

(ii) $R(s)$ and $Z(s)$ are coprime, and the degree of $Z(s)$ is strictly less than n.

(iii) $Q_r(s)$ and $Z(s)$ are coprime.

With these assumptions, we can define the output tracking error as

$$e_1 = \frac{Z(s)}{R(s)}u - y_r. \tag{2.17}$$

Filtering both sides of (2.17) by $\frac{Q_r(s)}{\Lambda(s)}$, where $\Lambda(s)$ is a monic Hurwitz polynomial of degree q, and also using Item (iii) of Assumption 2.3, we get

$$\begin{aligned} e_1 &= \frac{Z(s)\Lambda(s)}{R(s)Q_r(s)}\bar{u}, \\ \bar{u} &= \frac{Q_r(s)}{\Lambda(s)}u. \end{aligned} \tag{2.18}$$

Equation (2.18) transformed the tracking problem (2.17) into a regulation problem, that is, we need to choose $\bar{u}(t)$ to asymptotically take $e_1(t)$ to zero. At this point, we will solve the problem with the following state-space realization in canonical observable form:

$$\begin{aligned} \dot{e}(t) &= A_p e(t) + b_p \bar{u}(t), \\ e_1(t) &= c_p^\top e(t), \end{aligned}$$

where

$$\begin{aligned} A_p &= \left[\begin{array}{c|c} -a_p & \begin{matrix} \mathbb{I}_{n+q-1} \\ \hline 0 \end{matrix} \end{array}\right], \\ c_p &= \begin{bmatrix} 1 & 0 & \cdots & 0 \end{bmatrix}^\top, \end{aligned} \tag{2.19}$$

and a_p, b_p, $c_p \in \mathbb{R}^{n+q}$ are the coefficients of the vectors of $R(s)Q_r(s) - s^{n+q}$ and $Z(s)\Lambda(s)$, respectively. Consider the control law

$$\begin{aligned} \bar{u}(t) &= -K_c(t)\hat{e}(t), \\ u &= \frac{\Lambda(s)}{Q_r(s)}\bar{u}, \end{aligned} \tag{2.20}$$

where $\hat{e}(t)$ is the state estimate generated by the adaptive Luenberger observer

$$\dot{\hat{e}}(t) = \hat{A}_p(t)\hat{e}(t) + \hat{b}_p(t)\bar{u}(t) - K_o(t)\left(c_p^\top \hat{e}(t) - e_1(t)\right), \tag{2.21}$$

where $\hat{A}_p$ and $\hat{b}_p$ are the estimates of A_p and b_p, respectively, obtained by applying Proposition 2.5, i.e., they are the coefficients of the polynomials

$$\begin{aligned} \hat{R}(s,t)Q_r(s) - s^{n+q} &= \left(s^n + \hat{a}_p^\top(t)a_{n-1}^*(s)\right) Q_r(s) - s^{n+q}, \\ \hat{Z}(s,t)\Lambda(s) &= \hat{b}_p^\top(t)a_{n-1}^*(s)\Lambda(s), \end{aligned} \tag{2.22}$$

respectively. The vectors $K_o(t)$ and $K_c(t)$ are the solutions to

$$\begin{aligned} &K_o(t) = a^* - \hat{a}_p(t), \\ &\det\left(s\mathbb{I} - \hat{A}_p(t) + \hat{b}_p(t)K_c(t)\right) = A_c^*(s), \end{aligned}$$

respectively, a^* is chosen such that

$$A^* = \left[\begin{array}{c:c} -a^* & \begin{matrix} \mathbb{I}_{n+q-1} \\ 0 \end{matrix} \end{array}\right]$$

is Hurwitz, and $A_c^*(s) \in \mathbb{R}^{n+q}$ is a monic Hurwitz polynomial representing the desired closed-loop locations of the poles.

Proposition 2.6. *Assume that the polynomials $\hat{Z}(s,t)$ and $\hat{R}(s,t)Q_r(s)$ are strongly coprime at each time t. Then, all the signals of the closed-loop adaptive pole placement control scheme (2.16) to (2.18) and (2.20) to (2.22) are uniformly bounded, and the tracking error e_1 converges to zero asymptotically with time.*

Chapter 3

Multiple-Model Parameter Identification (MMPI)

In this chapter, we restrict our attention to the online parameter identification of an uncertain system of continuous-time plants using multiple models. The core of this chapter will deal with systems where the states are available for feedback, and the final part of this chapter will consider output feedback systems. In both cases, the online parameter identification will consist of the following three steps:

1. Create a parametric model using multiple models considering all unknown parameters of the system.

2. Set up an estimation model that has the same form as the parametric model. This will allow us to have an *estimation error*, which reflects the distance from the estimated parameters to the real parameters weighted by some signal. Finally, we design an online parameter identification law using optimization techniques and Lyapunov stability arguments.

3. The final step consists of finding conditions that guarantee that the estimates converge to the real parameters over time. This step consists of imposing a minimum requirement on the information that the input signal is carrying.

At the end, we show how to develop a Multiple-Model State Estimation (MMSE) by using the output-feedback Multiple-Model Parameter Identification (MMPI).

3.1 State-Feedback MMPI

Consider the Multiple-Input, Multiple-Output (MIMO), Linear, Time-Invariant (LTI) system

$$\dot{x}_p(t) = A_p x_p(t) + B_p u(t),\ x_p(0) = x_{p0},\ t \geq 0, \tag{3.1}$$

where $A_p \in \mathbb{R}^{n\times n}$ and $B_p \in \mathbb{R}^{n\times m}$ are unknown constant matrices with polytopic uncertainty, A_p is Hurwitz, $x_p(t) \in \mathbb{R}^n$ is the state of the system, $u(t) \in \mathbb{R}^m$ is a known, bounded, piecewise continuous control signal. We assume that $x_p(t)$ is measurable.

In order to perform online parameter identification of the system matrices

$$\Theta_p \coloneqq \begin{bmatrix} A_p & B_p \end{bmatrix} \tag{3.2}$$

we will assume that a compact, convex, uncertainty polytope is known for the system. This polytope is such that it includes all uncertainty of the system, as well as any trajectory for time-varying parameters. For every extreme point of the polytope, also referred to as corner, there is a fixed model

$$\dot{x}_i(t) = A_i x_i(t) + B_i u(t), \tag{3.3}$$

with system matrices $\begin{bmatrix} A_i & B_i \end{bmatrix} =: \Theta_i$, $i \in \{1, \cdots, N\}$. We define the set

$$\mathcal{S} \coloneqq \left\{ \begin{bmatrix} A_1 & B_1 \end{bmatrix}, \cdots, \begin{bmatrix} A_N & B_N \end{bmatrix} \right\} \tag{3.4}$$

consisting of every corner model.

Assumption 3.1. *There exist a finite set $\mathcal{S}$ of known system matrices $\begin{bmatrix} A_i & B_i \end{bmatrix} \in \mathbb{R}^{n\times(n+m)}$, such that $\begin{bmatrix} A_p & B_p \end{bmatrix} \in \operatorname{int}(\operatorname{conv}(\mathcal{S}))$.* △

Assumption 3.1 can be achieved by a system identification process for many systems of interest, such as mechanical and electrical applications. Every point of the polytope $\operatorname{conv}(\mathcal{S})$ can be expressed as a convex combination of the corner models $\begin{bmatrix} A_i & B_i \end{bmatrix}$, which implies that the following set is non-empty:

$$\mathcal{W} \coloneqq \left\{ w \in [0,1]^N : \begin{bmatrix} A_p & B_p \end{bmatrix} = \sum_{i=1}^{N} w_i \begin{bmatrix} A_i & B_i \end{bmatrix}, \sum_{i=1}^{N} w_i = 1 \right\}. \tag{3.5}$$

Consequently, the problem of identifying the unknown system matrix $\begin{bmatrix} A_p & B_p \end{bmatrix}$ is equivalent to the problem of identifying a vector $w \in \mathcal{W}$. Allowing fewer inputs than states and an arbitrary number of corner models makes this approach an interesting option when there are fewer actuators than sensors.

Remark 3.1. *Systems with structured uncertainties of the form $(A_p(\eta), B_p(\eta))$, where $A_p(\eta) \in \mathbb{R}^{n\times n}$ and $B_p(\eta) \in \mathbb{R}^{n\times m}$ are unknown constant matrices dependent on the uncertain parameter vector $\eta \in S \subset \mathbb{R}^q$, belonging to a compact set, simplify the identification process and fewer corner models are required to define the set $\mathcal{W}$. Moreover, if some entries of matrices A_p and B_p are known, we can isolate them on the left-hand side of the equation and all uncertain parameters, which need to be estimated, on the right-hand side of the equation.* △

In the following steps, we generate estimates $\begin{bmatrix}\hat{A}_p(t) & \hat{B}_p(t)\end{bmatrix}$ of $\begin{bmatrix}A_p & B_p\end{bmatrix}$ as a weighted sum of the corner models, and provide the stability and convergence analysis.

Step 1: Defining the Parametric Model using Multiple Models

Filtering both sides of (3.1) by the linear filter $\dfrac{1}{s+\lambda}$, where $\lambda > 0$ is a design parameter, we obtain the parametric model

$$z(t) \overset{\lambda}{=} \Theta_p \begin{bmatrix}\phi_1(t)\\ \phi_2(t)\end{bmatrix} =: \Theta_p \Phi(t), \tag{3.6}$$

where $\phi_1(t), z(t) \in \mathbb{R}^n$, $\phi_2(t) \in \mathbb{R}^m$ are generated by the filters

$$\begin{aligned}\begin{bmatrix}\dot{\phi}_1(t)\\ \dot{\phi}_2(t)\end{bmatrix} &= -\lambda \begin{bmatrix}\phi_1(t)\\ \phi_2(t)\end{bmatrix} + \begin{bmatrix}x_p(t)\\ u(t)\end{bmatrix}, \quad \begin{bmatrix}\phi_1(0)\\ \phi_2(0)\end{bmatrix} = \begin{bmatrix}0\\ 0\end{bmatrix},\\ z(t) &= \dot{\phi}_1(t) = -\lambda\phi_1(t) + x_p(t).\end{aligned} \tag{3.7}$$

The relation (3.6) can be verified by taking time derivatives of both sides and taking the difference, i.e., (3.7) implies for $e_z(t) = z(t) - \Theta_p\Phi(t)$ that

$$\begin{aligned}\dot{e}_z(t) &= \dot{z}(t) - \Theta_p\dot{\Phi}(t)\\ &= -\lambda\dot{\phi}_1(t) + \dot{x}_p - \Theta_p \begin{bmatrix}\dot{\phi}_1(t)\\ \dot{\phi}_2(t)\end{bmatrix}\\ &= -\lambda\dot{\phi}_1(t) + \Theta_p \begin{bmatrix}x_p(t)\\ u(t)\end{bmatrix} - \Theta_p \left(-\lambda \begin{bmatrix}\phi_1(t)\\ \phi_2(t)\end{bmatrix} + \begin{bmatrix}x_p(t)\\ u(t)\end{bmatrix}\right)\\ &= -\lambda\left(-\lambda\phi_1(t) + x_p(t)\right) + \lambda\Theta_p\Phi(t)\\ &= -\lambda\left(-\lambda\phi_1(t) + x_p(t) - \Theta_p\Phi(t)\right)\\ &= -\lambda e_z(t),\end{aligned} \tag{3.8}$$

which shows that $e_z(t)$ is an exponentially decaying signal.

Step 2: Defining the Estimation Error

To introduce multiple models into the identification scheme, we define for each of the fixed models

$$z_i(t) \coloneqq \Theta_i \begin{bmatrix} \phi_1(t) \\ \phi_2(t) \end{bmatrix} = \Theta_i \Phi(t), \ \forall i \in \{1, \cdots, N\}, \tag{3.9}$$

such that for any $w = \begin{bmatrix} w_1 & \cdots & w_N \end{bmatrix}^\top \in \mathcal{W}$, we obtain

$$z(t) = \sum_{i=1}^{N} w_i z_i(t) + e_z(t). \tag{3.10}$$

Then, the filtered state estimation error for each of the N fixed models is defined as

$$\varepsilon_i(t) \coloneqq \frac{z(t) - z_i(t)}{m_s^2(t)}, \forall i \in \{1, \cdots, N\}, \tag{3.11}$$

where $m_s^2(t) \coloneqq 1 + \alpha \|\Phi(t)\|^2$, $\alpha > 0$, is a normalization signal that guarantees that $\dfrac{\Phi(t)}{m_s(t)}$ is bounded. By Assumption 3.1 and (3.6) to (3.9), for any $w \in \mathcal{W}$, and using that $\sum_{i=1}^{N} w_i = 1$, (3.10) implies

$$\begin{aligned} e_z(t) &= \sum_{i=1}^{N} w_i z(t) - \sum_{i=1}^{N} w_i z_i(t) \\ &= \sum_{i=1}^{N} w_i \left(z(t) - z_i(t) \right) \\ &= \sum_{i=1}^{N} w_i \varepsilon_i(t) m_s^2(t). \end{aligned} \tag{3.12}$$

Adding $-\varepsilon_N(t) m_s^2(t)$ to both sides of (3.12), we obtain

$$e_z(t) - \varepsilon_N(t) m_s^2(t) = \sum_{i=1}^{N-1} w_i \left(\varepsilon_i(t) - \varepsilon_N(t) \right) m_s^2(t),$$

which implies, for any $w \in \mathcal{W}$, that

$$e_z(t) - \varepsilon_N(t) = \sum_{i=1}^{N-1} w_i \left(\varepsilon_i(t) - \varepsilon_N(t) \right). \tag{3.13}$$

Defining the $n \times (N-1)$ time-varying matrix

$$E(t) \coloneqq \begin{bmatrix} \varepsilon_1(t) - \varepsilon_N(t) & \cdots & \varepsilon_{N-1}(t) - \varepsilon_N(t) \end{bmatrix}, \tag{3.14}$$

we can rewrite (3.13) in matrix form as

$$E(t)\bar{w} = e_z(t) - \varepsilon_N(t), \tag{3.15}$$

where $\bar{w} \in \begin{bmatrix} w_1 & \cdots & w_{N-1} \end{bmatrix}^\top$.

Equation (3.15) motivates the use of the following recursive adaptive law [27] to generate estimate $\hat{w} = \begin{bmatrix} \hat{\bar{w}}^\top(t) & \hat{w}_N(t) \end{bmatrix}^\top \in \mathbb{R}^N$, such that $\lim_{t\to\infty} \sum_{i=1}^N \hat{w}_i(t) \begin{bmatrix} A_i & B_i \end{bmatrix} = \begin{bmatrix} A_p & B_p \end{bmatrix}$.

$$\begin{aligned} \dot{\hat{\bar{w}}}(t) &= -\Gamma E^\top(t) E(t) \hat{\bar{w}}(t) - \Gamma E^\top(t) \varepsilon_N(t), \\ \hat{w}_N(t) &= 1 - \sum_{i=1}^{N-1} \hat{w}_i(t), \end{aligned} \tag{3.16}$$

where the tuning parameter $\Gamma \in \mathbb{R}^{(N-1)\times(N-1)}$ is a symmetric positive definite matrix. Let w be some element in $\mathcal{W}$, and based on (3.16), the estimation error $\tilde{\bar{w}}(t) \coloneqq \hat{\bar{w}}(t) - \bar{w}$ satisfies

$$\begin{aligned} \dot{\tilde{\bar{w}}}(t) &= \dot{\hat{\bar{w}}}(t) - \dot{\bar{w}} = \dot{\hat{\bar{w}}}(t) \\ &= -\Gamma E^\top(t) E(t) \hat{\bar{w}}(t) - \Gamma E^\top(t) \varepsilon_N(t). \end{aligned} \tag{3.17}$$

Pre-multiplying (3.15) by $\Gamma E^\top(t)$ and moving all the terms to the left hand side, we obtain

$$\Gamma E^\top(t) E(t) \bar{w} + \Gamma E^\top(t) \varepsilon_N(t) - \Gamma E^\top(t) e_z(t) = 0. \tag{3.18}$$

Adding (3.18) to (3.17), we further obtain

$$\dot{\tilde{\bar{w}}}(t) = -\Gamma E^\top(t) E(t) \tilde{\bar{w}}(t) - \Gamma E^\top(t) e_z(t). \tag{3.19}$$

Step 3: Stability and Convergence Analysis

The main stability and convergence properties are established in the following theorems and corollaries. We use Barbalat's lemma from Section 2.4.3.

Theorem 3.2. *Consider the system (3.1) with the definitions (3.11) and (3.14). Let Assumption 3.1 hold, $w = \begin{bmatrix} \bar{w}^\top & w_N \end{bmatrix}^\top \in \mathcal{W}$ be an arbitrary vector within the set defined in (3.5), and $\tilde{\bar{w}}(t) \coloneqq \hat{\bar{w}}(t) - \bar{w}$. For any initial condition $\hat{\bar{w}}(0) \in \mathbb{R}^{N-1}$, the estimation scheme (3.16) guarantees that:*

(i) $\hat{\tilde{w}}$, $\tilde{\tilde{w}}$, $\dot{\tilde{\tilde{w}}}$ *and* E *are bounded signals.*

(ii) $E\tilde{\tilde{w}}$ *and* $\dot{\tilde{\tilde{w}}}$ *are square integrable.*

(iii) $\lim_{t\to\infty} E(t)\tilde{\tilde{w}}(t) = 0$.

(iv) $\hat{\tilde{w}}(t)$ *asymptotically converges to a constant vector* $\bar{\tilde{w}} \in \mathbb{R}^{N-1}$.

Proof. Consider the Lyapunov-like function

$$V_1(\tilde{\tilde{w}}(t), e_z(t)) = \frac{1}{2}\tilde{\tilde{w}}^\top(t)\Gamma^{-1}\tilde{\tilde{w}}(t) + \frac{1}{2\lambda}e_z^\top(t)e_z(t), \tag{3.20}$$

where $\Gamma \in \mathbb{R}^{(N-1)\times(N-1)}$ is a positive definite matrix that modifies the convergence speed of parameters, and $\lambda > 0$ is a design parameter for the filter in (3.6). Taking the time derivative of (3.20) along (3.19), we have

$$\begin{aligned}
\frac{\mathrm{d}V_1(t)}{\mathrm{d}t} &= \tilde{\tilde{w}}^\top(t)\Gamma^{-1}\dot{\tilde{\tilde{w}}}(t) + \frac{1}{\lambda}e_z^\top(t)\dot{e}_z(t) \\
&= -\tilde{\tilde{w}}^\top(t)\Gamma^{-1}\Gamma E^\top(t)E(t)\tilde{\tilde{w}}(t) \\
&\quad - \tilde{\tilde{w}}^\top(t)\Gamma^{-1}\Gamma E^\top(t)e_z(t) + \frac{1}{\lambda}e_z^\top\dot{e}_z \\
&= -\tilde{\tilde{w}}^\top(t)E^\top(t)E(t)\tilde{\tilde{w}}(t) - \tilde{\tilde{w}}^\top(t)E^\top(t)e_z(t) + \frac{1}{\lambda}e_z^\top\dot{e}_z \\
&= -\frac{1}{2}\|E(t)\tilde{\tilde{w}}(t)\|^2 + \frac{1}{2}\|e_z(t)\|^2 - \frac{1}{2}\|E(t)\tilde{\tilde{w}}(t) + e_z(t)\|^2.
\end{aligned} \tag{3.21}$$

Since $e_z(t)$ is an exponentially decaying signal, Equation (3.21) implies that $\dot{V}_1$ is bounded and there exists a time instant $t_1 > 0$ such that, for all $t \geq t_1$, $\dot{V}_1(t) \leq 0$. Hence. V_1, $\tilde{\tilde{w}}$, and $\hat{\tilde{w}}$ are bounded. Because of normalization (3.11), ε_i terms are bounded and hence E is bounded, which together with (3.19) also implies that $\dot{\tilde{\tilde{w}}}$ is bounded, finishing the proof of (i).

Since $V_1(t)$ is always positive, bounded, and decaying, the integral of (3.21) for $t = 0$ to ∞ is finite, and hence $E\tilde{\tilde{w}}$ and $E\tilde{\tilde{w}} + e_z(t)$ are square integrable. Since E is bounded, this, together with (3.19), further implies that $\dot{\tilde{\tilde{w}}}$ is square integrable, completing the proof of (ii).

Items (i) and (ii) together with Barbalat's Lemma imply (iii). Items (i) and (ii) further imply that $\lim_{t\to\infty}\tilde{\tilde{w}}(t)$ and, hence, $\lim_{t\to\infty}\hat{\tilde{w}}(t)$ exist and are finite, proving (iv). □

Theorem 3.2 implies that $\|E(t)\tilde{\bar{w}}(t)\|$ asymptotically converges to zero, but this does not mean that $\tilde{\bar{w}}(t)$ converges to the set $\mathcal{W}$. We can now state and prove the main result of the identification process.

Theorem 3.3. *Consider the system (3.1) with definitions (3.11), and (3.14), and the estimation scheme (3.16). Let Assumption 3.1 hold, $w = \begin{bmatrix}\bar{w}^\top & w_N\end{bmatrix}^\top \in \mathcal{W}$ be an arbitrary vector within the set defined in (3.5), $\tilde{\bar{w}}(t) \coloneqq \hat{\bar{w}}(t) - \bar{w}$, and Φ be bounded and satisfy the persistence of excitation condition (2.4). Then, for any initial condition $\hat{\bar{w}}(0) \in \mathbb{R}^{N-1}$, the estimated system matrix $\sum_{i=1}^{N} \hat{w}_i(t)\Theta_i$ asymptotically converges to Θ_p.*

Proof. Let $Q(t) \coloneqq \sum_{i=1}^{N-1}(\tilde{w}_i(t)(\Theta_N - \Theta_i)) \in \mathbb{R}^{n\times(n+m)}$. It is easily verifiable that if $Q(t) = 0$, then $\sum_{i=1}^{N} \hat{w}_i(t)\Theta_i = \Theta_p$, and $\hat{w}(t) \in \mathcal{W}$. Theorem 1 (iv) implies that $Q(t)$ asymptotically converges to a constant matrix $\bar{Q} \in \mathbb{R}^{n\times(n+m)}$. Hence, to establish that $\sum_{i=1}^{N} \hat{w}_i(t)\Theta_i$ asymptotically converges to Θ_p, we will show that $\bar{Q} = 0$.

Expressing Theorem 1 (iii) in summation form, we get

$$\begin{aligned}\lim_{t\to\infty} E(t)\tilde{\bar{w}}(t) &= \lim_{t\to\infty} Q(t)\frac{\Phi(t)}{1+\alpha\|\Phi(t)\|^2} \\ &= \lim_{t\to\infty} \bar{Q}\frac{\Phi(t)}{1+\alpha\|\Phi(t)\|^2} = 0. \end{aligned} \tag{3.22}$$

Since Φ is assumed to be bounded, (3.22) implies that

$$\lim_{t\to\infty} \bar{Q}\Phi(t) = 0.$$

and hence

$$\lim_{t\to\infty} \bar{Q}\Phi(t)\Phi^\top(t)\bar{Q}^\top = 0. \tag{3.23}$$

Since Φ satisfies the persistence of excitation condition (2.4), Equation (3.23) implies that $\bar{Q} = 0$, completing the proof. □

The recursive adaptive law (3.16) guarantees that $\sum_{i=1}^{N} \hat{w}_i(t) = 1$, but not that $\hat{w}(t) \in [0,1]^N$. Since the set $[0,1]^N$ is convex, the projection of $\hat{w}(t)$ into $[0,1]^N$ is well-defined.

Define the compact set

$$\Pi \coloneqq \left\{ \hat{\bar{w}} \in [0,1]^{N-1} : \sum_{i=1}^{N-1} \hat{\bar{w}}_i \leq 1 \right\}, \tag{3.24}$$

and let $\mathrm{Pr}_{\Pi,\hat{\hat{w}}} : \mathbb{R}^{N-1} \to \Pi \subset \mathbb{R}^{N-1}$ denote the parameter projection operator [27]. Choose $\hat{w}(0) \in \mathrm{int}(\Pi)$, then the recursive adaptive algorithm (3.16) with parameter projection is as follows:

$$\begin{aligned} \dot{\hat{\hat{w}}}(t) &= \mathrm{Pr}_{\Pi,\hat{\hat{w}}}\left(-\Gamma\left(E^{\top}(t)E(t)\hat{\hat{w}}(t) + E^{\top}(t)\varepsilon_N(t)\right)\right), \\ \hat{w}_N(t) &= 1 - \sum_{i=1}^{N-1} \hat{w}_i(t). \end{aligned} \tag{3.25}$$

The parameter projection operator enforces that Π is a positively invariant subset for the dynamics (3.25).

Corollary 3.4. *The gradient adaptive law with parameter projection (3.25) has all the properties established in Theorem 3.2 for the gradient adaptive law (3.16). Furthermore, we get the following properties:*

(i) If $\hat{w}(0) \in \Pi$, then $\hat{w}(t) \in \Pi$, $\forall t \geq 0$.

(ii) If $\hat{w}(0) \in \mathrm{int}(\Pi)$, then $\hat{w}(t)$ asymptotically converges to the set $\mathcal{W}$.

Proof. The proof follows by applying the result found in Section 2.4.5 to (3.16) combined with Theorems 3.2 and 3.3. □

3.1.1 Simulation Example

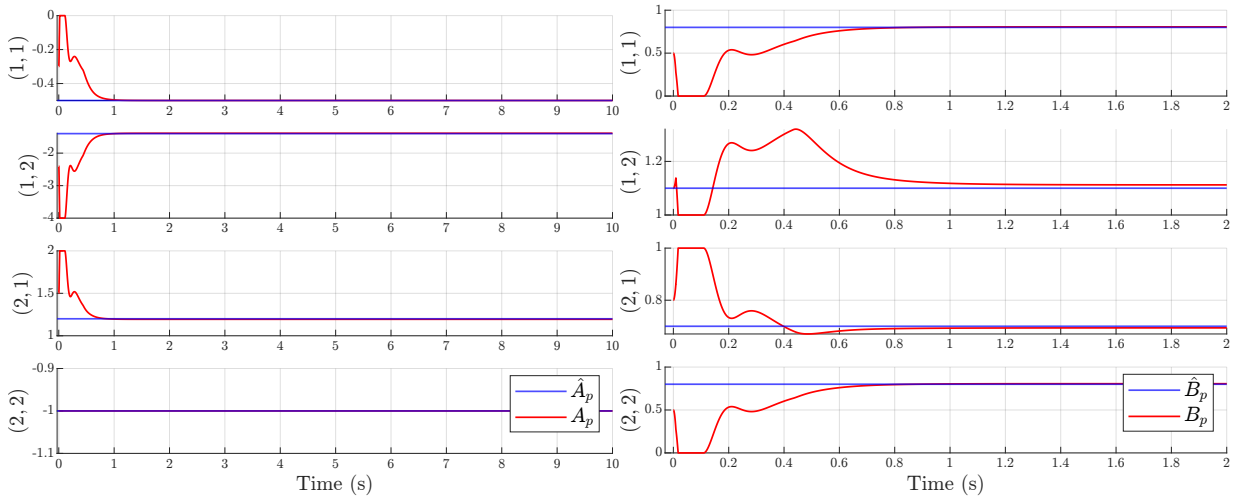
These simulation results are a modification to those found in our article published in [39]: we changed the signs of some corner models to have a Hurwitz A_p, and only considered the open-loop configuration.

We illustrate the stable behavior and performance of the proposed system identification scheme through a set of simulations when all the states are available for feedback of an uncertain model (3.1) with $n = 2$ and unknown system matrices

$$A_p = \begin{bmatrix} -0.5 & -1.4 \\ 1.2 & -1.0 \end{bmatrix}, \qquad B_p = \begin{bmatrix} 0.8 & 1.1 \\ 0.7 & 0.8 \end{bmatrix}.$$

The parameters used in the simulation are

$$A_1 = \begin{bmatrix} -1 & 0 \\ 1 & -1 \end{bmatrix}, \; A_2 = \begin{bmatrix} -1 & 2 \\ 0 & -1 \end{bmatrix}, \; A_3 = \begin{bmatrix} 0 & -4 \\ 2 & -1 \end{bmatrix},$$
$$B_1 = \begin{bmatrix} 1 & 0 \\ 1 & 1 \end{bmatrix}, \; B_2 = \begin{bmatrix} 2 & 2 \\ 0 & 2 \end{bmatrix}, \; B_3 = \begin{bmatrix} 0 & 1 \\ 1 & 0 \end{bmatrix}.$$



(a)Time evolution of the uncertain constant matrix A_p.

(b)Time evolution of the uncertain constant matrix B_p.

Figure 3.1: Time evolution of the uncertain constant matrices A_p and B_p.

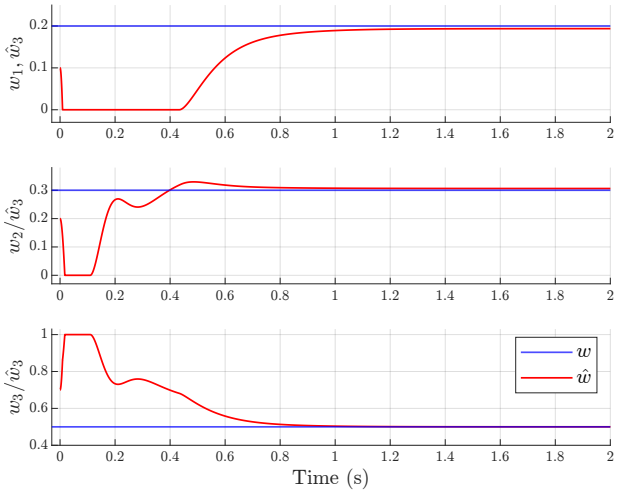


Figure 3.2: Time evolution of the weight vector $\hat{w}$.

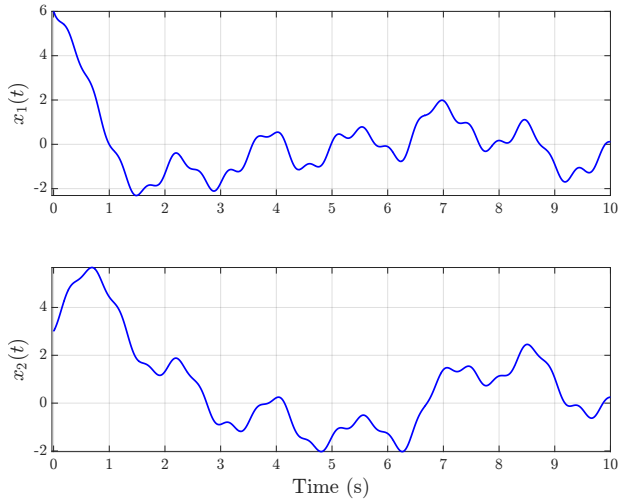


Figure 3.3: Time evolution of the states of the system. Note they are bounded.

The input to the system is taken to be the bounded control signals $u_1(t) = 4\sin(4t) + 2\sin(t) + 0.5\sin(2t)$ and $u_2(t) = 0.4\sin(9t) + \sin(7t) + 3\sin(13t)$, and the design parameter is $\Gamma = 100 I_{2\times 2}$.

We can verify that all assumptions are satisfied for this system:

- The eigenvalues of A_p are $-0.75 \pm j1.2718$, which makes A_p Hurwitz.
- $u(t)$ is known, bounded, and piecewise continuous.
- Taking $w = \begin{bmatrix} 0.2 & 0.3 & 0.5 \end{bmatrix}$ and defining $\mathcal{S} \coloneqq \left\{ \begin{bmatrix} A_1 & B_1 \end{bmatrix}, \begin{bmatrix} A_2 & B_2 \end{bmatrix}, \begin{bmatrix} A_3 & B_3 \end{bmatrix} \right\}$, we get that $\begin{bmatrix} A_p & B_p \end{bmatrix} \in \mathcal{S}$, satisfying Assumption 3.1.
- u is sufficiently rich; hence Φ is Persistently Exciting (PE).

The gradient identification scheme achieves asymptotic convergence of the uncertain plant matrices A_p and B_p, as seen in Figures 3.1(a) and 3.1(b). We can also verify that the weight vector $\hat{w}(t)$ remains bounded and is within the set $[0, 1]^3$ and always adds up to 1, as shown in Figure 3.2. Furthermore, the states of the system remain bounded, as shown in Figure 3.3.

3.2 Output-Feedback MMPI

Consider Single-Input, Single-Output (SISO), LTI plants of the form

$$\begin{aligned} \dot{x}_p(t) &= A_p x_p(t) + b_p u(t),\ x_p(0) = x_{p0},\ t \geq 0, \\ y_p(t) &= c_p^\top x_p(t), \end{aligned} \tag{3.26}$$

where $A_p \in \mathbb{R}^{n\times n}$, $b_p \in \mathbb{R}^n$ are unknown constant matrices with polytopic uncertainty, A_p is Hurwitz, $c_p \in \mathbb{R}^n$ is the output matrix, $y_p(t) \in \mathbb{R}$ is the measurable output of the system, and $u(t) \in \mathbb{R}$ is a known, bounded, piecewise continuous control signal.

Assumption 3.2. *The systems under consideration in* (3.26) *are in canonical observable form, that is, they have the following structure*

$$\begin{aligned} A_p &= \left[\begin{array}{c:c} -a_p & \begin{matrix} \mathbb{I}_{n-1} \\ 0 \end{matrix} \end{array}\right], \\ a_p &= \begin{bmatrix} a_{n-1} & a_{n-2} & \cdots & a_1 & a_0 \end{bmatrix}^\top \in \mathbb{R}^n, \\ b_p &= \begin{bmatrix} b_{n-1} & b_{n-2} & \cdots & b_1 & b_0 \end{bmatrix}^\top, \\ c_p &= \begin{bmatrix} 1 & 0 & \cdots & 0 \end{bmatrix}^\top. \end{aligned} \tag{3.27}$$

Note that the state-space representation of a system is not unique. Then, for any SISO, LTI transfer function $y = G(s)u$ we can *always* select the canonical observable representation and apply the results found in this section, making Assumption 3.2 a reasonable and applicable assumption to a large class of systems. We consider the uncertainty only in b_p and not in c_p since it represents the actuator uncertainty, which is commonly found in experimental settings.

To perform online parameter identification, we redefine the uncertain vector (3.2) as

$$\Theta_p \coloneqq \begin{bmatrix} b_p \\ a_p \end{bmatrix}, \tag{3.28}$$

and the corner fixed models (3.3) as

$$\begin{aligned} \dot{x}_i(t) &= A_i x_i(t) + b_i u(t), \quad x_i(0) = x_{i0}, \\ y_i(t) &= c_p^\top x_i(t), \end{aligned} \tag{3.29}$$

where

$$A_i = \left[\begin{array}{c:c} -a_i & \mathbb{I}_{n-1} \\ \hdashline & 0 \end{array}\right].$$

Combining the parameters of the corner models into a vector $\Theta_i \coloneqq \begin{bmatrix} b_i^\top & a_i^\top \end{bmatrix}^\top$, $i \in \{1, \cdots, N\}$, we can then fully define the set $\mathcal{S}$ from (3.4) and transform the problem of identifying the uncertain vector (3.28) to the equivalent problem of identifying an uncertain vector $w \in \mathcal{W}$, defined in (3.5).

Step 1: Defining the Parametric Model using Multiple Models

We begin by using the information contained in the signals u and y_p to obtain a multiple-model system identification scheme that guarantees perfect convergence of the estimate $\hat{\Theta}_p(t)$ to Θ_p.

Consider the transfer function corresponding to (3.26):

$$\frac{Y_p(s)}{U(s)} = \frac{b_{n-1}s^{n-1} + \cdots + b_1 s + b_0}{s^n + a_{n-1}s^{n-1} + \cdots + a_1 s + a_0}. \tag{3.30}$$

For any $w \in \mathcal{W}$, the transfer function (3.30) can be represented as

$$\frac{Y_p(s)}{U(s)} = \frac{\sum_{i=1}^N w_i b_{n-1(i)} s^{n-1} + \cdots + \sum_{i=1}^N w_i b_{0(i)}}{s^n + \sum_{i=1}^N w_i a_{n-1(i)} s^{n-1} + \cdots + \sum_{i=1}^N w_i a_{0(i)}},$$

where $a_{j(i)}(b_{j(i)})$ means the value of $a_j(b_j)$ corresponding to the corner i of the uncertainty polytope $\mathcal{W}$. The equation above can be written in polynomial form as

$$\left(s^n + \sum_{i=1}^N w_i a_{n-1(i)} s^{n-1} + \cdots + \sum_{i=1}^N w_i a_{0(i)}\right) Y_p(s) = \left(\sum_{i=1}^N w_i b_{n-1(i)} s^{n-1} + \cdots + \sum_{i=1}^N w_i b_{0(i)}\right) U(s).$$

Returning to the time domain and isolating the n-th derivative of y_p

$$y_p^{(n)} = \sum_{i=1}^N w_i b_{n-1(i)} u^{(n-1)} + \cdots + \sum_{i=1}^N w_i b_{0(i)} u - \sum_{i=1}^N w_i a_{n-1(i)} y_p^{(n-1)} - \cdots - \sum_{i=1}^N w_i a_{0(i)} y_p. \tag{3.31}$$

If some parameters are known, then the statement in Remark 3.1 can be applied and not all entries need to be identified, they can be grouped in the left hand side of (3.31).

Filtering both sides of (3.31) by $\frac{1}{\Lambda(s)}$, where $\Lambda(s)$ is a Hurwitz polynomial

$$\Lambda(s) \coloneqq s^n + \lambda_{n-1}s^{n-1} + \cdots + \lambda_1 s + \lambda_0,$$

where $\lambda_i \in \mathbb{R}$, $i = \{0, \cdots, n-1\}$, are design parameters. Rewriting the filtered version of (3.31) in matrix form, we get

$$z \overset{\lambda}{\coloneqq} \frac{s^n}{\Lambda(s)} y_p = w^\top M \phi \in \mathbb{R},$$

where

$$M = \begin{bmatrix} b_{n-1(1)} & \cdots & b_{0(1)} & a_{n-1(1)} & \cdots & a_{0(1)} \\ b_{n-1(2)} & \cdots & b_{0(2)} & a_{n-1(2)} & \cdots & a_{0(2)} \\ \vdots & \ddots & \vdots & \vdots & \ddots & \vdots \\ b_{n-1(N)} & \cdots & b_{0(N)} & a_{n-1(N)} & \cdots & a_{0(N)} \end{bmatrix} \in \mathbb{R}^{N \times 2n},$$

$$\phi = \begin{bmatrix} \frac{s^{n-1}}{\Lambda(s)} u & \cdots & \frac{1}{\Lambda(s)} u & -\frac{s^{n-1}}{\Lambda(s)} y_p & \cdots & -\frac{1}{\Lambda(s)} y_p \end{bmatrix}^\top \in \mathbb{R}^{2n}.$$

Note that for any $w \in \mathcal{W}$, we have that $M^\top w = \Theta_p$.

Step 2: Defining the Estimation Error

Define $\phi_p \coloneqq M\phi$, and let $\hat{w}$ denote an estimate of w. We can define the estimation model as

$$\hat{z} = \hat{w}^\top \phi_p \in \mathbb{R},$$

and the corresponding filtered output estimation error

$$\varepsilon = \frac{z - \hat{z}}{m_s^2} = \frac{z - \hat{w}^\top \phi_p}{m_s^2} \in \mathbb{R},$$

where $m_s^2 = 1 + \alpha \|\phi\|^2$, $\alpha > 0$ is a normalization signal designed to bound ϕ from above. With these definitions we can apply a gradient algorithm by defining the cost function $J(\hat{w})$ as

$$J(\hat{w}) = \frac{\varepsilon^2 m_s^2}{2} = \frac{(z - \hat{w}^\top \phi_p)^2}{2m_s^2} \in \mathbb{R},$$

and obtaining the solution to the following problem:

$$\begin{aligned} &\min\ J(\hat{w}) \\ &\hat{w} \in \mathbb{R}^N. \end{aligned} \tag{3.32}$$

Then, the gradient algorithm takes the form

$$\dot{\hat{w}} = -\Gamma \nabla J(\hat{w}) = \Gamma \varepsilon \phi_p \in \mathbb{R}^N, \tag{3.33}$$

where $\Gamma \in \mathbb{R}^{N\times N}$ is a symmetric, positive definite, design matrix known as adaptation gain. For any $w \in \mathcal{W}$ the estimation error is $\tilde{w}(t) \coloneqq \hat{w}(t) - w$, which gives the following dynamics for the estimation error

$$\dot{\tilde{w}} = \dot{\hat{w}} = \Gamma \varepsilon \phi_p. \tag{3.34}$$

Step 3: Stability and Convergence Analysis

The main stability and convergence properties are established in the following theorems and corollaries.

Theorem 3.5. *Consider the system (3.26) with Assumptions 3.1 and 3.2. Let $w \in \mathcal{W}$ be an arbitrary vector, then for any initial condition $\hat{w}_0 \in \mathbb{R}^N$, the estimation scheme (3.33) guarantees that:*

(i) The signals $\hat{w}$, $\tilde{w}$, $\dot{\tilde{w}}$, $M^\top \tilde{w}$, $M^\top \dot{\tilde{w}}$, ε are bounded.

(ii) $\lim_{t\to\infty} \dfrac{\phi^\top(t) M^\top \tilde{w}(t)}{1 + \|\phi(t)\|^2} = 0.$

(iii) If $M^\top \tilde{w}(t) = 0$, then $M^\top \hat{w}(t) = \Theta_p$.

(iv) If ϕ is PE, then $\lim_{t\to\infty} M^\top \tilde{w}(t) = 0$.

Proof. Let $w \in \mathcal{W}$, and $\hat{w}_0 \in \mathbb{R}^N$ be constant vectors and $\Gamma \in \mathbb{R}^{N\times N}$ be a symmetric, positive definite, constant matrix. Recall that u is bounded and A_p is Hurwitz, hence y_p is bounded and furthermore, ϕ, ϕ_p, m_s and m_s^2 are bounded.

Considering the estimation error dynamics (3.34)

$$\begin{aligned}\dot{\tilde{w}} &= \Gamma\varepsilon\phi_p \\ &= -\Gamma\frac{\phi_p\phi_p^\top}{m_s^2}\tilde{w} \\ &= -\Gamma\frac{M\phi\phi^\top M^\top}{m_s^2}\tilde{w} \in \mathbb{R}^N.\end{aligned}$$

Consider the Lyapunov-like function

$$V_p(\tilde{w}) = \frac{1}{2}\tilde{w}^\top\Gamma^{-1}\tilde{w} \in \mathbb{R}.$$

Taking the derivative along the solution of $\tilde{w}$ yields

$$\begin{aligned}\dot{V}_p &= \tilde{w}^\top\Gamma^{-1}\left(-\Gamma\frac{\phi_p\phi_p^\top}{m_s^2}\tilde{w}\right) \\ &= -\tilde{w}^\top\frac{\phi_p\phi_p^\top}{m_s^2}\tilde{w} = -\tilde{w}^\top\frac{M\phi\phi^\top M^\top}{m_s^2}\tilde{w} \\ &= -\varepsilon^2 m_s^2 \leq 0.\end{aligned}$$

Therefore, since V_p is a non-negative function, it follows that

$$\lim_{t\to\infty} V_p(\tilde{w}(t)) = V_{p\infty} < \infty,$$

and V_p, $\tilde{w}$ and $\hat{w}$ are bounded. Finally, $M^\top\tilde{w}$, $\dot{\tilde{w}}$, ε and εm_s are the product of bounded signals, hence they are bounded, finishing the proof of (i).

To prove (ii) we will apply Barbalat's Lemma to the signal $f(t) = \phi(t)M^\top\tilde{w}(t)$. It follows from (i) that $f(t)$ and $\dot{f}(t) = \phi(t)M^\top\dot{\tilde{w}}(t) + \dot{\phi}(t)M^\top\tilde{w}(t)$ are bounded because they are the product and sum of bounded signals. Considering that $V_p(t)$ is positive semi-definite, bounded, and $\dot{V}_p(t)$ is negative semi-definite, then

$$\begin{aligned}\int_0^\infty \dot{V}_p(\tilde{w}(\tau))\mathrm{d}\tau &= -\int_0^\infty \left\|\frac{\phi^\top(\tau)M^\top\tilde{w}(\tau)}{m_s(\tau)}\right\|^2 \mathrm{d}\tau \\ &= \lim_{t\to\infty} V_p(\tilde{w}(t)) - V_p(\tilde{w}(0)) < \infty,\end{aligned}$$

proving that $f(t)$ is square integrable. Combining all of these facts with Barbalat's Lemma we get that $\lim_{t\to\infty}\phi(t)M^\top\tilde{w}(t) = 0$, completing the proof of (ii).

For (iii), let $t^* \geq 0$ be a time such that $M^\top \tilde{w}(t^*) = 0$. Then

$$\begin{aligned} & M^\top \left(\hat{w}(t^*) - w^* \right) = 0 \\ \Rightarrow \quad & M^\top \hat{w}(t^*) = M^\top w^* = \Theta_p. \end{aligned}$$

Finally, for (iv), recall that ϕ is bounded which implies, by (ii), that

$$\lim_{t \to \infty} \frac{\phi^\top(t) M^\top \tilde{w}(t)}{m_s^2(t)} = \lim_{t \to \infty} \frac{\phi^\top(t)}{1 + \alpha \|\phi(t)\|^2} M^\top \tilde{w}(t) = 0.$$

But since ϕ is persistently exciting, $\lim_{t\to\infty} \phi(t) \neq 0$, and we conclude that $\lim_{t\to\infty} M^\top \tilde{w}(t) = 0$, completing the proof. □

Remark 3.6. *Theorem 3.5 assumes that $w \in \mathcal{W}$ but this assumption can be relaxed to w being a linear combination of elements in $\mathcal{S}$. This relaxation allows for the identification of uncertain systems whose model parameters lie outside the polytope of uncertainty. This result differs from the one presented in Section 3.1 by allowing for bounded linear combinations of the corner models, instead of all $\hat{w}_i(t)$ having to sum to one.* △

Under the conditions of Theorem 3.5, the adaptive algorithm in (3.33) guarantees that

$$\lim_{t \to \infty} \sum_{i=1}^{N} \hat{w}_i(t) \Theta_i = \Theta_p$$

without imposing any restrictions on the values of $\hat{w}_i$. From Assumption 3.1 we have some *a priori* knowledge of Θ_p that we can use to constrain the online estimation to a compact set, rather than minimizing over $\mathbb{R}^N$, i.e., we want to transform the minimization problem (3.32) to

$$\begin{aligned} \min \ & J(\hat{w}) \\ & \hat{w} \in S, \end{aligned} \tag{3.35}$$

where

$$S = \left\{ \hat{w} \in \mathbb{R}^N : \hat{w} \in [0,1]^N, \ \sum_{i=1}^{N} \hat{w}_i = 1 \right\}.$$

With this definition of $S \subset \mathbb{R}^N$ we see that the gradient algorithm becomes

$$\dot{\hat{w}} = \mathrm{Pr}\left(\Gamma \varepsilon \phi_p\right) = \begin{cases} \Gamma \varepsilon \phi_p, & \text{if } \hat{w} \in S^0 \text{ or } \hat{w} \in \delta(S) \\ & \text{and } (\Gamma \varepsilon \phi_p)^\top \nabla g \leq 0, \\ \Gamma \varepsilon \phi_p - & \Gamma \dfrac{\nabla g \nabla g^\top}{\nabla g^\top \Gamma \nabla g} \Gamma \varepsilon \phi_p, \ \text{otherwise}, \end{cases} \tag{3.36}$$

where $\delta(S) = \{\theta \in \mathbb{R}^n : g(\theta) = 0\}$, $S^0 = \{\theta \in \mathbb{R}^n : g(\theta) < 0\}$ denote the boundary and interior of S, respectively, and $\hat{w}(0) \in S$.

Theorem 3.7 (See Section 2.4.5)**.** *The gradient adaptive law with projection modification retains all the properties established in the absence of projection. In addition, guarantees that $\hat{w}(t) \in S, \forall t \geq 0$, provided that $\hat{w}(0) \in S$, and $w \in S$.*

3.3 State Estimation of Output-Feedback Systems using Multiple Models

In this section, we use the results from Section 3.2 to develop a MMSE. Consider a LTI, SISO system

$$\begin{aligned} \dot{x}_p(t) &= A_p x_p(t) + b_p u(t),\ x_p(0) = x_{p0},\ t \geq 0, \\ y_p(t) &= c_p^\top x_p(t), \end{aligned} \tag{3.37}$$

where $A_p \in \mathbb{R}^{n\times n}$, $b_p \in \mathbb{R}^n$ are unknown constant matrices, A_p is Hurwitz, $c_p \in \mathbb{R}^n$ is known, $x_p(t) \in \mathbb{R}^n$ is the state of the system, $y_p(t) \in \mathbb{R}$ is the measurable output of the system, $u(t) \in \mathbb{R}$ is a known, bounded, piecewise continuous control input.

The objective is to design a multiple-model state estimator using the parameter identification scheme from Section 3.2. The observer needs to guarantee boundedness of all signals and drive the estimated states to the real states of the system. To achieve this target, we make the following assumption.

Assumption 3.3. *The matrix pair $(A_p, c_p^\top)$ is observable. Moreover, the system (3.37) is in observable canonical form as in Assumption 3.2.* △

Our approach to solving the problem described above involves online parameter identification of the uncertain vector

$$\Theta_p \coloneqq \begin{bmatrix} b_p \\ a_p \end{bmatrix} \tag{3.38}$$

using multiple models as we explain in Section 3.2. For the set $\mathcal{S}$ we impose the following assumption.

Assumption 3.4. *There exist a finite set $\mathcal{S}$ of known system matrices, such that*

(i) $\Theta_p \in \operatorname{int}(\operatorname{conv}(\mathcal{S}))$.

(ii) For each $i \in \{1, \cdots, N\}$, the pair $(A_i, c_p^\top)$ is observable.

$\triangle$

Item (i) of Assumption 3.4 is a natural consequence of performing system identification. We require Item (ii) to ensure that we can recreate the states at every time. The fixed models correspond to each of the corners of the uncertainty bounding set explained in [6]. Every point of the polytope $\text{conv}\,(\mathcal{S})$ can be expressed as a convex combination of the corner models Θ_i. Consequently, we solve the problem of identifying a vector $w \in \mathcal{W}$ as defined in (3.5).

As motivation for developing a multiple-model state estimator, we start by considering the case in which there is no uncertainty [43]. Given a set of n desired eigenvalues with conjugate symmetry, let A_o^* be the matrix

$$A_o^* = \left[\begin{array}{c:c} -a_o^* & \mathbb{I}_{n-1} \\ \hdashline & 0 \end{array}\right]$$

with the desired eigenvalues. y Assumption 3.2, for each $i \in \{1, 2, \cdots, N\}$, the gain vector $K_{oi} = a_o^* - a_i$ is such that

$$\sigma(A_i - K_{oi} c_p^\top) = \sigma(A_o^*).$$

Using these gains, we assign an observer to each corner model of the form

$$\dot{\hat{x}}_i(t) = A_i \hat{x}_p(t) + b_i u(t) + K_{oi}(c_p^\top \hat{x}_p(t) - y_p(t))$$

where, with $w \in \mathcal{W}$, the signal $\hat{x}_p$ is a blending of the state vectors from each corner model observer

$$\hat{x}_p(t) = \sum_{i=1}^{N} w_i \hat{x}_i(t). \tag{3.39}$$

To show that this (uncertainty free) state estimate asymptotically converges to the plant's

state, let $e_o \coloneqq x_p - \hat{x}_p$ and observe that

$$\begin{aligned}
\dot{e}_o(t) &= A_p x_p(t) + b_p u(t) - \sum_{i=1}^{N} w_i \dot{\hat{x}}_i(t) \\
&= A_p x_p(t) + b_p u(t) - \sum_{i=1}^{N} w_i \left(A_i \hat{x}_p(t) + b_i u(t) + K_{oi}(c_p^\top \hat{x}_p(t) - y_p(t)) \right) \\
&= A_p e_o(t) - \sum_{i=1}^{N} w_i K_{oi}(c_p^\top \hat{x}_p(t) - y_p(t)) \\
&= A_p e_o(t) - (a_o^* - a_p) c_p^\top (\hat{x}_p(t) - x_p(t)) \\
&= A_o^* e_o(t).
\end{aligned}$$

Consequently, if all the desired eigenvalues have negative real part, then this observer produces a state estimate $\hat{x}_p$ that exponentially converges to x_p [27]. Nevertheless, since $w \in \mathcal{W}$ is unknown, this observer is not implementable and so we instead replace w with its estimate $\hat{w}$ to obtain an implementable multiple model observer:

$$\begin{aligned}
\dot{\hat{x}}_i(t) &= A_i \hat{x}_p(t) + b_i u(t) + K_{oi}(c_p^\top \hat{x}_p(t) - y_p(t)), \\
\hat{x}_p(t) &= \sum_{i=1}^{N} \hat{w}_i(t) \hat{x}_i(t), \\
K_{oi} &= a_o^* - a_i.
\end{aligned} \tag{3.40}$$

Remark 3.8. *The multiple model observer (3.40) can also be written in the form*

$$\begin{aligned}
\dot{\hat{x}}_p(t) &= \hat{A}_p(t) \hat{x}_p(t) + \hat{b}_p(t) u(t) + \hat{K}_o(t)(c_p^\top \hat{x}_p(t) - y_p(t)), \\
\hat{A}_p(t) &= \sum_{i=1}^{N} \hat{w}_i(t) A_i, \\
\hat{b}_p(t) &= \sum_{i=1}^{N} \hat{w}_i(t) b_i, \\
\hat{K}_o(t) &= a_o^* - \sum_{i=1}^{N} \hat{w}_i(t) a_i
\end{aligned}$$

which may be preferable from an implementation point of view because it requires fewer state variables. △

Theorem 3.9. *Consider the system (3.37) with Assumptions 3.3 and 3.4 and the multiple-model system identification with projection (3.36). The adaptive observer (3.40) guarantees that for any initial condition $\hat{x}_p(0)$:*

1. *All signals are bounded.*
2. *If u is sufficiently rich of order N, the state estimation error $\tilde{x}_p(t) \coloneqq \hat{x}_p(t) - x_p(t)$ converges to zero asymptotically.*

Proof. From Theorem 3.7 we know that the signals $\hat{w}_p$, $\tilde{w}_p$, $\dot{\tilde{w}}_p$, $M^\top \tilde{w}_p$, $M^\top \dot{\tilde{w}}_p$, ε are bounded. Estimates $\hat{A}_p$ and $\hat{b}_p$, and the adaptive gain $\hat{K}_o$ are convex combinations of $\hat{w}$ and bounded parameters, and hence they are bounded. By the same logic $\dot{\hat{x}}_p$ is also bounded, and note that we can rewrite it as

$$\begin{aligned}
\dot{\hat{x}}_p(t) &= \hat{A}_p(t)\hat{x}_p(t) + \hat{b}_p(t)u(t) + \hat{K}_o(t)(c_p^\top \hat{x}_p(t) - y_p(t)) \\
&= A_o^* \hat{x}_p(t) + \hat{b}_p(t)u(t) + (\hat{A}_p - A_o^*)x_p(t) \\
&= A_o^* \hat{x}_p(t) + \hat{b}_p(t)u(t) + (\hat{a}_p - a_o^*)c_p^\top x_p(t) \\
&= A_o^* \hat{x}_p(t) + \hat{b}_p(t)u(t) + (\hat{a}_p - a_o^*)y_p(t).
\end{aligned}$$

Since A_o^* is Hurwitz and x_p is bounded, we get that $\hat{x}_p$ is bounded.

Let $e_o(t) \coloneqq x_p(t) - \hat{x}_p(t)$ be the state estimation error, then the state estimation error dynamics are

$$\begin{aligned}
\dot{e}_o(t) &= \dot{\hat{x}}_p(t) - \dot{x}_p(t) \\
&= A_o^* e_o(t) + \tilde{b}_p(t)u(t) - \tilde{a}_p(t)y_p(t),
\end{aligned} \tag{3.41}$$

where $\tilde{a}_p(t) = \hat{a}_p(t) - a_p$, $\tilde{b}_p(t) = \hat{b}_p(t) - b_p$ are the parameter errors. Since u is sufficiently rich, we get that $\sum_{i=1}^{N} \hat{w}_i(t)\Theta_i \to \Theta_p$ asymptotically. This implies that $\tilde{a}_p$ and $\tilde{b}_p$ asymptotically converge to zero, which finally proves that $\tilde{x}_p$ asymptotically goes to zero, finishing the proof. □

3.3.1 Simulation Example

Consider the following uncertain LTI, SISO transfer function

$$y = \frac{s^3 + 2s^2 + 3s + b_{p0}}{s^4 + 17s^3 + 81s^2 + a_{p3}s + a_{p4}}u,$$

where b_{p0}, a_{p3} and a_{p4} are uncertain parameters in the interior of the convex polytope defined by

$$\begin{aligned}
0.7a_{p3} = a_{p3\,\min} < a_{p3} < a_{p3\,\max} = 1.5a_{p3} \\
0.7a_{p4} = a_{p4\,\min} < a_{p4} < a_{p4\,\max} = 1.5a_{p4} \\
0.5b_{p4} = b_{p4\,\min} < b_{p4} < b_{p4\,\max} = 2.5b_{p4}.
\end{aligned}$$

We will perform system identification of these parameters and estimate the states of the observable canonical realization of the system. In this representation, Equation (3.27) is redefined as follows:

$$\begin{aligned}
a_p &= \begin{bmatrix} 17 & 81 & a_{p3} = \underline{115} & a_{p4} = \underline{50} \end{bmatrix}^\top, \\
b_p &= \begin{bmatrix} 1 & 2 & 3 & b_{p4} = \underline{4} \end{bmatrix}^\top, \\
c_p &= \begin{bmatrix} 1 & 0 & 0 & 0 \end{bmatrix}^\top.
\end{aligned}$$

Defining $\Lambda(s) = (s+5)^4$ and using Remark 3.1 we isolate all terms that are known on the left-hand side of the equality as

$$\begin{aligned}
z &= \frac{s^4 + 17s^3 + 81s^2}{\Lambda(s)} y_p - \frac{s^3 + 2s^2 + 3s}{\Lambda(s)} u = w_p^\top M \phi, \\
w_p^\top &= \begin{bmatrix} w_1 & w_2 & \cdots & w_8 \end{bmatrix}^\top, \\
M &= \begin{bmatrix} b_{0(1)} & a_{1(1)} & a_{0(1)} \\ b_{0(2)} & a_{1(2)} & a_{0(2)} \\ \vdots & \vdots & \vdots \\ b_{0(8)} & a_{1(8)} & a_{0(8)} \end{bmatrix}, \\
\phi &= \begin{bmatrix} \frac{1}{\Lambda(s)} u & -\frac{s}{\Lambda(s)} y_p & -\frac{1}{\Lambda(s)} y_p \end{bmatrix}^\top.
\end{aligned}$$

The simulations are compared with the equivalent adaptive technique that uses a single-model for identification found in Section 2.4.7. The initial estimate of the multiple-model approach is

$$\hat{w}_p(0) = \hat{w}_{p0} = \begin{bmatrix} 0.1 & 0.1 & 0.1 & 0.1 & 0.1 & 0.1 & 0.1 & 0.3 \end{bmatrix}^\top,$$

which corresponds to

$$\hat{\Theta}_p(0) = \hat{\Theta}_{p0} = \begin{bmatrix} 6.8 & 135.7 & 59 \end{bmatrix}^\top.$$

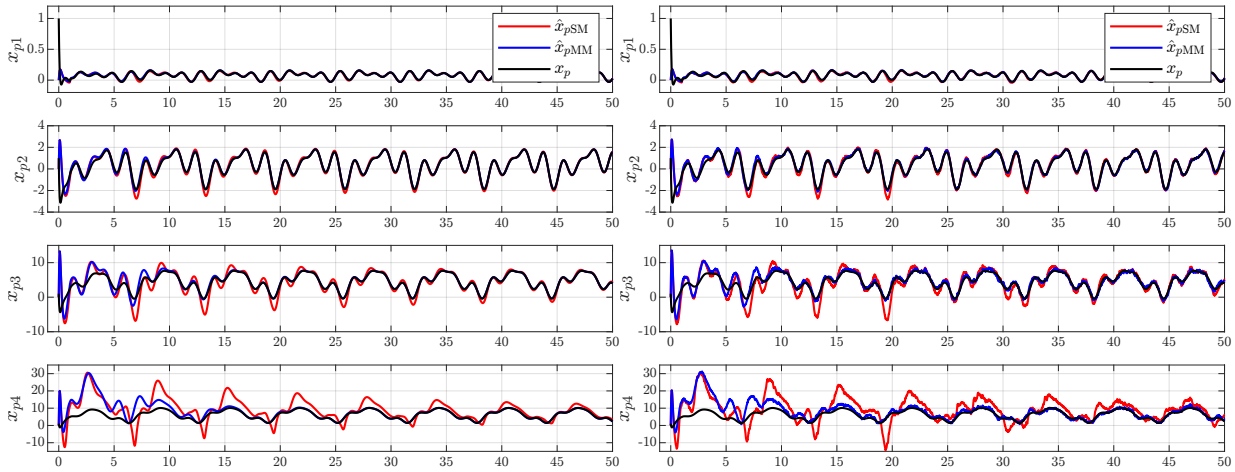
The initial condition for the state estimator is $\hat{x}(0) = \begin{bmatrix} 0 & 0 & 0 & 0 \end{bmatrix}^\top$. The matrices set for convergence speed are $\Gamma_{\text{SM}} = 10^7 \mathbb{I}_{3\times 3}$ and $\Gamma_p = 10^2 \mathbb{I}_{8\times 8}$. These matrices were chosen to have convergence times in the same order of magnitude. The input signal is set to $u(t) = 1 + \sin(t) + \sin(3t) + \sin(4t)$, which is sufficiently rich of order 9, making it a PE signal for the systems using a single identification model and multiple identification models.

In Figures 3.4(a) and 3.4(b) we present the time evolution of the states for the uncertain plant using a single identification model and multiple identification models. We see that the single-model and the multiple-model approach are able to estimate the states in the presence of measurement noise and in the absence of it. We see that for the same control input, the estimated states converge faster in the case of multiple models, as also shown in Figures 3.5(a) and 3.5(b). This behavior is clearly seen when comparing the 2-norm of the state estimation error in Figures 3.6(a) and 3.6(b), where we can also see that the multiple-model approach is better at filtering high-frequency noise. By subtracting the state estimates without noise and the state estimates with noise, we are left with the amplification of the noise. In Figure 3.7 we see that the amplification of the noise using a single-model approach is greater than using multiple models in the open-loop configuration.

To compare the effects of using a single model, or multiple models, we ran a series of 1000 simulations with randomly generated initial conditions, lasting 100 seconds in open-loop, and 20 seconds in closed-loop. The results are presented as box-and-whisker plots and a table. Outliers are presented as box-and-whisker plots as circles and represent values outside 99.3% of the distribution.

The first test was the identification error of the uncertain parameter θ. In Figure 3.8(a) we see that the multiple-model approach has smaller 2-norm, on average, in noiseless and measurement noise cases. It is interesting to note that the single-model approach has outliers that outperformed the best cases of the multiple-model approach; on average, the multiple-model obtained better results. This was then analyzed in the state estimation error, which was reduced by half in the 2-norm as seen in Figure 3.8(b).

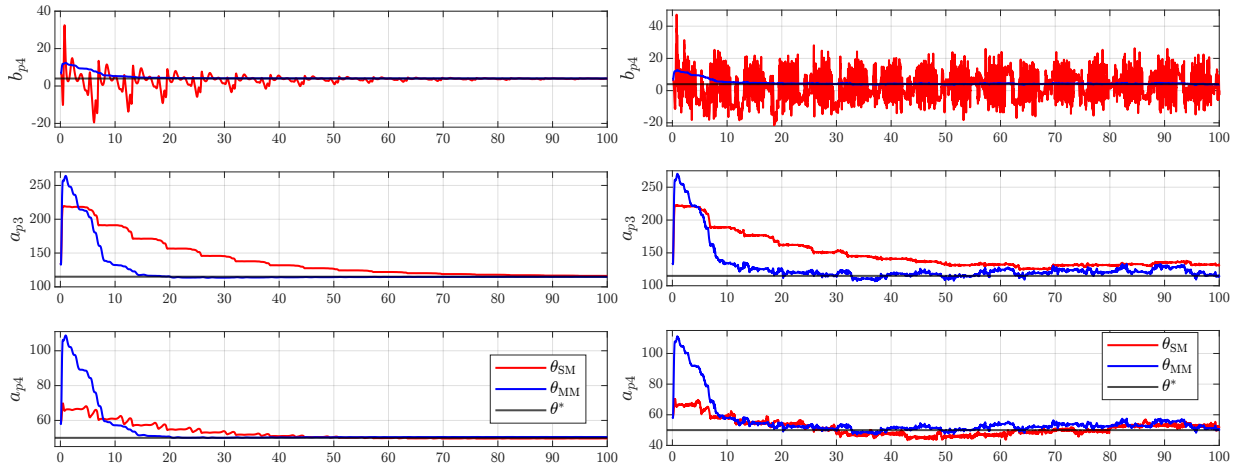
Finally, we studied the amplification of the noise in the system by subtracting the estimated states of the system with noise and the system without noise, in the single-model and multiple-model approach. The use of multiple models allows us to filter the noise and obtain a system that can perform better in the presence of noise, as seen in Figure 3.8(c). A summary of the results of the statistical analysis can be seen in Table 3.1. In summary, the simulations show that using a multiple-model approach, we can achieve better performance that is retained even in the case of measurement noise.



(a)Time evolution of the state estimates without uncertain dynamics and measurement noise.

(b)Time evolution of the state estimates with uncertain dynamics and measurement noise.

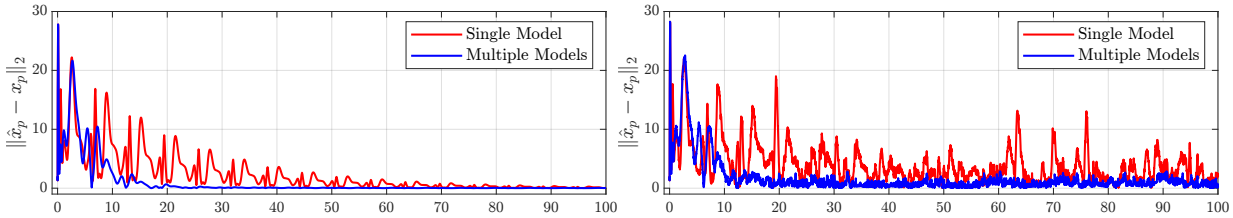
Figure 3.4: Time evolution of the state estimates without and with uncertain dynamics and measurement noise, on the left and right, respectively.



(a)Time evolution of $\hat{\Theta}_p$ without uncertain dynamics and measurement noise.

(b)Time evolution of $\hat{\Theta}_p$ with uncertain dynamics and measurement noise.

Figure 3.5: Time evolution of $\hat{\Theta}_p$ without and with uncertain dynamics and measurement noise, on the left and right, respectively.



(a)Time evolution of $\|\hat{x}_p - x_p\|$ without uncertain dynamics and measurement noise.

(b)Time evolution of $\|\hat{x}_p - x_p\|$ with uncertain dynamics and measurement noise.

Figure 3.6: Time evolution of $\|\hat{x}_p - x_p\|$ without and with uncertain dynamics and measurement noise, on the left and right, respectively.

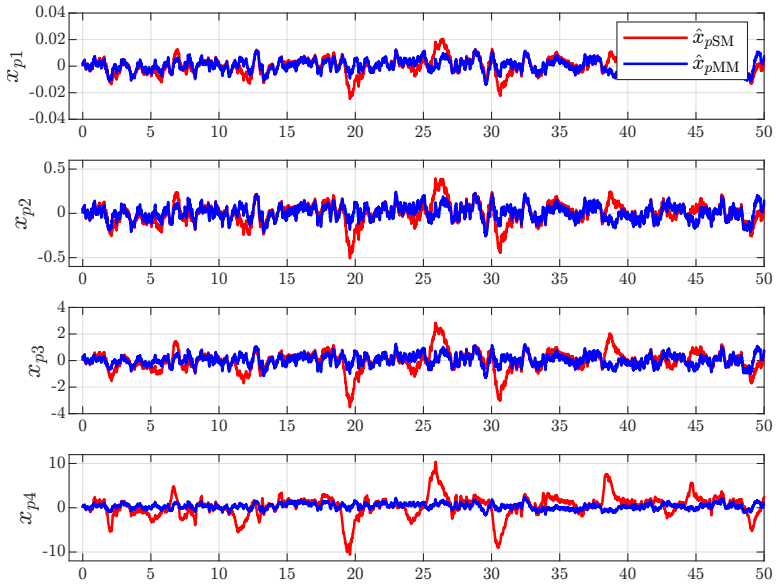
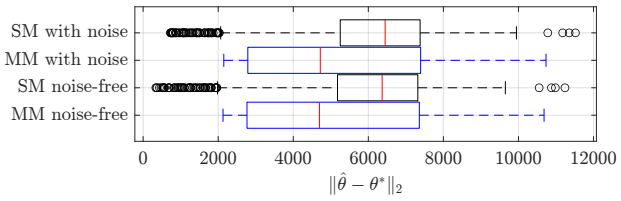
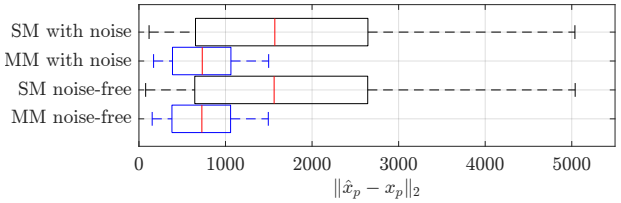


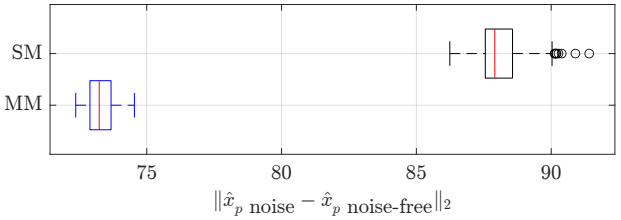
Figure 3.7: Amplification of the noise in each state in open-loop.



(a)Whisker-plot of the estimation of the plant dynamics in open-loop configuration.



(b)Whisker-plot of the estimation of the states in open-loop configuration.



(c)Whisker-plot of the noise amplification in open-loop configuration.

Figure 3.8: Statistical analysis for open-loop state estimation using multiple models.

Table 3.1: Summary of results of the statistical analysis in open-loop.

2-norm of the identification error					
	Minimum	Q1	Median	Q3	Maximum
SM noise	728	5251	6448	7397	11517
MM noise	2149	2789	4720	7393	10734
SM noise-free	338	5178	6368	7318	11238
MM noise-free	2128	2766	4697	7358	10681
2-norm of the state estimation error					
	Minimum	Q1	Median	Q3	Maximum
SM noise	117	653	1569	2645	5036
MM noise	169	387	731	1062	1498
SM noise-free	77	645	1561	2642	5039
MM noise-free	153	381	727	1058	1494
2-norm of the noise amplification					
	Minimum	Q1	Median	Q3	Maximum
SM	86	87	88	89	91
MM	72	72	73	73	74

Chapter 4

Multiple Model Reference Adaptive Control (MMRAC) with Blending

This chapter combines Multiple-Model Parameter Identification (MMPI) from Chapter 3 with the Model Reference Adaptive Control (MRAC) approach to obtain a Multiple-Model Reference Adaptive Control (MMRAC) scheme with blending. The desired plant behavior is expressed through a reference model that captures the ideal transient and steady-state behavior. The adaptive law is then designed to adjust the controller parameters so that the plant states track the response of this model and ensuring robustness against plant uncertainties. The development of the controller and the stability analysis can be found in Section 4.1. In addition, we include statistical analysis that shows the improvements in performance compared to single-model approaches. In Section 4.2 we tackle an interesting control problem of side-slip of vehicles due to loss of traction of the tires with the road. The simulations demonstrate that the use of multiple-model techniques improves the performance with similar control efforts.

4.1 MMRAC in State Space

The results found in this section were published in [42]. Consider the Multiple-Input, Multiple-Output (MIMO), Linear, Time-Invariant (LTI) system

$$\dot{x}_p(t) = A_p x_p(t) + B_p u(t),\ x_p(0) = x_{p0},\ t \geq 0, \tag{4.1}$$

where $A_p \in \mathbb{R}^{n\times n}$ and $B_p \in \mathbb{R}^{n\times m}$ are unknown constant matrices, B_p is full column rank, $x_p(t) \in \mathbb{R}^n$, $u(t) \in \mathbb{R}^m$ are the state of the system and the control input, respectively. We assume that $x_p(t)$ is available for feedback.

We aim to design a controller such that the state x_p of the plant (4.1) asymptotically tracks the trajectory x_r generated by the reference model

$$\dot{x}_r(t) = A_r x_r(t) + B_r r(t),\ x_r(0) = x_{r0},\ t \geq 0, \tag{4.2}$$

where $A_r \in \mathbb{R}^{n\times n}$ and $B_r \in \mathbb{R}^{n\times m}$ are known constant matrices, A_r is Hurwitz, and $r : [0, \infty) \to \mathbb{R}^m$ is a known, bounded, piecewise continuous reference signal. It is assumed that the plant (4.1) and the reference model (4.2) satisfy the exact matching conditions [77], as stated in the following assumption.

Assumption 4.1. *There exist matrices $K^* \in \mathbb{R}^{m\times n}$ and $L^* \in \mathbb{R}^{m\times m}$ such that*

$$A_p + B_p K^* = A_r, \tag{4.3}$$

$$B_p L^* = B_r. \tag{4.4}$$

△

Assumption 4.1 is a reasonable assumption, since it is a necessary and sufficient condition to guarantee the existence of a solution to the tracking problem when the plant model (4.1) is known and there are no uncertainties [77]. In addition, (4.4) is equivalent to $\operatorname{Im} B_r \subseteq \operatorname{Im} B_p$, which means that, without loss of generality, we can assume that $\operatorname{Im} B_p = \operatorname{Im} B_r$.

Our approach to solving the aforementioned control design problem involves online parameter identification of the system matrices $\Theta_p = \begin{bmatrix} A_p & B_p \end{bmatrix}$, applying the results from Section 3.1. With the definition of (3.4), we modify Assumption 3.1 for the MMRAC case.

Assumption 4.2. *There exists a finite set $\mathcal{S}$ of known system matrices $\begin{bmatrix} A_i & B_i \end{bmatrix} \in \mathbb{R}^{n\times(n+m)}$, such that*

i) $\begin{bmatrix} A_p & B_p \end{bmatrix} \in \operatorname{int}(\operatorname{conv}(\mathcal{S}))$.

ii) Every convex combination of B_i is full column rank. △

The first item of Assumption 4.2 is further explained for the case of MMRAC in Section 4.1.1. We require Assumption 4.2 (ii) to ensure that we do not have redundant inputs, or we do not drop the rank of the number of inputs, losing control authority of the system. Given a set $\mathcal{S}$, there exist numerical methods to verify whether all convex combinations of B_i's are full rank [33].

4.1.1 Corner Model Selection

Consider a set $\mathcal{S}$ that satisfies Assumption 4.2 and has N elements. In this subsection, we develop a constructive procedure that, starting with $\mathcal{S}$, produces a new set

$$\mathcal{S}' = \left\{ \begin{bmatrix} A'_1 & B'_1 \end{bmatrix}, \cdots, \begin{bmatrix} A'_{N'} & B'_{N'} \end{bmatrix} \right\}, \tag{4.5}$$

that also satisfies Assumption 4.2, and such that for every $i \in \{1, \cdots, N\}$ there exist matrices $K_i \in \mathbb{R}^{m \times n}$ and $L_i \in \mathbb{R}^{m \times m}$ such that,

$$A'_i + B'_i K_i = A_r, \tag{4.6}$$
$$B'_i L_i = B_r. \tag{4.7}$$

Satisfying the Matching Conditions

In the next proposition, we show how to use the information of Assumption 4.1 and a set $\mathcal{S}$ that satisfies Assumption 4.2 to obtain a new set $\mathcal{S}'$ such that for every element of $\mathcal{S}'$ there exist matrices $K_i \in \mathbb{R}^{m \times n}$ and $L_i \in \mathbb{R}^{m \times m}$ that satisfy (4.6) and (4.7).

Proposition 4.1. *Suppose that the plant (4.1) and reference model (4.2) are such that Assumption 4.1 is satisfied. If there exists a set $\mathcal{S}$ that satisfies Assumption 4.2, then there exists a set $\mathcal{S}'$ that also satisfies Assumption 4.2, and furthermore*

1. $\text{conv}(\mathcal{S}') \subseteq \text{conv}(\mathcal{S})$.
2. *For each $i \in \{1, \cdots, N\}$, there exist matrices $K_i \in \mathbb{R}^{m \times n}$ and $L_i \in \mathbb{R}^{m \times m}$ such that (4.6) and (4.7) are satisfied.*

Proof. Let (A_p, B_p) and (A_r, B_r) be the matrix pairs that represent a plant, and a reference model, respectively. Assume that they satisfy Assumption 4.1. Moreover, assume that there exists a set $\mathcal{S}$ with N elements that satisfies Assumption 4.2. The first, and trivial case, is if for every $i = 1, \cdots, N$, there exist matrices $K_i \in \mathbb{R}^{m \times n}$ and $L_i \in \mathbb{R}^{m \times m}$ such that every corner model $[A'_i \;\; B'_i] := [A_i \;\; B_i]$ satisfies (4.6) and (4.7). In that case, we can define $\mathcal{S}' = \mathcal{S}$, and we have satisfied Assumptions 4.1 and 4.2.

For the case when there exists some $j \in \{1, \cdots, N\}$ such that $[A'_j \;\; B'_j] := [A_j \;\; B_j] \in \mathcal{S}$ does not satisfy (4.6) or (4.7), consider the closed convex hull of $\mathcal{S}$, i.e., $\text{conv}\,(\mathcal{S})$. The set $\text{conv}\,(\mathcal{S})$ is a compact, convex polytope, and it is non-empty since $\begin{bmatrix} A_p & B_p \end{bmatrix}$ is an element of

conv $(\mathcal{S})$ by Assumption 4.2 (i). Next, take the set of matrices that satisfy Equations (4.3) and (4.4):

$$\mathcal{T} \coloneqq \left\{ \begin{bmatrix} A_x & B_x \end{bmatrix} \in \mathbb{R}^{n\times(n+m)} : A_x + B_x K = A_r, B_x L = B_r, L \in \mathbb{R}^{m\times m}, K \in \mathbb{R}^{m\times n} \right\}.$$

The set $\mathcal{T}$ is a hyperplane, since it can be written as $n(n+m)$ linear equations (see Section 2.2.1 of [10]), therefore it is a convex polytope. From Assumption 4.1, we see that if we replace K and L by K^* and L^*, respectively, the element $\begin{bmatrix} A_p & B_p \end{bmatrix}$ belongs to $\mathcal{T}$, which means $\mathcal{T}$ is non-empty. The intersection set

$$\mathcal{P} \coloneqq \text{conv}\,(\mathcal{S}) \cap \mathcal{T}.$$

is also non-empty, since $\begin{bmatrix} A_p & B_p \end{bmatrix}$ is an element of both conv $(\mathcal{S})$ and $\mathcal{T}$. Moreover, the intersection of a compact, convex polytope and a convex polytope is another compact, convex polytope (see Section 2.3.1 of [10]), which in turn implies that we can obtain N' corner models $\begin{bmatrix} A'_i & B'_i \end{bmatrix}$ such that

$$\mathcal{P} = \text{conv}\left(\underbrace{\left\{ \begin{bmatrix} A'_1 & B'_1 \end{bmatrix}, \cdots, \begin{bmatrix} A'_{N'} & B'_{N'} \end{bmatrix} \right\}}_{=:\mathcal{S}'} \right).$$

Every convex combination of the matrices B'_i can be written as a convex combination of the original B_i matrices, and every convex combination of the B_i's is full column rank by Assumption 4.2, which implies that every convex combination of the B'_i is also full column rank. The vertices, edges and faces of $\mathcal{P}$ are obtained by intersecting the previous vertices, edges and faces from conv$(\mathcal{S})$ with the set $\mathcal{T}$. Since $\begin{bmatrix} A_p & B_p \end{bmatrix}$ is not on a vertex, edge or face of conv$(\mathcal{S})$ it cannot be on a vertex, edge or face of $\mathcal{P}$ and must be in the interior. Hence, the set $\mathcal{S}'$ satisfies Assumption 4.2, and also every element of $\mathcal{S}'$ satisfies (4.6) and (4.7). □

Remark 4.2. *The results provided in Proposition 4.1 deal with systems that do not have the same number of inputs as states; the special case of $n = m$ is solved trivially, i.e., we have $\mathcal{S} = \mathcal{S}'$. Since every convex combination of B_i is full column rank, that means that B_i can be inverted for all $i \in \{1, \cdots, N\}$, and the gains can be obtained as*

$$K_i = B_i^{-1}(A_r - A_i)$$
$$L_i = B_i^{-1} B_r.$$

△

Obtaining the sets $\mathcal{S}$ and $\mathcal{S}'$

The modeling uncertainty in (4.1) is taken to be parametric uncertainty in the matrices in this state-space system model. There is an implicit assumption here that the state-space system model (4.1) is derived from physical laws rather than from a state-space realization of an input-output system model. If we consider the full range of values that each entry of A_p, and B_p can take, we get that we can bound $a_{ij} \in [a_{ij}^-, a_{ij}^+]$ and $b_{ij} \in [b_{ij}^-, b_{ij}^+]$. When we consider the minimums and maximums of every entry we write the following matrices

$$\begin{aligned} A_p^- &= \left[a_{ij}^-\right], i, j \in \{1, \cdots, n\}, \\ A_p^+ &= \left[a_{ij}^+\right], i, j \in \{1, \cdots, n\}, \\ B_p^- &= \left[b_{ij}^-\right], i \in \{1, \cdots, n\}, j \in \{1, \cdots, m\}, \\ B_p^+ &= \left[b_{ij}^+\right], i \in \{1, \cdots, n\}, j \in \{1, \cdots, m\}. \end{aligned}$$

Let $\mathcal{S}$ be the set of all possible binary combinations of system matrices $\begin{bmatrix} A_p & B_p \end{bmatrix}$, where each entry takes either a minimum value from $\begin{bmatrix} A_p^- & B_p^- \end{bmatrix}$ or a maximum value from $\begin{bmatrix} A_p^+ & B_p^+ \end{bmatrix}$. Note that, by construction, $\mathcal{S}$ satisfies Assumption 4.2 (i). The number of elements in $\mathcal{S}$ is $N = 2^{n(n+m)}$. If the entries can be parameterized by an uncertainty vector $\eta \in \mathbb{R}^q$, then $\mathcal{S}$ can be defined in terms of 2^q elements (see Remark 3.1). A final remark is that, the more information of the underlying structure of the system we have, the less elements the set $\mathcal{S}$ will have; a clever parametrization of the uncertainty can greatly reduce the total number of models.

The corner model selection process described above guarantees that $\begin{bmatrix} A_p & B_p \end{bmatrix} \in \text{int}\left(\text{conv}\left(S\right)\right)$. However, it is not evident that Assumption 4.2 (ii) is satisfied. The results from [33] can be used to verify this condition. If Assumption 4.2 (ii) is satisfied, then the last step is to the use constructive procedure from the proof of Proposition 4.1 to obtain $\mathcal{S}'$.

Example

In this example, we consider a system with two states and one input. We assume that the plant only has uncertainty in the B_p matrix. The *unknown* input matrix to the system is $B_p = \begin{bmatrix} 2 \\ 2 \end{bmatrix}$. The reference models input's matrix is $B_r = \begin{bmatrix} 10 \\ 10 \end{bmatrix}$. Note that by taking $L^* = 5$ we can satisfy (4.4), and Assumption 4.1 is satisfied. The polytopic uncertainty for B_p is given by

$$B_p^- = \begin{bmatrix} 1 \\ 1 \end{bmatrix}, B_p^+ = \begin{bmatrix} 4 \\ 5 \end{bmatrix}.$$

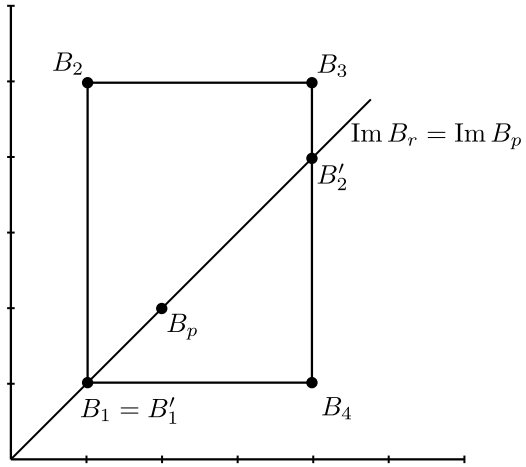


Figure 4.1: Graphic illustration of the projection process to select corner models.

Using the selection procedure from Section 4.1.1 we can take all possible combinations of the minimums and maximums of every entry of B_p^- and B_p^+ to get

$$B_1 = \begin{bmatrix} 1 \\ 1 \end{bmatrix}, B_2 = \begin{bmatrix} 1 \\ 5 \end{bmatrix}, B_3 = \begin{bmatrix} 4 \\ 5 \end{bmatrix}, B_4 = \begin{bmatrix} 4 \\ 1 \end{bmatrix}.$$

Since A_p is completely known, we need to redefine the sets $\mathcal{S}$ and $\mathcal{T}$ as

$$\begin{aligned} \mathcal{S} &= \{B_1, \cdots, B_4\}, \\ \mathcal{T} &= \left\{B_x \in \mathbb{R}^{2\times 1} : B_x L = B_r, L \in \mathbb{R}\right\}. \end{aligned}$$

It is easily verifiable that $B_p \in \operatorname{int}(\operatorname{conv}(\mathcal{S}))$, and that any convex combination of B_i is full column rank. Nevertheless, if we consider B_2, B_3, or B_4 we cannot satisfy (4.7). Using the proof of Proposition 4.1 we solve for the set $\mathcal{P}$ graphically (closed line segment going from B_1 to B_2'), as shown in Figure 4.1 to obtain

$$\mathcal{P} = \operatorname{conv}(\mathcal{S}) \cap \mathcal{T} = \operatorname{conv}\left(\underbrace{\left\{\begin{bmatrix} 1 \\ 1 \end{bmatrix}, \begin{bmatrix} 4.5 \\ 4.5 \end{bmatrix}\right\}}_{\mathcal{S}'}\right).$$

Note that $B_p \in \operatorname{int}(\mathcal{P})$. In addition, every convex combination of B_1 and B_2' is full column rank, and we can satisfy (4.7) with $L_1 = 10$, and $L_{2'} = 20/9$.

4.1.2 Control Design

In this subsection, we combine the system identification scheme of Section 3.1 with a Model Reference Control (MRC) framework to achieve asymptotic tracking of the reference system (4.2). We use the recursive adaptive algorithm with parameter projection (3.25) to design a MMRAC scheme to achieve the adaptive state tracking control task stated in Section 4.1. We utilize Theorem 3.2 (iii) to construct the proposed MMRAC scheme.

If $w \in \mathcal{W}$, then multiplying both sides of (4.7) by w_i and summing over i yields

$$\sum_{i=1}^{N} w_i B_i L_i = \sum_{i=1}^{N} w_i B_r = B_r,$$

which implies, together with (4.4) from Assumption 4.1, that

$$B_p L^* = \sum_{i=1}^{N} w_i B_i L_i. \tag{4.8}$$

Applying the same steps on (4.6) we get

$$\begin{aligned} A_r = \sum_{i=1}^{N} w_i A_r &= \sum_{i=1}^{N} w_i \big(A_i + B_i K_i\big) \\ &= A_p + \sum_{i=1}^{N} w_i B_i K_i. \end{aligned} \tag{4.9}$$

Comparing (4.9) to (4.3) we get that

$$B_p K^* = \sum_{i=1}^{N} w_i B_i K_i. \tag{4.10}$$

Equations (4.8) and (4.10) motive us to generate estimates of the gains K^* and L^* using the estimates $\hat{w}(t)$, keeping in mind the rank supposition in Assumption 4.2, as

$$\hat{K}(t) = \hat{B}_p^{\dagger}(t) \sum_{i=1}^{N} \hat{w}_i(t) B_i K_i, \tag{4.11}$$

$$\hat{L}(t) = \hat{B}_p^{\dagger}(t) \sum_{i=1}^{N} \hat{w}_i(t) B_i L_i, \tag{4.12}$$

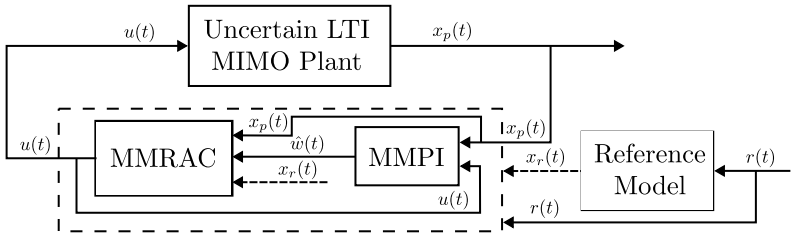


Figure 4.2: Block diagram of the proposed MMRAC.

where $\hat{B}_p^\dagger(t)$ is the Moore-Penrose inverse of

$$\hat{B}_p(t) = \sum_{i=1}^{N} \hat{w}_i(t) B_i. \tag{4.13}$$

Equations (4.8) and (4.10) to (4.12), together with Corollary 3.4 further imply the following:

Corollary 4.3. *Consider the system (4.1) with definitions (3.11) and (3.14), and the reference model (4.2). If $\Phi(t)$ satisfies the persistence of excitation condition with constants $\alpha_{\Phi 1}$, $\alpha_{\Phi 2}$, and T_Φ, then the estimates $\hat{K}(t)$ and $\hat{L}(t)$ defined in (4.11) and (4.12) are bounded, and asymptotically converge to K^* and L^*, respectively.*

Proof. Since Π is compact, we get that $\hat{B}_p(t)$ belongs to a compact set, which means the Moore-Penrose inverse of $\hat{B}_p(t)$ exists, and it is bounded. Furthermore, from Assumption 4.2, we have that $\hat{B}_p(t)$ is full column rank, which means that we can write

$$\hat{B}_p^\dagger(t) = \left(\hat{B}_p^\top(t)\hat{B}_p(t)\right)^{-1} \hat{B}_p^\top(t). \tag{4.14}$$

Combining Equations (4.11), (4.12) and (4.14) we get that $\hat{K}(t)$, and $\hat{L}(t)$ are bounded. The proof to show asymptotic convergence is the same as Theorem 3.2 (iii). □

The control law we will consider to achieve asymptotic tracking of the reference model is

$$u(t) \coloneqq \hat{K}(t)x_p(t) + \hat{L}(t)r(t). \tag{4.15}$$

The complete schematics of the MMRAC approach can be seen in Figure 4.2.

4.1.3 Stability Analysis

The main result of the MMRAC scheme is now presented.

Theorem 4.4. *Consider the plant (4.1) and the reference model (4.2). If $\Phi(t)$ satisfies the persistence of excitation condition (2.4), and Assumptions 4.1 and 4.2 hold, then the MMRAC scheme (3.7), (3.9), (3.11), (3.25) and (4.11) to (4.15) guarantees that for any*

(i) initial conditions of the plant (4.1),

(ii) initial conditions of the reference model (4.2), and

(iii) piecewise continuous and bounded signal $r : [0, \infty) \to \mathbb{R}^m$ in (4.2),

all closed-loop signals are bounded and $x_p(t)$ asymptotically converges to $x_r(t)$.

Proof. Let $x_p(0) = x_{p0}$ and $x_r(0) = x_{r0}$ be arbitrary initial plant and reference model states, and $r(t)$ be any known, bounded, piecewise continuous signal. Substituting (4.15) into (4.1) we get

$$\begin{aligned}\dot{x}_p(t) &= A_p x_p(t) + B_p u(t) \\ &= A_p x_p(t) + B_p \hat{K}(t) x_p(t) + B_p \hat{L}(t) r(t).\end{aligned}$$

Adding and subtracting $B_p K^* x_p(t)$ and $B_p L^* r(t)$, defining $\tilde{K}(t) \coloneqq \hat{K}(t) - K^*$, $\tilde{L}(t) \coloneqq \hat{L}(t) - L^*$, and using Assumption 4.1 we get

$$\dot{x}_p(t) = A_r x_p(t) + B_r r(t) + B_p \tilde{K}(t) x_p(t) + B_p \tilde{L}(t) r(t).$$

For the tracking error $e(t) \coloneqq x_p(t) - x_r(t)$, this implies

$$\begin{aligned}\dot{e}(t) &= A_r e(t) + B_p \tilde{K}(t) x_p(t) + B_p \tilde{L}(t) r(t) \\ &= \left(A_r + B_p \tilde{K}(t)\right) e(t) + B_p \tilde{K}(t) x_r(t) + B_p \tilde{L}(t) r(t).\end{aligned} \tag{4.16}$$

Let $Q \in \mathbb{R}^{n \times n}$ be a fixed, symmetric, and positive definite matrix. Then we can define $P \in \mathbb{R}^{n \times n}$ to be the unique positive definite and symmetric solution of $PA_r + A_r^\top P + Q = 0$. Consider the positive definite function

$$V\left(e(t)\right) = e^\top(t) P e(t). \tag{4.17}$$

Taking the derivative of (4.17) along solutions of (4.16) we get

$$\begin{aligned}\dot{V}\left(e(t)\right) &= 2e^{\top}(t)P\dot{e}(t)\\ &= 2e^{\top}(t)PA_re(t) + 2e^{\top}(t)PB_p\tilde{K}(t)x_p(t) + 2e^{\top}(t)PB_p\tilde{L}(t)r(t).\end{aligned} \tag{4.18}$$

The first term satisfies

$$\begin{aligned}2e^{\top}(t)PA_re(t) &= e^{\top}(t)PA_re(t) + e^{\top}(t)PA_re(t)\\ &= e^{\top}(t)\left(PA_r + A_r^{\top}P\right)e(t)\\ &= -e^{\top}(t)Qe(t).\end{aligned}$$

Hence, (4.18) can be rewritten as

$$\dot{V}\left(e(t)\right) = -e^{\top}(t)Qe(t) + 2e^{\top}(t)PB_p\tilde{K}(t)x_p(t) + 2e^{\top}(t)PB_p\tilde{L}(t)r(t).$$

Substituting $x_p(t) = e(t) + x_r(t)$, we get

$$\dot{V}\left(e(t)\right) = -e^{\top}(t)\left(Q - PB_p\tilde{K}(t)\right)e(t) + 2e^{\top}(t)PB_p\tilde{K}(t)x_r(t) + 2e^{\top}(t)PB_p\tilde{L}(t)r(t).$$

Defining

$$c_1(t) \coloneqq \|PB_p\tilde{K}(t)\|,$$

and

$$c_2(t) \coloneqq 2\|PB_p\tilde{K}(t)\|\|x_r(t)\| + 2\|PB_p\tilde{L}(t)\|\|r(t)\|,$$

we have

$$\dot{V}(e(t)) \leq -\left(\lambda_{\min}(Q) - c_1(t)\right)\|e(t)\|^2 + c_2(t)\|e(t)\|, \tag{4.19}$$

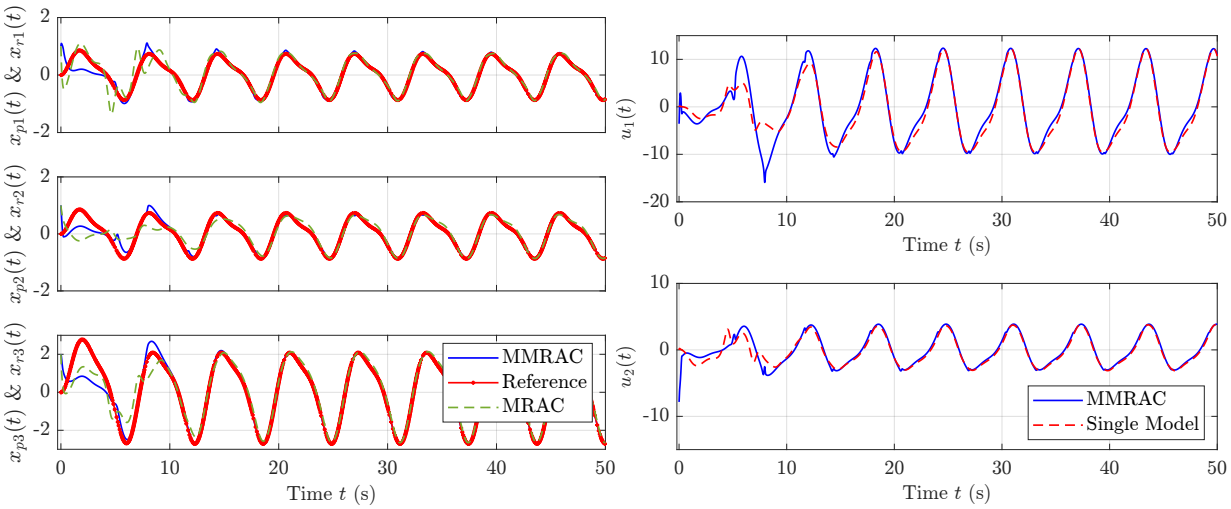
where $\lambda_{\min}(Q) > 0$ is the minimum eigenvalue of Q. Note that (4.16) does not have a finite escape time; from Corollary 4.3 we have that $\hat{K}(t)$ and $\hat{L}(t)$ are continuous and bounded, which means that $\tilde{K}(t)$ and $\tilde{L}(t)$ are also continuous and bounded, hence (4.16) may only go to infinity as time goes to infinity. Moreover, if $\Phi(t)$ is Persistently Exciting (PE), then $\tilde{K}(t)$ and $\tilde{L}(t)$ converge to zero asymptotically, which lets us conclude that $c_1(t)$ is bounded, and there exists $t_1 \geq 0$ such that $\lambda_{\min}(Q) > c_1(t)$ for all $t \geq t_1$. We can define

$$\bar{c}_1 = \sup\{c_1(t), t \geq t_1\}, \tag{4.20}$$

$$\bar{c}_2 = \sup\{c_2(t), t \geq t_1\}. \tag{4.21}$$

This implies that for all $t \geq t_1$ we get that if

$$\|e(t)\| > \frac{\bar{c}_2}{\lambda_{\min}(Q) - \bar{c}_1},$$



(a)State of the system $x_p(t)$, and state of the reference model $x_r(t)$.

(b)Control efforts for MMRAC and a single-model MRAC.

Figure 4.3: On the left: Time evolution of the states of the system and the reference model for MRAC and MMRAC. On the right: Control effort for MRAC and MMRAC.

then $\dot{V} < 0$, and we can conclude that e is bounded. This further implies that x_p is bounded, which finally implies that u is bounded, showing that all signals in the closed-loop system are bounded. Combining this with Corollary 4.3 we get

$$\lim_{t\to\infty} \left(\dot{V}(e(t)) + e^\top(t) Q e(t) \right) = 0.$$

This implies that $e(t)$ converges to 0, asymptotically, i.e., $x_p(t)$ asymptotically converges to $x_r(t)$. □

4.1.4 Simulation Example

We illustrate the behavior and performance of the proposed MMRAC scheme through a set of simulation tests performed on an uncertain model (4.1), a reference model (4.2), and a set $\mathcal{S}$ (3.4) that defines the polytopic uncertainty and satisfies Assumption 4.2. Statistical analysis comparing the performance of both control schemes is presented at the end of the subsection.

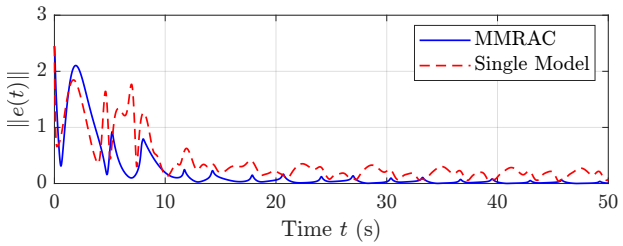


Figure 4.4: Euclidean norm of the tracking error for MMRAC and a single-model MRAC.

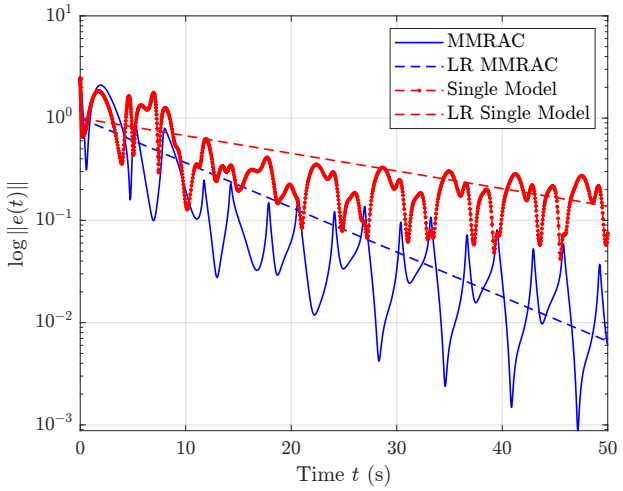


Figure 4.5: Semilog plot for the norm 2 of the tracking errors, and the linear regressions (LR) for MMRAC and a single-model.

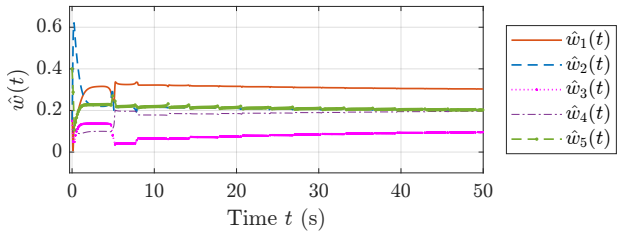
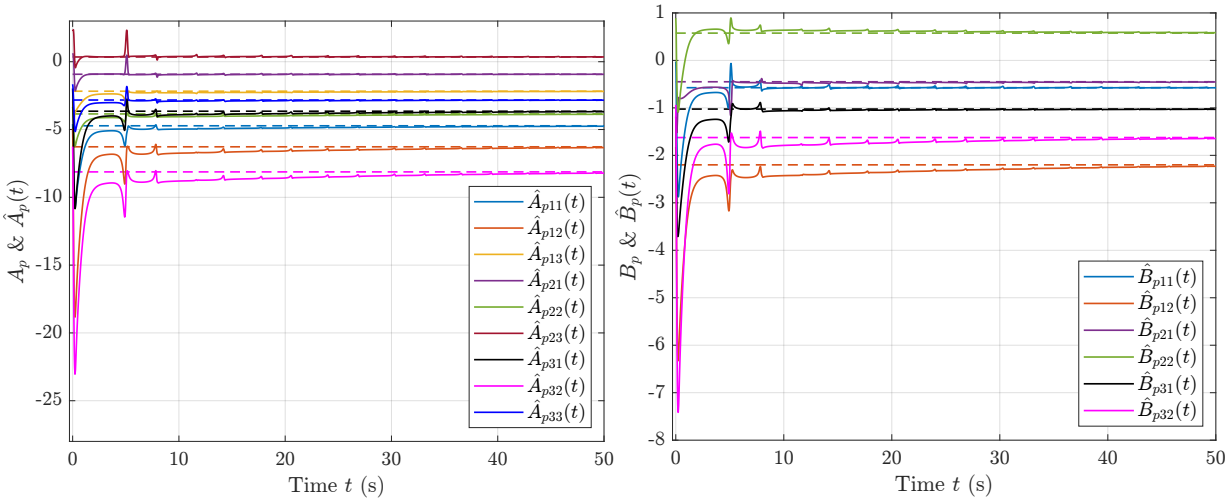


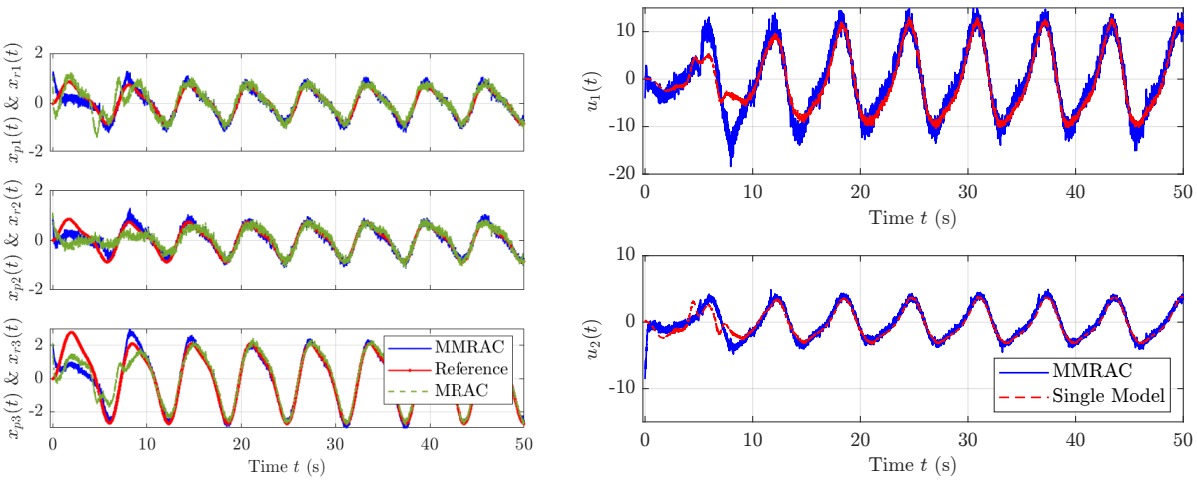
Figure 4.6: Evolution of the estimates $\hat{w}(t)$.



(a)Estimation of each entry of A_p. The dashed line is the true value.

(b)Estimation of each entry of B_p. The dashed line is the true value.

Figure 4.7: Time evolution of the estimates of A_p and B_p.



(a)State of the system $x_p(t)$, and state of the reference model $x_r(t)$ with measurement noise.

(b)Control efforts for MMRAC and a single-model MRAC with measurement noise.

Figure 4.8: Simulations with measurement noise. On the left: Time evolution of the states of the system and the reference model for MRAC and MMRAC. On the right: Control effort for MRAC and MMRAC.

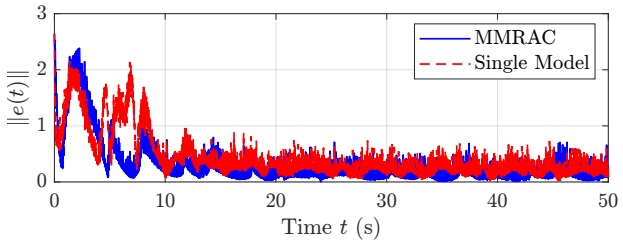


Figure 4.9: Euclidean norm of the tracking error for MMRAC and a single-model MRAC with measurement noise.

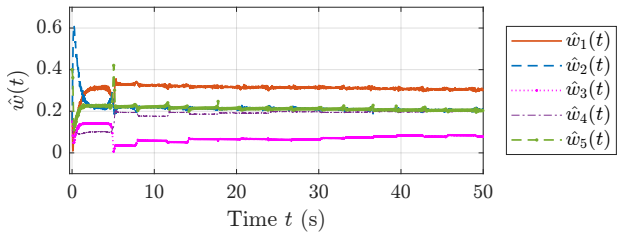
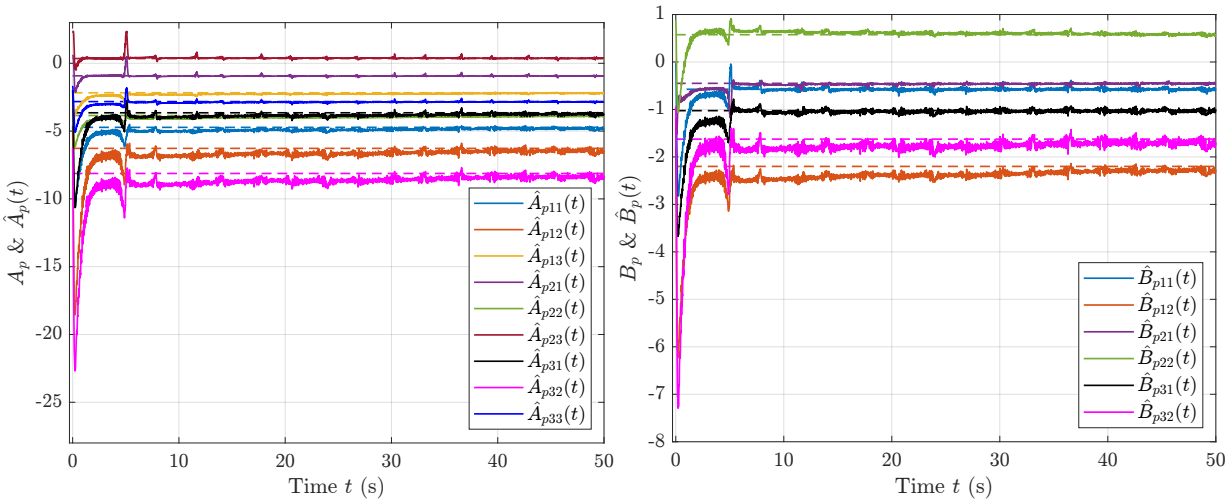


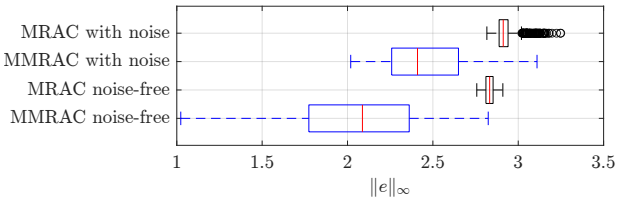
Figure 4.10: Evolution of the estimates $\hat{w}(t)$ with measurement noise.



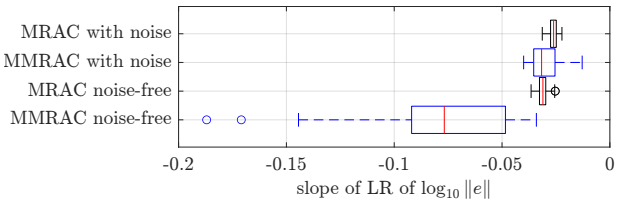
(a)Estimation of each entry of A_p with measurement noise. The dashed line is the true value.

(b)Estimation of each entry of B_p with measurement noise. The dashed line is the true value.

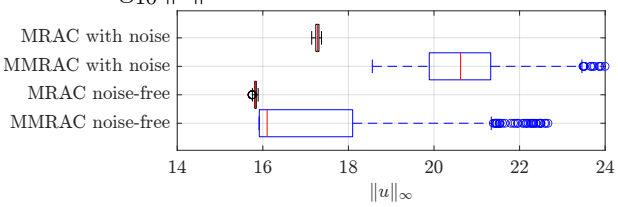
Figure 4.11: Time evolution of the estimates of A_p and B_p with measurement noise.



(a)Whisker plot of the infinity norm of the tracking error.



(b)Whisker plot of the slopes of the linear regression of $\log_{10}\|e\|$.



(c)Whisker plot of the norm infinity of the control effort.

Figure 4.12: Compilation of Whisker plots of the ∞-norm of the tracking error (top), slopes of the linear regression (middle), and control efforts (bottom).

Table 4.1: Summary of results of the statistical analysis.

Infinity norm of the tracking error					
	Minimum	Q1	Median	Q3	Maximum
MRAC noise	2.83	2.90	2.93	2.95	3.22
MMRAC noise	1.50	2.26	2.54	2.77	3.30
MRAC noise-free	2.76	2.81	2.83	2.85	2.91
MMRAC noise-free	1.02	1.77	2.09	2.36	2.82
Tracking error convergence speed [$\times 10^{-2}$]					
	Minimum	Q1	Median	Q3	Maximum
MRAC noise	-3.13	-2.79	-2.65	-2.51	-2.24
MMRAC noise	-4.00	-3.51	-3.21	-2.72	-1.35
MRAC noise-free	-3.65	-3.26	-3.10	-2.97	-2.53
MMRAC noise-free	-18.6	-9.19	-7.67	-4.84	-3.40
Infinity norm of the control effort					
	Minimum	Q1	Median	Q3	Maximum
MRAC noise	17.09	17.18	17.21	17.24	17.29
MMRAC noise	17.90	18.81	19.47	20.86	23.66
MRAC noise-free	15.74	15.81	15.83	15.85	15.89
MMRAC noise-free	15.91	15.92	16.10	18.10	22.66

Consider the uncertain system with $n = 3$, $m = 2$ given by the matrices

$$A_p = \begin{bmatrix} -4.725 & -6.275 & -2.175 \\ -0.925 & -3.85 & 0.35 \\ -3.65 & -8.125 & -2.825 \end{bmatrix}, \; B_p = \begin{bmatrix} -0.575 & -2.2 \\ -0.45 & 0.575 \\ -1.025 & -1.625 \end{bmatrix}.$$

The reference model (4.2) is

$$A_r = \begin{bmatrix} -1 & 0 & 0 \\ 0 & -1 & 0 \\ 1 & 1 & -1 \end{bmatrix}, \; B_r = \begin{bmatrix} 1 & 0 \\ 0 & 1 \\ 1 & 1 \end{bmatrix}.$$

It can be verified that Assumption 4.1 is satisfied by defining the matrices

$$K^* = \begin{bmatrix} -3.16 & -7.48 & -0.36 \\ -0.87 & -0.89 & -0.89 \end{bmatrix}, \; L^* = \begin{bmatrix} -0.44 & -1.66 \\ -0.34 & 0.44 \end{bmatrix}.$$

Considering the following 5 matrix pairs

$$A_1 = \begin{bmatrix} -0.75 & 0.25 & 0.25 \\ -3.75 & -4.75 & -3.75 \\ -2.5 & -2.5 & -4.5 \end{bmatrix}, \; B_1 = \begin{bmatrix} 0.25 & -0.5 \\ 1.25 & 2.5 \\ 1.5 & 2 \end{bmatrix},$$

$$A_2 = \begin{bmatrix} -16 & -30 & -5 \\ -3.5 & -8.5 & -1.5 \\ -17.5 & -36.5 & -7.5 \end{bmatrix}, \; B_2 = \begin{bmatrix} -5 & -10 \\ -1 & -2.5 \\ -6 & -12.5 \end{bmatrix},$$

$$A_3 = \begin{bmatrix} 2 & 0 & -1 \\ -0.5 & -1.5 & -0.5 \\ -0.5 & 0.5 & -2.5 \end{bmatrix}, \; B_3 = \begin{bmatrix} -1 & 1 \\ -0.5 & 0 \\ -1.5 & 1 \end{bmatrix},$$

$$A_4 = \begin{bmatrix} -1.5 & -0.75 & -0.75 \\ -0.25 & -0.875 & 1.125 \\ 0.25 & 0.375 & -0.625 \end{bmatrix}, \; B_4 = \begin{bmatrix} 0.25 & 0.25 \\ 0.125 & -0.375 \\ 0.375 & -0.125 \end{bmatrix},$$

$$A_5 = \begin{bmatrix} -4 & -1 & -5 \\ 5 & -2 & 8 \\ 3 & -1 & 2 \end{bmatrix}, \; B_5 = \begin{bmatrix} 2 & -1 \\ -3 & 2 \\ -1 & 1 \end{bmatrix},$$

we can define the set

$$\mathcal{S} = \left\{ \begin{bmatrix} A_1 & B_1 \end{bmatrix}, \cdots, \begin{bmatrix} A_5 & B_5 \end{bmatrix} \right\}.$$

The set $\mathcal{S}$ satisfies Assumption 4.2. The design parameters for the estimation scheme and the controller are $\Gamma = 2I_{5\times 5}$, $\lambda = 0.5$, and $\alpha = 0.01$, with the initial condition $\hat{w}(0) = \begin{bmatrix} 0.2 & 0.15 & 0.15 & 0.1 & 0.4 \end{bmatrix}^\top$. The input to the reference model is taken to be $r_1(t) = r_2(t) = \sin(t) + 0.5 \sin 2t$. With these definitions the full controller is

$$\begin{aligned}
\begin{bmatrix} \dot{\phi}_1(t) \\ \dot{\phi}_2(t) \end{bmatrix} &= -\lambda \begin{bmatrix} \phi_1(t) \\ \phi_2(t) \end{bmatrix} + \begin{bmatrix} x_p(t) \\ u(t) \end{bmatrix}, \\
\dot{\hat{w}}(t) &= \mathrm{Pr}_{\Pi,\hat{w}} \left(-\Gamma \left(E^\top(t) E(t) \hat{w}(t) + E^\top(t) \varepsilon_5(t) \right) \right), \\
\hat{w}_5(t) &= 1 - \sum_{i=1}^{4} \hat{w}_i(t), \\
\hat{K}(t) &= \hat{B}_p^\dagger(t) \sum_{i=1}^{5} \hat{w}_i(t) B_i K_i, \\
\hat{L}(t) &= \hat{B}_p^\dagger(t) \sum_{i=1}^{5} \hat{w}_i(t) B_i L_i, \\
u(t) &= \hat{K}(t) x_p(t) + \hat{L}(t) r(t).
\end{aligned}$$

MMRAC simulations are compared to a direct adaptive control technique using a single-model MRAC from Section 2.4.6. The simulations consider the same initial condition for the system, the same reference, and the initial gains are calculated according to (4.11), and (4.12), with $t = 0$.

The first set of results are performed for the case of no measurement or process noise. In Figure 4.3(a) we see the time evolution of each of the states for the reference model, the states generated by the MMRAC, and the states generated by MRAC. Convergence is achieved for both controllers, with a clear advantage of the multiple-model technique while using approximately the same control effort, as depicted in Figure 4.3(b). The convergence speed is a key factor to consider, and there is a clear advantage of using multiple models when we analyze the dynamics of the error. In Figure 4.4 we compare the time evolution of the norm of the error for the case of MMRAC, and MRAC. To better visualize the advantage in convergence speed, we present the norm of the error in log-scale in Figure 4.5, and we perform a linear regression (LR) on each of the signals. The slope coefficient of the LR provides insight into the rate at which the error decreases, i.e., a the largest negative

slope indicates a faster reduction in the error magnitude. The slope coefficients of the LR are -0.0333 for the MMRAC case, and -0.0103 for the single-model controller. This shows that the MMRAC scheme is approximately two orders of magnitude faster than the single-model approach, for this simulation. This matches with the conjecture in [61]. Finally, as mentioned in Section 3.1, we achieve asymptotic convergence of the estimated system's matrices. In Figures 4.7(a) and 4.7(b) we see the asymptotic convergence of each entry of the matrix pairs $\begin{bmatrix}\hat{A}_p(t) & \hat{B}_p(t)\end{bmatrix}$ to $\begin{bmatrix}A_p & B_p\end{bmatrix}$, respectively, and in Figure 4.6 we present the time evolution of the estimate $\hat{w}(t)$. Note that for every time, the sum of all of the $\hat{w}_i(t) = 1$.

The second set of results are performed for the case of measurement and process white noise with a mean value of 0 and a variance of 0.01. In Figure 4.8(a) we present the time response of the states generated by the MMRAC and the MRAC, as well as the reference states $x_r(t)$. The error between the reference states and the states of the plant remain bounded (as seen in Figure 4.9), and the control effort for both controllers is similar, as shown in Figure 4.8(b). We obtain estimates $\begin{bmatrix}\hat{A}_p(t) & \hat{B}_p(t)\end{bmatrix}$ whose errors remain bounded. The time evolution of $\hat{A}_p(t)$, $\hat{B}_p(t)$, and $\hat{w}(t)$ can be seen in Figures 4.10, 4.11(a) and 4.11(b), respectively. Note that for every time, the sum of all of the $\hat{w}_i(t) = 1$. In the simulation, we observe that the performance is preserved in the presence of noise.

Finally, we perform a statistical study of the performance of the controllers without noise and with noise. For the system explained above, we ran 1000 experiments with random initial conditions, lasting 30 seconds each. The results are presented as box-and-whisker plots and a table. The outliers are presented in the box-and-whisker plots as circles, and represent values that are outside of the 99.3% of the distribution. In Figure 4.12(a) we see that the MMRAC reduces the infinity norm of the tracking error in both the noisy and noise free cases. Moreover, performing a LR on $\log_{10}\|e\|$ and analyzing the slopes, the simulations show that the tracking error converges to zero faster for the MMRAC case, as presented in Figure 4.12(b). This improvement of the convergence speed increases the median control effort by less than 10%, as shown in Figure 4.12(c). A summary of the results is presented in Table 4.1.

In summary, the simulations show that using MMRAC we can achieve better performance by moderately increasing the control effort. This behavior is maintained even in the case of measurement and process noise.

4.2 Application of MMRAC to Motion Control of Lateral Vehicle Dynamics

In this section, we apply the MMRAC scheme to the problem of motion control of lateral vehicle dynamics. The results were published in [40]. We begin by describing the problem.

Consider the following widely used simplifying modeling assumptions [64]:

- All forces act on a plane flat road. The effect of the altitude of the center of gravity is neglected.
- The equations of motion are linearized. The tire force is assumed proportional to the slip angle.

Under these assumptions, the free-body diagram of the lateral vehicle dynamics using a bicycle model is presented in Figure 4.13. The system is represented by the state-space model

$$\dot{x}_p(t) = A_p(\eta)x_p(t) + B_p(\eta)u(t),\ x_p(0) = x_{p0}, \tag{4.22}$$

with state $x_p(t) \coloneqq \begin{bmatrix}\beta(t) & \dot{\psi}(t)\end{bmatrix}^\top \in \mathbb{R}^2$ and input $u(t) \coloneqq \begin{bmatrix}\delta(t) & M_z(t)\end{bmatrix}^\top \in \mathbb{R}^2$, where β is the side-slip angle, r is the yaw rate, M_z is the yaw moment about the z-axis, $\delta = \delta_d + \delta_c$ is the total steering angle of the front wheels resulting from addition of the driver command δ_d and the corrective steering control input δ_c. The system matrices $A_p(\eta) \in \mathbb{R}^{2\times 2}$ and $B_p(\eta) \in \mathbb{R}^{2\times 2}$ are unknown due to uncertain variations in cornering stiffness and longitudinal force capacities of the tires and are parameterized in the form

$$\begin{aligned} A_p(\eta) &= A_{p1} + \eta_f A_{p2} + \eta_r A_{p3}, \\ B_p(\eta) &= \eta_f B_{p1} + \eta_x B_{p2}, \end{aligned} \tag{4.23}$$

where

$$\begin{aligned} A_{p1} &= \begin{bmatrix} 0 & -1 \\ 0 & 0 \end{bmatrix}, A_{p2} = \begin{bmatrix} \frac{-C_f}{mv_x} & \frac{l_f C_f}{mv_x^2} \\ \frac{-l_f C_f}{I_z} & \frac{-l_f^2 C_f}{I_z v_x} \end{bmatrix}, A_{p3} = \begin{bmatrix} \frac{-C_r}{mv_x} & \frac{l_r C_r}{mv_x^2} \\ \frac{l_r C_r}{I_z} & \frac{-l_r^2 C_r}{I_z v_x} \end{bmatrix}, \\ B_{p1} &= \begin{bmatrix} \frac{C_f}{mv_x} & 0 \\ \frac{l_f C_f}{I_z} & 0 \end{bmatrix}, B_{p2} = \begin{bmatrix} 0 & 0 \\ 0 & \frac{1}{I_z} \end{bmatrix}, \end{aligned} \tag{4.24}$$

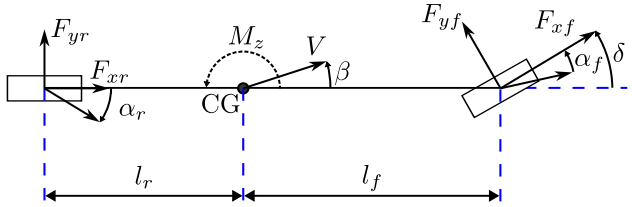


Figure 4.13: Free-body diagram for lateral vehicle dynamics using a bicycle model.

where m is the mass of the vehicle, I_z is the moment of inertia about the z-axis, v_x is the longitudinal velocity, l_f and l_r are the distance from the center of gravity to the front and rear wheels, respectively, C_f and C_r are the cornering stiffness coefficients for the front and rear tires, respectively. The entries of $\eta = \begin{bmatrix}\eta_f & \eta_r & \eta_x\end{bmatrix}^\top$, in order, parameterize the uncertainties in front tire cornering stiffness, rear tire cornering stiffness, and longitudinal tire force capacity, where $\eta = \begin{bmatrix}1 & 1 & 1\end{bmatrix}^\top$ represents the nominal model case. The upper and lower bounds of the uncertainty parameters η_i for $i \in \{f, r, x\}$ are assumed to be known in the form

$$\eta_{i\,\min} \leq \eta_i \leq \eta_{i\,\max}, \tag{4.25}$$

where $0 < \eta_{i\,\min} < 1$ and $\eta_{i\,\max} > 1$. These parameter ranges correspond to the polytope generated by taking the minimum and maximum values of every entry of the matrices A_p and B_p. Under these assumptions, the model is fit to accurately describe the dynamics under normal driving conditions [18].

Problem Definition

The control objective is to design a state-feedback controller such that the closed-loop plant state x_p asymptotically tracks the desired state x_r generated by the reference model (4.2), which represents ideal driving behavior on optimal dry road conditions. The constant matrices $A_r \in \mathbb{R}^{2\times 2}$ and $B_r \in \mathbb{R}^{2\times 2}$ are known, A_r is Hurwitz, and $r : [0, \infty) \to \mathbb{R}^2$ is a known, bounded, piecewise continuous input to the reference model. For the case of lateral vehicle dynamics, we expect the car to achieve the yaw rate, with the minimum possible side-slip, i.e., we expect the car to behave as if the road had a very high friction coefficient.

Assumption Verification

We begin by verifying that the model (4.22) satisfies Assumptions 4.1 and 4.2 for any physically meaningful values of the plant parameters. First, to verify Assumption 4.1 we

need to be able to invert the matrix B_p. Re-writing (4.23) with the definitions from (4.24) we obtain

$$B_p(\eta) = \eta_f \begin{bmatrix} \frac{C_f}{mv_x} & 0 \\ \frac{l_f C_f}{I_z} & 0 \end{bmatrix} + \eta_x \begin{bmatrix} 0 & 0 \\ 0 & \frac{1}{I_z} \end{bmatrix}. \tag{4.26}$$

Note that the parameters C_f, m, v_x, l_f, and I_z need to be strictly greater than zero to be physically meaningful during forward motion. This implies that, since the values of $\eta_{f\,\min}$ and $\eta_{x\,\min}$ are strictly positive, the matrix B_p will be lower triangular with positive values on the main diagonal, hence it will always have a positive determinant, which implies that it will always be invertible. With these considerations we can calculate K^* and L^* from (4.3) and (4.4), respectively.

To satisfy Assumption 4.2 we need to select the fixed models pairs $\begin{bmatrix} A_i & B_i \end{bmatrix}$, for $i \in \{1, \cdots, N\}$. We consider all possible combination of minimums and maximums of η_f, η_r, and η_x to obtain eight corner models. This selections guarantees that B_p is in the interior of some convex combination of the corner model, and Assumption 4.2 is satisfied. Note that this selection process does not minimize the number of corner models. The corner model pairs are as follows:

$$\begin{aligned} A_i &= A_{p1} + \eta_{fi} A_{p2} + \eta_{ri} A_{p3}, \\ B_i &= \eta_{fi} B_{p1} + \eta_{xi} B_{p2}, \end{aligned} \tag{4.27}$$

where $i \in \{1, \cdots, 8\}$, and

$$\begin{aligned} \eta_{fi} &= \begin{cases} \eta_{f\,\min}, & \text{if } i = \{1,3,5,7\} \\ \eta_{f\,\max}, & \text{if } i = \{2,4,6,8\}, \end{cases} \\ \eta_{ri} &= \begin{cases} \eta_{r\,\min}, & \text{if } i = \{1,2,5,6\} \\ \eta_{r\,\max}, & \text{if } i = \{3,4,7,8\}, \end{cases} \\ \eta_{xi} &= \begin{cases} \eta_{x\,\min}, & \text{if } i = \{1,2,3,4\} \\ \eta_{x\,\max}, & \text{if } i = \{5,6,7,8\}. \end{cases} \end{aligned} \tag{4.28}$$

From (4.23) and (4.24) and strictly positive η_f and η_x are, the determinant of B_i is strictly greater than zero, for every $i \in \{1, \cdots, 8\}$. This implies that any convex combination of the B_i matrices will have a strictly positive determinant, which further implies that any convex combination of the B_i matrices is invertible, hence the proposed controller can be applied to the uncertain model of lateral vehicle dynamics.

Table 4.2: Values used to run simulations.

Symbol	Value	Meaning
m	1140 kg	Mass of the car
I_z	1020 kgm^2	Moment of inertia about the yaw-axis
l_f	1.165 m	Distance from CG to the front wheel
l_r	1.165 m	Distance from CG to the rear wheel
v_x	100 m/s	Longitudinal velocity
C_f	86849 N/rad	Front tire cornering stiffness
C_r	90950 N/rad	Rear tire cornering stiffness
λ	20	Linear filter design parameter
Γ	$50\mathbb{I}_{7\times 7}$	Symmetric matrix to tune convergence speed

Finally, we can calculate the gains K_i and L_i, for $i \in \{1, 2 \cdots, 8\}$ as

$$K_i = B_i^{-1}(A_r - A_i),$$
$$L_i = B_i^{-1}B_r.$$

Selecting a value of $\lambda > 0$, and a positive definite matrix $\Gamma \in \mathbb{R}^{7\times 7}$, the full controller is described by Equations (3.7), (3.25), (4.11), (4.12) and (4.15), with $N = 8$.

Simulation Results

The simulation results are presented here, and we compare the performance of the MMRAC scheme with other controllers. The parameters used to run the simulations are in Table 4.2. Moreover, all the uncertainty of the system and the time-variations satisfies (4.25) with

$$\eta_{i\min} = 0.1,\ \eta_{i\max} = 1.3,\ i \in \{f, r, x\}. \tag{4.29}$$

With these values, we fixed the corner systems, and we track the states generated by the reference model defined by

$$A_r = \begin{bmatrix} -13.6 & 1.96 \\ 17 & -18.85 \end{bmatrix},\ B_r = \begin{bmatrix} 6.8 & 0 \\ 124.67 & 0.001 \end{bmatrix}.$$

First, we present a set of simulations that assumes a constant unknown value of $\eta_f = \eta_r = \eta_x = 1$. We compare the proposed multiple-model technique with a single model

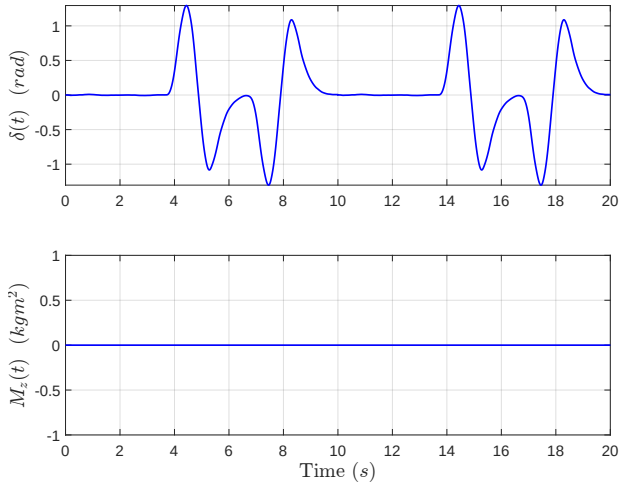
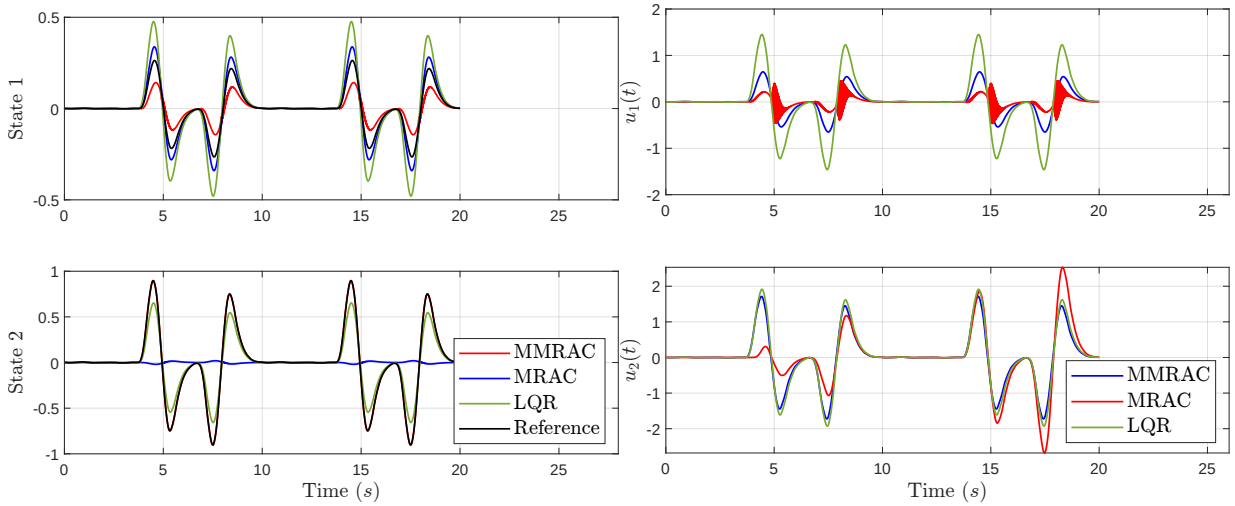


Figure 4.14: $r(t)$ for the reference model.



(a)States of the system for different control techniques assuming $\eta = \begin{bmatrix} 1 & 1 & 1 \end{bmatrix}^\top$.

(b)Control effort of the different control techniques assuming $\eta = \begin{bmatrix} 1 & 1 & 1 \end{bmatrix}^\top$.

Figure 4.15: Constant $\eta = \begin{bmatrix} 1 & 1 & 1 \end{bmatrix}^\top$. On the left: Time evolution of the states of the system and the reference model for MRAC and MMRAC. On the right: Control effort for MRAC and MMRAC.

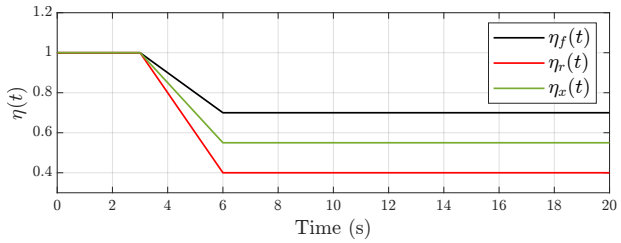
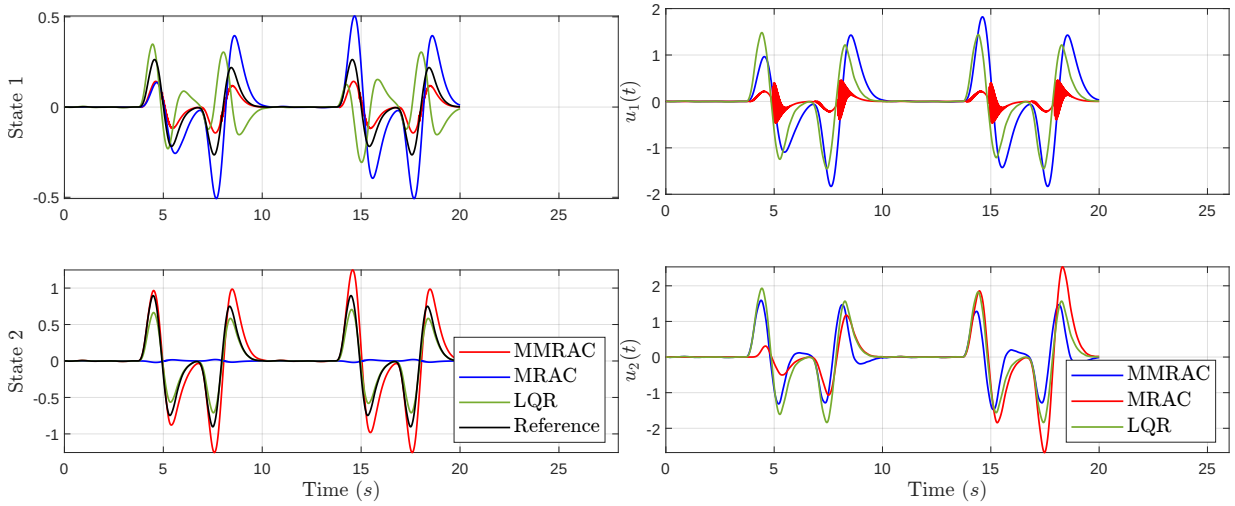


Figure 4.16: Time-variation of $\eta(t)$.



(a)States of the system for different control techniques assuming $\eta = \eta(t)$.

(b)Control effort of the different control techniques assuming $\eta = \eta(t)$.

Figure 4.17: The vector $\eta(t)$ changes as shown in Figure 4.16. On the left: Time evolution of the states of the system and the reference model for MRAC and MMRAC. On the right: Control effort for MRAC and MMRAC.

reference adaptive controller, and a single model optimal LQR controller. The reference signal $r(t)$ shown in Figure 4.14 represents a change of lanes, and was obtained on CarSim. In Figure 4.15(a) we observe that MMRAC and MRAC are able to track the desired side-slip and LQR has the largest error. When we look at the yaw rate instead, we see that LQR and MMRAC are able to track the desired state, but not the MRAC control. As observed in Figure 4.15(b) the control efforts applied are comparable, which suggests that there is an advantage in using the proposed MMRAC scheme.

Finally, we present a set of simulations that assumes that the unknown parameter η is slowly time-varying, and takes values contained in the set (4.29) as shown in Figure 4.16. Once again, we compare the results with an MRAC technique and an LQR controller. In Figure 4.17(a) we observe that the MMRAC scheme alone tracks the desired side-slip, and MMRAC and LQR are able to track the desired yaw rate, with similar control efforts, as shown in Figure 4.17(b). Simulations with time-varying parameters show clear advantages of using the proposed MMRAC scheme over single model controllers.

Chapter 5

Multiple-Model Adaptive Pole Placement Control (MMAPPC) with Blending

This chapter deals with pole placement of uncertain systems using multiple models, defined as Multiple-Model Adaptive Pole Placement Control (MMAPPC). In Section 5.1, the attention is focused on systems where all the states are available for feedback. For this type of system, we analyze the performance of the controller on the problem of motion control of lateral vehicle dynamics. In the end, we combine a Multiple-Model Parameter Identification (MMPI) with a Multiple-Model State Estimation (MMSE) to develop an output-feedback MMAPPC. Performance is evaluated, and statistical analysis shows the advantages over single-model approaches.

5.1 State-Feedback MMAPPC of Square MIMO Systems

Consider the Multiple-Input, Multiple-Output (MIMO), Linear, Time-Invariant (LTI) system

$$\dot{x}_p(t) = A_p x_p(t) + B_p u(t),\ x_p(0) = x_{p0},\ t \geq 0, \tag{5.1}$$

where $A_p \in \mathbb{R}^{n\times n}$ and $B_p \in \mathbb{R}^{n\times n}$ are unknown constant matrices, $x_p(t) \in \mathbb{R}^n$ is the state of the system and available for feedback, $u(t) \in \mathbb{R}^n$ is the control input.

The goal is to design a state feedback controller of the form

$$u(t) = K(t)x_p(t), \tag{5.2}$$

where $K(t) \in \mathbb{R}^{n\times n}$, which drives all the states of the system to zero, by placing the poles of the closed-loop system at desired locations, i.e., satisfying

$$\sigma(A_p + B_pK) = \Lambda, \tag{5.3}$$

where Λ is a conjugate symmetric set of n closed-loop desired poles in $\mathbb{C}^-$. In order to do that, we will assume that B_p is invertible to guarantee that there exists K^* such that $\sigma(A_p + B_pK^*) = \Lambda$ [87]. The regulation control problem described above involves online parameter identification of the system matrices $\Theta_p = \begin{bmatrix} A_p & B_p \end{bmatrix}$, as explained in Section 3.1. Defining $\mathcal{S}$ as in (3.4), we make the following assumption.

Assumption 5.1. *There exist a finite set $\mathcal{S}$ of known system matrices $\begin{bmatrix} A_i & B_i \end{bmatrix} \in \mathbb{R}^{n\times(2n)}$, such that*

(i) $\begin{bmatrix} A_p & B_p \end{bmatrix} \in \text{int}\,(\text{conv}\,(\mathcal{S}))$.

(ii) Every convex combination of the B_i is non-singular.

The first item of Assumption 5.1 is a natural consequence of performing system identification. We require Assumption 5.1 (ii) to ensure that we do not have redundant inputs, or we do not drop rank of the number of inputs, losing control authority of the system. Given a set $\mathcal{S}$, there exist numerical methods to verify whether every convex combinations of the B_i's is non-singular [33].

Every point of the polytope $\text{conv}\,(\mathcal{S})$ can be expressed as a convex combination of the corner models $\begin{bmatrix} A_i & B_i \end{bmatrix}$, which implies that $\mathcal{W}$ defined in (3.5) is non-empty, and the problem of identifying the unknown system matrix $\begin{bmatrix} A_p & B_p \end{bmatrix}$ is equivalent to the problem of identifying a vector $w \in \mathcal{W}$.

5.1.1 Control Design

Our MMAPPC design will utilize a blending-based MMPI scheme defined in Section 3.1 that generates estimates $\begin{bmatrix} \hat{A}_p(t) & \hat{B}_p(t) \end{bmatrix}$ of $\begin{bmatrix} A_p & B_p \end{bmatrix}$, as a weighted sum of the corner models. The weights are used to blend the information coming from every corner model

to generate a single gain K^* that drives all states of the plant to zero. In this section, we provide the design, stability and convergence analysis of the MMAPPC scheme.

The process of creating the multiple-model controller begins with an offline design stage in which N gains are calculated. Let $A_r \in \mathbb{R}^{n\times n}$ be *any* matrix such that $\sigma(A_r) = \Lambda$. Then, let $K_i \in \mathbb{R}^{n\times n}, i \in \{1, \cdots, N\}$, be defined as

$$K_i = B_i^{-1}(A_r - A_i), \tag{5.4}$$

which in turn implies that

$$A_i + B_i K_i = A_r \tag{5.5}$$

Let $K^* \in \mathbb{R}^{n\times n}$ be defined as

$$K^* \coloneqq B_p^{-1}(A_r - A_p), \tag{5.6}$$

and let $w \in \mathcal{W}$. From (5.5) and (5.6) we have

$$\begin{aligned} B_p K^* &= \sum_{i=1}^{N} w_i (A_i + B_i K_i) - A_p \\ &= \sum_{i=1}^{N} w_i B_i K_i. \end{aligned} \tag{5.7}$$

Comparing the left and right hand side of (5.7) we can isolate the gain K^* as

$$K^* = B_p^{-1} \sum_{i=1}^{N} w_i B_i K_i. \tag{5.8}$$

The final step is to use the certain equivalence principle and replace the values of B_p and w_i by the estimates obtained using the recursive adaptive algorithm with parameter projection (3.25) to design a MMAPPC scheme to achieve the adaptive state tracking control task stated in Section 5.1. Equation (5.8) motivates the following estimate of K^*

$$K(t) = \hat{B}_p^{-1}(t) \sum_{i=1}^{N} \hat{w}_i(t) B_i K_i, \tag{5.9}$$

where $\hat{B}_p^{-1}(t)$ is the inverse of

$$\hat{B}_p(t) = \sum_{i=1}^{N} \hat{w}_i(t) B_i. \tag{5.10}$$

The complete schematics of the state-feedback MMAPPC approach can be seen in Figure 5.1.

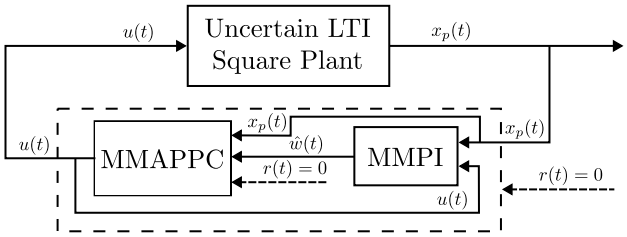


Figure 5.1: Block diagram of the proposed state-feedback MMAPPC.

5.1.2 Stability Analysis

The stability result is now presented.

Theorem 5.1. *Consider the plant (5.1). If Φ satisfies the persistence of excitation condition (2.4), B_p is invertible, and Assumption 5.1 holds, then the MMAPPC scheme (3.7), (3.9), (3.11), (3.25), (5.2), (5.9) and (5.10) guarantees that for any initial conditions of the plant (5.1), all closed-loop signals are bounded and $x_p(t)$ asymptotically converges to zero.*

Proof. Let $x_p(0) = x_{p0}$ be an arbitrary initial state of the plant. Fix $\Lambda \subset \mathbb{C}^-$ to be a conjugate symmetric set of n complex numbers, and let $A_r \in \mathbb{R}^{n\times n}$ be *any* matrix such that $\sigma(A_r) = \Lambda$.

Using the fact that B_p is non-singular, then the equation $A_p + B_p K^* = A_r$ has a unique solution. Combining this with Equations (5.8) and (5.9) and Corollary 4.3 we get that $K(t)$ is bounded, and asymptotically converges to K^*. This is because Π is compact and every convex combination of B_i is non-singular by Assumption 5.1, then the inverse of $\hat{B}_p(t)$ exists, and it is bounded. Combining this fact with Equation (5.9) we get that $K(t)$ is bounded. The remainder of the argument that $K(t)$ converges to K^* is similar to the proof of Corollary 4.3.

Substituting (5.2) into (5.1) we get

$$\begin{aligned}\dot{x}_p(t) &= A_p x_p(t) + B_p u(t)\\ &= (A_p + B_p K(t)) x_p(t).\end{aligned}$$

Adding and subtracting $B_p K^* x_p(t)$, defining $\tilde{K}(t) \coloneqq K(t) - K^*$, we get

$$\begin{aligned}\dot{x}_p(t) &= (A_p + B_p K^*) x_p(t) + B_p \tilde{K}(t) x_p(t)\\ &= A_r x_p(t) + B_p \tilde{K}(t) x_p(t).\end{aligned}$$

Let $Q \in \mathbb{R}^{n\times n}$ be a fixed, symmetric, and positive definite matrix. Then take $P \in \mathbb{R}^{n\times n}$ to be the unique positive definite and symmetric solution of $PA_r + A_r^\top P + Q = 0$. Consider the positive definite function

$$V\left(x_p(t)\right) = x_p^\top(t) P x_p(t). \tag{5.11}$$

Taking the time derivative of (5.11) we get

$$\dot{V}\left(x_p(t)\right) = 2x_p^\top(t) P \dot{x}_p(t) = x_p^\top(t)(PA_r + A_r^\top P)x_p(t) + 2x_p^\top(t) B_p \tilde{K}(t) x_p(t). \tag{5.12}$$

Hence, (5.12) can be rewritten as

$$\dot{V}\left(x_p(t)\right) = -x_p^\top(t) Q x_p(t) + 2x_p^\top(t) B_p \tilde{K}(t) x_p(t).$$

Defining $c(t) \coloneqq 2\|B_p \tilde{K}(t)\|$, we have

$$\dot{V}(x_p(t)) \leq -\left(\lambda_{\min}(Q) - c(t)\right)\|x_p(t)\|^2, \tag{5.13}$$

where $\lambda_{\min}(Q) > 0$ is the minimum eigenvalue of Q. If $\Phi(t)$ is Persistently Exciting (PE), then $\tilde{K}(t)$ converges to zero asymptotically, which lets us conclude that $c(t)$ is bounded, and there exists $t_1 \geq 0$ such that $\lambda_{\min}(Q) > c(t)$ for all $t \geq t_1$.

This implies that for all $t \geq t_1$ we get that $\dot{V} < 0$, and we can conclude that x_p is bounded, which finally implies that u is bounded, showing that all signals in the closed-loop system are bounded. Combining this with the fact that $K(t)$ is bounded, and asymptotically converges to K^*, we get

$$\lim_{t\to\infty} \left(\dot{V}(x_p(t)) + x_p^\top(t) Q x_p(t)\right) = 0.$$

This implies that $x_p(t)$ converges asymptotically to 0. Lastly, we can see that

$$\lim_{t\to\infty} \sum_{i=1}^{N} \hat{w}_i(t)\left(A_i + B_i K_i\right) = A_p + B_p K^*, \tag{5.14}$$

obtaining the desired eigenvalues for the closed-loop system. □

Since the selection of A_r is not unique, different choices based on *a priori* knowledge of the plant may help reduce numerical problems and improve performance.

5.2 Application of MMAPPC with State Feedback to the Motion Control of Lateral Vehicle Dynamics

In this subsection, we apply the state-feedback MMAPPC scheme from Section 5.1 to the motion control of lateral vehicle dynamics with uncertainty described in Section 4.2. The parameters used to run the simulations are in Table 4.2. The results are compared to a single-model optimal pole placement control scheme. Dynamical uncertainty and measurement noise are considered.

Since we are using the same values as in Section 4.2, then Assumption 5.1 is satisfies, because Assumption 4.2 is also satisfied. The corner model pairs are defined as in (4.27), where $i \in \{1, \cdots, 8\}$, and the η's are defined as in (4.28) and represent the extreme values found in (4.29). With these values, each matrix B_i is invertible so Assumption 5.1 is satisfied. Note that for the nominal value $\eta = \begin{bmatrix} 1 & 1 & 1 \end{bmatrix}^\top$, B_p is also invertible. The desired closed-loop poles for the system are $\Lambda = \{-11.67, -22.23\}$, and we select A_r as

$$A_r = \begin{bmatrix} 0 & 1 \\ -256.42 & -33.9 \end{bmatrix}. \tag{5.15}$$

The single-model adaptive pole placement control scheme follows the steps shown in [27] with the same closed-loop poles and initial condition as the MMAPPC. This optimal controller is designed using a constant nominal model using the nominal model (A, B), where

$$A = \sum_{i=1}^{8} \hat{w}_i(0) A_i,$$
$$B = \sum_{i=1}^{8} \hat{w}_i(0) B_i,$$

and $\hat{w}(0) = [0.05,\ 0.1,\ 0.03,\ 0.08,\ 0.1,\ 0.02,\ 0.2,\ 0.42]^\top$. For the Riccati equations we use $Q = \text{diag}(4, 10^4)$ and $R = \text{diag}(10^4, 1)$, which places the poles optimally at $\Lambda = \{-11.67, -22.23\}$.

Simulation Results

We present a set of simulations in which the parameter η slowly varies over time, within the set generated by (4.25) and (4.29), as shown in Figure 4.16. The system begins with

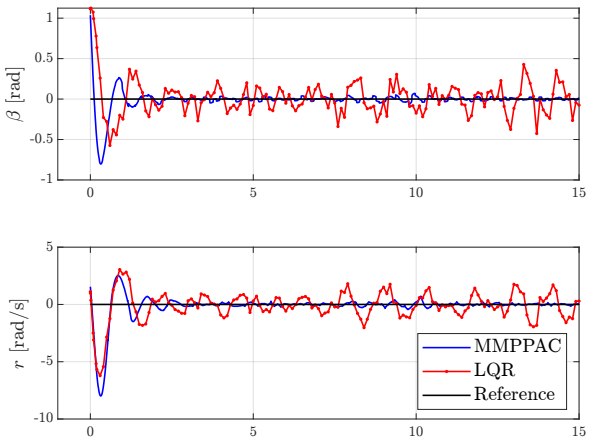


Figure 5.2: States of the system for different control techniques assuming $\eta = \eta(t)$.

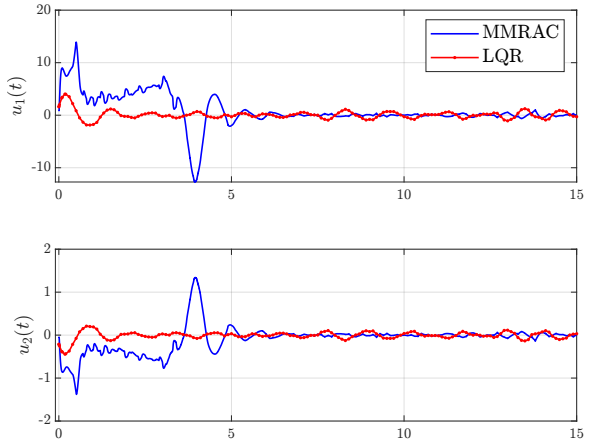


Figure 5.3: Control effort of the different control techniques assuming $\eta = \eta(t)$.

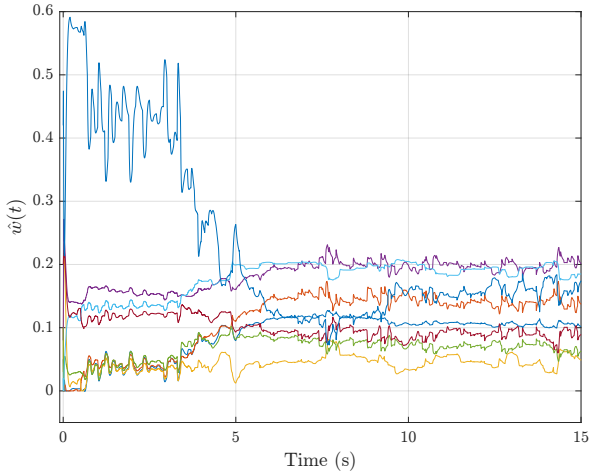


Figure 5.4: Time evolution of the weight vector $\hat{w}(t)$ when $\eta = \eta(t)$.

an initial condition not equal to zero, and we show how the states get regulated. To show the robustness of the algorithm, we include dynamical uncertainty, as well as measurement noise in the form of white noise with a variance of 0.01. In Figure 5.2 we see that the states of the system are driven to zero by both the MMAPPC and the LQR controllers, in a similar time. It was observed that the MMAPPC behaved better in the presence of noise; the effects of uncertainty and noise were more evident in the simulations of LQR. This robustness to noise comes with a small increase in control effort, as seen in Figure 5.3. In Figure 5.4 we see the time evolution of the estimate $\hat{w}(t)$. Note that for every time, the sum of all $\hat{w}_i(t) = 1$.

5.3 Output-Feedback MMAPPC of SISO Systems

Consider a linear, time-invariant, single-input, single-output system

$$\begin{aligned} \dot{x}_p(t) &= A_p x_p(t) + B_p u(t),\ x_p(0) = x_{p0},\ t \geq 0, \\ y_p(t) &= c_p^\top x_p(t), \end{aligned} \tag{5.16}$$

where $A_p \in \mathbb{R}^{n\times n}$, $b_p \in \mathbb{R}^n$ are unknown constant matrices, $c_p \in \mathbb{R}^n$, $x_p(t) \in \mathbb{R}^n$ is the state of the system, $y_p(t) \in \mathbb{R}$ is the measurable output of the system, $u(t) \in \mathbb{R}$ is the control input.

The objective is to design a controller that drives all states of the system (5.16) to zero and that guarantees boundedness of all closed-loop signals. The approach that we take to

solve the aforementioned control problem is to design an output-feedback controller that first estimates the states of the plant x_p as shown in Section 3.2. With these estimates, we develop an adaptive pole placement controller using multiple models that places the closed-loop eigenvalues of the system at a desired predetermined location selected by the control designed as in Section 3.3. For this purpose, we make the following standing assumption.

Assumption 5.2. *The uncertain matrix pairs* (A_p, b_p) *and* $\left(A_p, c_p^\top\right)$ *are controllable and observable, respectibly. Moreover, the system* (5.16) *is in observable canonical form.* △

In particular, Assumption 5.2 imposes that the matrices (5.16) have the structure of (3.27). The state-space representation of a system is not unique; any rational scalar transfer function $G(s)$ has an observable (canonical) realization. This means that Assumption 5.2 holds for a large class of systems.

Our approach to solving the problem described above involves online parameter identification of the uncertain vector $\Theta_p = \begin{bmatrix} b_p \\ a_p \end{bmatrix}$ by defining a compact, convex, uncertainty polytope such that at every extreme point of the polytope there is a known corner model as explained in Section 3.2. We combine the corner model's parameters in a vector $\Theta_i \coloneqq \begin{bmatrix} b_i^\top & a_i^\top \end{bmatrix}^\top$, $i \in \{1, \cdots, N\}$ to redefine $\mathcal{S} = \{\Theta_1, \cdots, \Theta_N\}$.

Assumption 5.3. *There exist a finite set* $\mathcal{S}$ *of known system matrices, such that*

(i) $\Theta_p \in \operatorname{int}(\operatorname{conv}(\mathcal{S}))$.

(ii) Every convex combination of the (A_i, b_i) *and* $\left(A_i, c_p^\top\right)$ *is strongly controllable and strongly observable, respectively.*

△

Item (ii) is a technical result needed to ensure that the generated estimates of the system are both controllable and observable, at all times. The fixed models correspond to each of the corners of the uncertainty bounding set explained in [6].

Every point of the polytope $\operatorname{conv}(\mathcal{S})$ can be expressed as a convex combination of the corner models Θ_i, which implies that the following set is non-empty:

$$\mathcal{W} \coloneqq \left\{ w \in [0,1]^N : \Theta_p = \sum_{i=1}^{N} w_i \Theta_i, \sum_{i=1}^{N} w_i = 1 \right\}. \tag{5.17}$$

Consequently, the problem of identifying the unknown vector Θ_p is equivalent to the problem of identifying a vector $w \in \mathcal{W}$.

5.3.1 Control Design

Here, we design the control input signal $u(t)$ so that all states of the system are driven to zero by placing the eigenvalues of the closed-loop state matrix at the desired locations selected by the control designer. As motivation, we first consider the problem assuming known plant parameters and then use certain equivalence to replace the unknown parameters in the control law with their estimates. In the end, we provide a complete stability and convergence analysis of the closed-loop system.

The recursive adaptation law with parameter projection (3.36) is used in combination with the state estimator (3.40) and Remark 3.8 to develop a MMAPPC scheme that satisfies the control requirements.

Given a set of n desired eigenvalues with conjugate symmetry and negative real part, let A_c^* be the matrix

$$A_c^* = \left[\begin{array}{c|c} -a_c^* & \mathbb{I}_{n-1} \\ \hline 0 & \end{array}\right]$$

with the desired eigenvalues. In the absence of uncertainty, we can define K_c as the gain matrix which satisfies

$$\sigma(A_p - b_p K_c) = \sigma(A_c^*).$$

Then, we can design a multiple model pole placement controller by using the state estimate (3.39) to obtain

$$u(t) = -K_c \hat{x}_p(t). \tag{5.18}$$

In the absence of uncertainty, the control law (5.18) guarantees that all closed-loop signals are bounded, and the estimated state $\hat{x}_p$ converges exponentially fast to x_p. In addition, x_p converges to zero exponentially fast [27]. When we introduce uncertainty and use certain equivalence, the control law (5.18) becomes

$$u(t) = -\hat{K}_c(t) \hat{x}_p(t), \tag{5.19}$$

where $\hat{K}_c(t)$ is the solution to

$$\sigma(\hat{A}_p(t) - \hat{b}_p(t)\hat{K}_c(t)) = \sigma(A_c^*). \tag{5.20}$$

The solution $\hat{K}_c(t)$ to (5.20) exists by Assumption 5.3, and is computed in real-time using Ackermann's formula [86].

The complete schematics of the output-feedback MMAPPC approach can be seen in Figure 5.5.

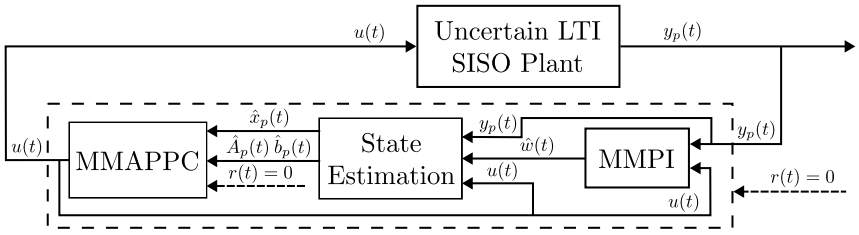


Figure 5.5: Block diagram of the proposed output-feedback MMAPPC.

5.3.2 Stability Analysis

The main stability result is now presented.

Theorem 5.2. *Consider the plant (5.16) that satisfies Assumptions 5.2 and 5.3. Then, the MMAPPC scheme consisting of (3.36), (3.40), (5.19) and (5.20) guarantees that for any*

(i) initial conditions of the plant (5.16),

(ii) initial conditions of the state estimator (3.40),

(iii) Hurwitz matrices A_o^* and A_c^*,

all closed-loop signals are bounded and x_p converges asymptotically to zero.

The proof of this theorem is based on the following result.

Theorem 5.3 ([27, Theorem 6.4.3])**.** *Consider the Single-Input, Single-Output (SISO), LTI plant*

$$y_p = G_p(s)u, \quad G_p(s) = \frac{Z_p(s)}{R_p(s)},$$

where $G_p(s)$ is strictly proper, $R_p(s)$ is monic of known degree n, $Z_p(s)$ and $R_p(s)$ are coprime.

Let $\hat{Z}_p$ and $\hat{R}_p$ be the estimates of $Z_p(s)$ and $R_p(s)$, respectively. Assume that $\hat{Z}_p$ and $\hat{R}_p$ are strongly coprime at each time t. Then, all signals in the closed-loop adaptive pole

placement control scheme

$$
\begin{aligned}
\varepsilon(t) &= \frac{z(t) - \hat{w}^\top(t)\phi_p(t)}{m_s^2(t)}, \\
m_s^2(t) &= 1 + \|\phi(t)\|^2, \\
\dot{\hat{w}}_p(t) &= \Gamma\varepsilon(t)\phi_p(t), \\
\hat{A}_p(t) &= \sum_{i=1}^{N} \hat{w}_i(t) A_i, \\
\hat{b}_p(t) &= \sum_{i=1}^{N} \hat{w}_i(t) b_i, \\
\hat{K}_o(t) &= a_0^* - \hat{a}_p(t), \\
\dot{\hat{x}}_p(t) &= \hat{A}_p(t)\hat{x}_p(t) + \hat{b}_p(t)u(t) - \hat{K}_o(t)C\hat{x}_p(t), \\
\sigma(A_c^*) &= \sigma(\hat{A}_p(t) - \hat{b}_p(t)\hat{K}_c(t)), \\
u(t) &= -\hat{K}_c(t)\hat{x}_p(t),
\end{aligned}
$$

are uniformly bounded, and y_p converges to zero asymptotically with time.

Proof. Let $x_p(0) = x_{p0}$, $\hat{x}_p(0) = \hat{x}_{p0}$, A_o^* and A_c^* be fixed Hurwitz matrices. To study the closed-loop stability, we will develop the closed-loop error equations. Replacing (5.19) into the observer error dynamics equation (3.41) we get

$$
\dot{e}_o(t) = A_o^* e_o(t) - \tilde{a}_p(t) y_p(t) - \tilde{b}_p(t)\hat{K}_c(t)\hat{x}_p(t). \tag{5.21}
$$

Replacing (5.19) into (3.40) we get

$$
\begin{aligned}
\dot{\hat{x}}_p(t) &= \hat{A}_p(t)\hat{x}_p(t) - \hat{b}_p(t)\hat{K}_c(t)\hat{x}_p(t) + \hat{K}_o(t)(c_p^\top \hat{x}_p(t) - y_p(t)) \\
&= (\hat{A}_p(t) - \hat{b}_p(t)\hat{K}_c(t))\hat{x}_p(t) - \hat{K}_o(t)c_p^\top e_o(t) \\
&= A_c^*\hat{x}_p(t) - \hat{K}_o(t)c_p^\top e_o(t).
\end{aligned} \tag{5.22}
$$

Combining (5.21) and (5.22) we get that the output error can be computed as

$$
\begin{aligned}
y_p(t) &= c_p^\top x_p(t) \\
&= c_p^\top e_o(t) + c_p^\top \hat{x}_p(t).
\end{aligned} \tag{5.23}
$$

The overall closed-loop system dynamics are

$$\dot{e}_o(t) = A_o^* e_o(t) - \tilde{a}_p(t) y_p(t) - \tilde{b}_p(t) \hat{K}_c(t) \hat{x}_p(t) \tag{5.24}$$

$$\dot{\hat{x}}_p(t) = A_c^* \hat{x}_p(t) - \hat{K}_o(t) c_p^\top e_o(t) \tag{5.25}$$

$$y_p(t) = c_p^\top e_o(t) + c_p^\top \hat{x}_p(t). \tag{5.26}$$

At this point, we can invoke Theorem 5.3 to complete the proof. □

5.3.3 Simulation Example

Here, we extend the results presented in Section 3.3.1 to closed loop. To simplify the reading, we repeat the problem definition.

Consider the following uncertain LTI, SISO transfer function

$$y = \frac{s^3 + 2s^2 + 3s + b_{p4}}{s^4 + 17s^3 + 81s^2 + a_{p3}s + a_{p4}} u,$$

where b_{p0}, a_{p3} and a_{p4} are uncertain parameters in the interior of the convex polytope defined by

$$\begin{aligned} 0.7a_{p3} = a_{p3\,\min} < a_{p3} < a_{p3\,\max} = 1.5a_{p3} \\ 0.7a_{p4} = a_{p4\,\min} < a_{p4} < a_{p4\,\max} = 1.5a_{p4} \\ 0.5b_{p4} = b_{p4\,\min} < b_{p4} < b_{p4\,\max} = 2.5b_{p4}. \end{aligned}$$

We will perform system identification of these parameters and estimate the states of the observable canonical realization of the system. In this representation, Equation (3.27) is redefined as follows:

$$\begin{aligned} a_p &= \begin{bmatrix} 17 & 81 & a_{p3} = \underline{115} & a_{p4} = \underline{50} \end{bmatrix}^\top, \\ b_p &= \begin{bmatrix} 1 & 2 & 3 & b_{p4} = \underline{4} \end{bmatrix}^\top, \\ c_p &= \begin{bmatrix} 1 & 0 & 0 & 0 \end{bmatrix}^\top. \end{aligned}$$

Defining $\Lambda(s) = (s+5)^4$ and using Remark 3.1 we isolate all terms that are known on the

left-hand side of the equality as

$$z = \frac{s^4 + 17s^3 + 81s^2}{\Lambda(s)} y_p - \frac{s^3 + 2s^2 + 3s}{\Lambda(s)} u = w_p^\top M \phi,$$

$$w_p^\top = \begin{bmatrix} w_1 & w_2 & \cdots & w_8 \end{bmatrix}^\top,$$

$$M = \begin{bmatrix} b_{0(1)} & a_{1(1)} & a_{0(1)} \\ b_{0(2)} & a_{1(2)} & a_{0(2)} \\ \vdots & \vdots & \vdots \\ b_{0(8)} & a_{1(8)} & a_{0(8)} \end{bmatrix},$$

$$\phi = \begin{bmatrix} \frac{1}{\Lambda(s)} u & -\frac{s}{\Lambda(s)} y_p & -\frac{1}{\Lambda(s)} y_p \end{bmatrix}^\top.$$

The simulations are compared with the equivalent adaptive technique that uses a single-model for identification found in Section 2.4.7. The initial estimate of the multiple-model approach is

$$\hat{w}_p(0) = \hat{w}_{p0} = \begin{bmatrix} 0.1 & 0.1 & 0.1 & 0.1 & 0.1 & 0.1 & 0.1 & 0.3 \end{bmatrix}^\top,$$

which corresponds to

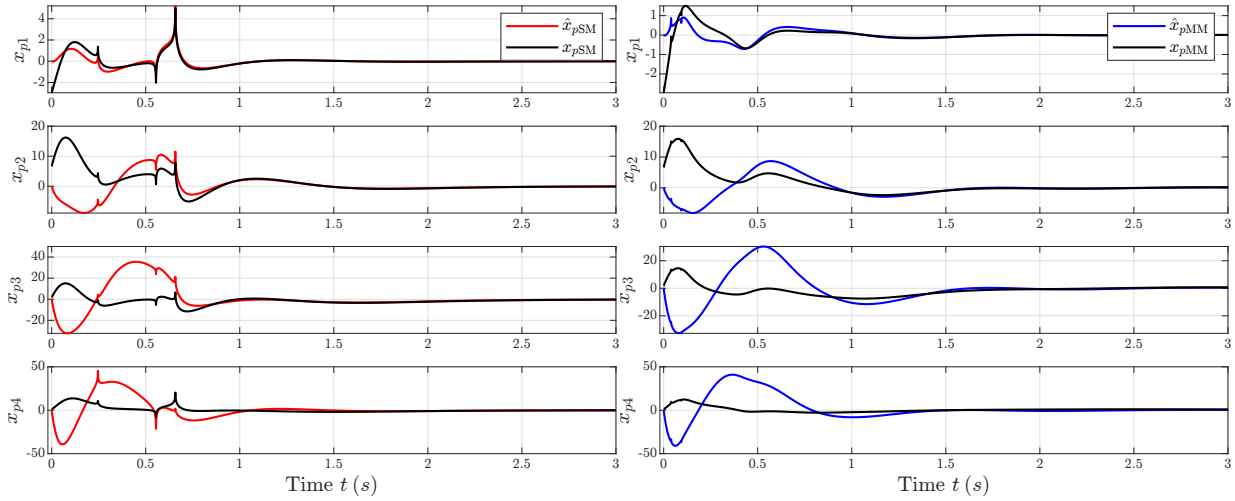
$$\hat{\Theta}_p(0) = \hat{\Theta}_{p0} = \begin{bmatrix} 6.8 & 135.7 & 59 \end{bmatrix}^\top.$$

The initial condition for the state estimator is $\hat{x}(0) = \begin{bmatrix} 0 & 0 & 0 & 0 \end{bmatrix}^\top$. The matrices set for convergence speed are $\Gamma_{\text{SM}} = 10^7 \mathbb{I}_{3\times 3}$ and $\Gamma_p = 10^2 \mathbb{I}_{8\times 8}$. These matrices were chosen to have convergence times in the same order of magnitude.

We design controllers for a single-model and a multiple-model approach, as explained in Sections 2.4.8 and 5.3, respectively. In Figures 5.6(a) and 5.6(b) we see that the states and of the closed-loop system converge to zero. In addition, we see that the estimated states of the multiple-model approach track the actual states more accurately. This faster state estimation is also experienced when we look at the case of measurement noise in Figures 5.7(a) and 5.7(b). In Figure 5.8 we see that the amplification of the noise using a single-model approach is greater than using multiple models in closed-loop configuration.

Statistical and Robustness Analysis

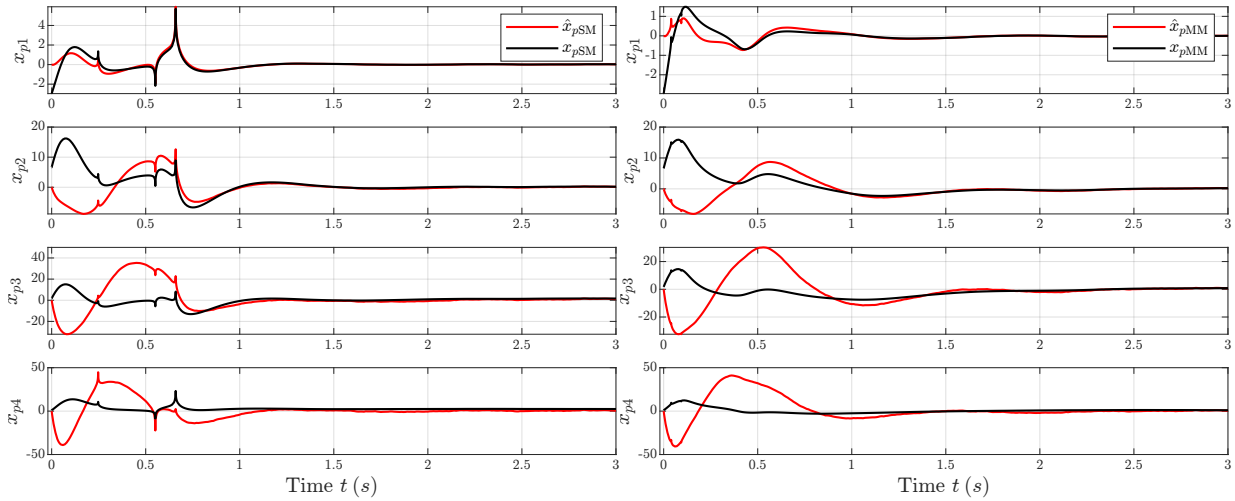
To compare the effects of using a single model, or multiple models, we ran a series of 1000 simulations with randomly generated initial conditions, lasting 100 seconds in open-loop,



(a)Time evolution of x_p and $\hat{x}_p$ for a single model without measurement noise.

(b)Time evolution of x_p and $\hat{x}_p$ for multiple models without measurement noise.

Figure 5.6: Time evolution of x_p and $\hat{x}_p$ for multiple models without measurement noise. On the left we present a single-model approach, and on the right a multiple-model approach.



(a)Time evolution of x_p and $\hat{x}_p$ for a single model with measurement noise.

(b)Time evolution of x_p and $\hat{x}_p$ for multiple models with measurement noise.

Figure 5.7: Time evolution of x_p and $\hat{x}_p$ for multiple models with measurement noise. On the left we present a single-model approach, and on the right a multiple-model approach.

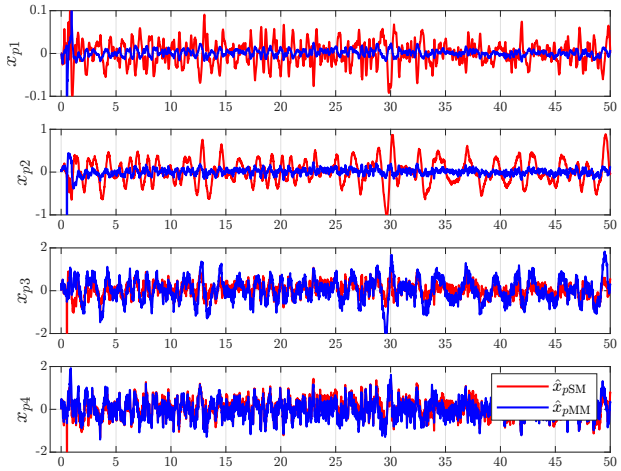


Figure 5.8: Amplification of the noise in each state in closed loop.

and 20 seconds in closed-loop. The results are presented as box-and-whisker plots and a table. Outliers are presented on box-and-whisker plots as circles and represent values outside 99.3% of the distribution.

The first test was the identification error of the uncertain parameter θ. In Figure 5.9(a) we see that the multiple-model approach has smaller 2-norm and ∞-norm error, on average, in noiseless and measurement noise cases. It is interesting to note that the single-model approach has outliers that outperformed the best cases of the multiple-model approach; on average, the multiple models obtained better results. This was then analyzed in the state estimation error, which was reduced by half in the 2-norm, with very similar ∞-norm values, as seen in Figure 5.9(b). For the closed-loop system, we analyzed the regulation performance and noted that the multiple-model approach improved the performance, particularly by reducing the width of the distribution. This behavior is not free; in order to achieve this improvement we have to increase the control effort by approximately 33% on average, as seen in Figures 5.10(a) and 5.10(b). Finally, we studied the amplification of the noise in the system by subtracting the estimated states of the system with noise and the system without noise, in the single-model and multiple-model approach. The use of multiple models allows us to filter the noise and obtain a system that can perform better in the presence of noise, as seen in Figure 5.10(c). A summary of the statistical analysis results can be seen in Table 5.2.

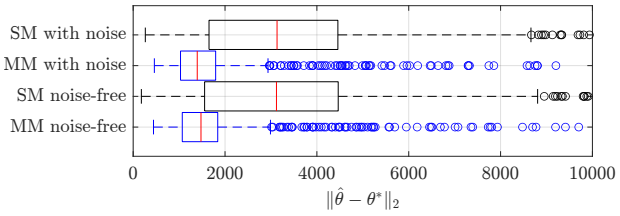
In summary, the simulations show that using a multiple-model approach, we can achieve better performance by moderately increasing the control effort. This behavior is maintained even in the case of measurement noise.

Table 5.1: Summary of results of the statistical analysis in open-loop.

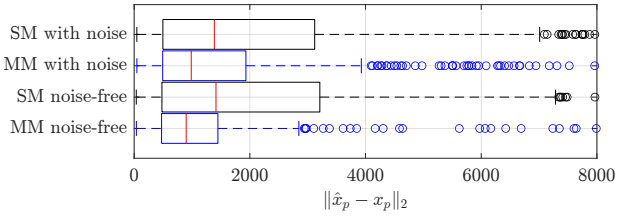
2-norm of the identification error					
	Minimum	Q1	Median	Q3	Maximum
SM noise	728	5251	6448	7397	11517
MM noise	2149	**2789**	**4720**	7393	10734
SM noise-free	338	5178	6368	7318	11238
MM noise-free	2128	**2766**	**4697**	7358	10681
2-norm of the state estimation error					
	Minimum	Q1	Median	Q3	Maximum
SM noise	117	653	1569	2645	5036
MM noise	169	**387**	**731**	1062	1498
SM noise-free	77	645	1561	2642	5039
MM noise-free	153	**381**	**727**	1058	1494
2-norm of the noise amplification					
	Minimum	Q1	Median	Q3	Maximum
SM	**86**	87	88	89	91
MM	72	72	73	73	**74**

Table 5.2: Summary of results of the statistical analysis in closed-loop.

2-norm of the identification error					
	Minimum	Q1	Median	Q3	Maximum
SM noise	264	1651	3132	4457	36176
MM noise	461	1030	**1395**	1795	10835
SM noise-free	178	1555	3119	4464	51925
MM noise-free	442	1069	**1476**	1840	10715
2-norm of the state estimation error					
	Minimum	Q1	Median	Q3	Maximum
SM noise	45	496	1385	3120	267947
MM noise	46	493	**986**	1931	81439
SM noise-free	36	480	1414	3209	330923
MM noise-free	38	473	**899**	1447	104740
2-norm of the regulation error					
	Minimum	Q1	Median	Q3	Maximum
SM noise	36	264	831	2226	428177
MM noise	33	231	**537**	1205	204951
SM noise-free	34	258	802	2519	552085
MM noise-free	31	226	**482**	903	133686
2-norm of the control effort					
	Minimum	Q1	Median	Q3	Maximum
SM noise	20	1983	**4484**	8160	115644
MM noise	21	1408	**5963**	9624	152507
SM noise-free	11	1867	**4125**	5868	93553
MM noise-free	12	1395	**5717**	8554	202313
2-norm of the noise amplification					
	Minimum	Q1	Median	Q3	Maximum
SM	21	58	**392**	2379	340424
MM	23	33	**203**	973	247628

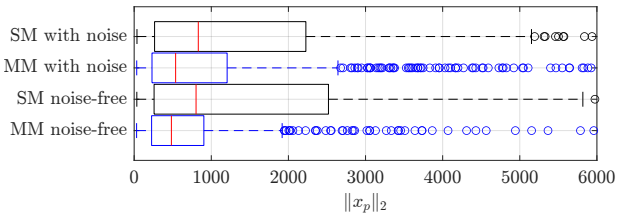


(a)Whisker-plot of the estimation of the plant dynamics in closed-loop configuration.

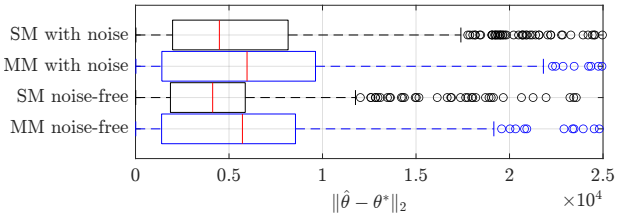


(b)Whisker-plot of the estimation of the states in closed-loop configuration.

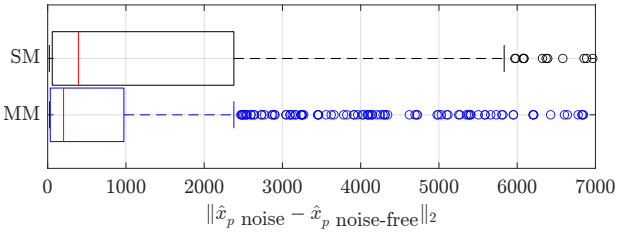
Figure 5.9: Compilation of Whisker plots of the 2-norm of the closed-loop parameter estimation (top) and state estimation (bottom).



(a)Whisker-plot of the regulation of the states in closed-loop configuration.



(b)Whisker-plot of the control effort in closed-loop configuration.



(c)Whisker-plot of the noise amplification in closed-loop configuration.

Figure 5.10: Compilation of Whisker plots of the 2-norm of the closed-loop state regulation (top), control effort (middle) and noise amplification (bottom).

Chapter 6

Conclusions

In this chapter, we conclude the thesis. First, we present a summary of all the results developed and obtained in this work. Then, noting that several interesting research questions emerged during the development of this thesis, we present a brief list of open problems.

6.1 Summary

In this thesis, we studied the problem of controlling Multiple-Input, Multiple-Output (MIMO), Linear, Time-Invariant (LTI) systems with large parametric uncertainty. The approach selected was multiple models with blending. The control scheme consists of an online parameter identification using multiple models, and a Model Reference Control (MRC) or Pole Placement Control (PPC) framework.

Considering that the entries of the state and input matrices are within a *known*, compact, and convex polytope of uncertainty, we developed a Multiple-Model Parameter Identification (MMPI) scheme that under the condition of persistence of excitation achieves the asymptotic convergence of the estimation error to zero rapidly and is robust to noise. In Chapter 3, we develop the MMPI to address state-feedback and output-feedback problems. Moreover, we present how to develop a state estimator for the output-feedback case. The simulation results showcase the effectiveness of our approach, obtaining faster parameter convergence to the true values, while also being more robust to noise.

Taking into account the MRC framework, we develop a novel approach for Multiple-Model Reference Adaptive Control (MMRAC) with blending. The states x_p of the uncertain plant are shown to perfectly asymptotically track the states x_r generated by a *known*

reference model that has a *known*, bounded and piecewise continuous input and has a nominal or ideal performance. All closed-loop signals remain bounded. Statistical analysis shows that the convergence rate of the state tracking error is approximately one order of magnitude faster than the single-model approach with a small increase in control effort.

A Multiple-Model Adaptive Pole Placement Control (MMAPPC) with blending was developed in Chapter 5 by combining the MMPI with an Adaptive Pole Placement Control (APPC) scheme that guarantees asymptotic regulation of all states by placing the closed-loop poles at the desired predetermined positions. We consider the case where the states are available for feedback, for square, multivariate, LTI systems with polytopic uncertainty. For output-feedback systems, we combine MMPI with a state-estimator using multiple models to achieve perfect regulation. Performance was shown in simulation to surpass the case of single-model approaches by moderately increasing the control effort. Statistical analysis shows that MMAPPC is more robust to noise compared to single-model approaches.

The MMRAC and MMAPPC frameworks were evaluated on the interesting problem of motion control of lateral vehicle dynamics, where the adhesion of the car tires and the road decreases and the car experiences side-slip. We observed an increase in performance that suggests that the use of multiple-model techniques could improve the implementation of existing safety features in cars.

6.2 Open Problems and Future Research

This section provides suggestions on possible research directions to continue the work done in this thesis. These ideas consider (i) how to improve the current theory for implementation and (ii) how to extend this theory to a larger class of systems.

6.2.1 Extension to Discrete-Time Systems

Consider the system presented in Chapter 3 in discrete time.

$$\begin{aligned} x_p[k+1] &= A_p x_p[k] + B_p u[k],\ x_p[0] = x_{p0},\ k \in \mathbb{N} \cup \{0\}, \\ y_p[k] &= C_p x_p[k], \end{aligned}$$

where $A_p \in \mathbb{R}^{n\times n}$ and $B_p \in \mathbb{R}^{n\times m}$ are unknown constant matrices with parametric uncertainty, A_p is Schur, $C_p \in \mathbb{R}^{q\times n}$ is *known*, $x_p[k] \in \mathbb{R}^n$ is the state of the system, $u[k] \in \mathbb{R}^m$ is a control signal. The question is then what are the conditions to extend the results of

this thesis to discrete time systems, and formalize them for future implementation in microcontrollers. It should be noted that proofs for discrete-time Model Reference Adaptive Control (MRAC) have only been published last year in [78, 79].

6.2.2 Persistence of Excitation Considerations

In the heart of the parameter identification problem, we find the assumption of persistence of excitation. If the input does not carry enough information to "sufficiently excite" the system over time, then the parameters cannot be uniquely and stably identified. The difficulties are as follows.

- Global richness; Excitation is not required at some times, but at **all** times, continuously. The input is usually selected to satisfy a task and may not persistently excite all modes.
- The controllers are designed to regulate the system to a desired trajectory, i.e., asymptotically drive the states of the system to those generated by a reference model. Once regulation is achieved, the control input and tracking error tend to become steady or very small, which means that Φ loses excitations. The better we track, the worse our parameter convergence is.
- Online verification that an input is sufficiently rich is a non-trivial problem, making it a practicably uncheckable assumption.

Some results in the literature [14] show a way to introduce an exogenous signal into a system to guarantee some degree of excitation to guarantee the convergence of the parameters. By introducing a diminishing Persistently Exciting (PE) signal into the system, convergence of the estimated parameters to the true values is guaranteed, although not exponentially fast. The problem is then how to construct such a signal that guarantees a diminishing PE condition. In [16], an example of an adaptive scheme for localization of a target from distance measurements and motion control of a mobile agent to pursue this target is shown, where an external signal is introduced to guarantee the persistence of excitation condition.

An interesting line of research would be to extend the results to multi-input systems. If this were the case, then we could relax the persistence of excitation condition of our theorems.

6.2.3 Combining Switching and Blending Techniques

In the literature review, a clear distinction is made between using Multiple-Model Adaptive Control (MMAC) to switch between the models or blend the information obtained from all of them. For switching control, all models need to be simulated, which means that obtaining a blending model is not computationally challenging; one of the models to choose from could be a blended option.

A different possibility occurs when the uncertainty set consists of disconnected polytopes of uncertainty. In this case, we can run the blending algorithms for each disconnected set and switch to the one in which the true plant is.

6.2.4 Extension of MMAPPC to General MIMO Systems

In Chapter 5, the MMAPPC problem is presented and solved for square, LTI, multivariate systems with state-feedback, and for Single-Input, Single-Output (SISO), LTI systems with output-feedback via a state-estimation step. A reasonable extension of the work presented in this thesis is to solve the general MIMO, LTI case with output-feedback.

6.2.5 Extension to a Class of Nonlinear Systems

When it comes to nonlinear systems, there are almost no results except for a recent paper [94], where they show that second-level adaptation can be applied to a class of SISO, discrete-time nonlinear systems. Specifying a particular class of nonlinear system is necessary to reduce the difficulty of the problem and take advantage of existing results. An interesting and reasonable starting point would be to extend the results of this thesis to fully actuated Euler-Lagrange equations. This class of systems is present in different applications, such as robotics, satellites, CNC machines, and 3D printers.

References

[1] T. H. S. Abdelaziz and M. Valasek. Direct algorithm for pole placement by state-derivative feedback for multi-input linear systems : Nonsingular case. *Kybernetika*, 41(5):637–660, 2005. 11

[2] N. Ahmadian, A. Khosravi, and P. Sarhadi. A New Approach to Adaptive Control of Multi-Input Multi-Output Systems Using Multiple Models. *ASME Journal of Dynamic Systems, Measurement, and Control*, 137(9):091009, September 2015. 15

[3] B. D. O. Anderson, T. Brinsmead, D. Liberzon, and A. S. Morse. Multiple model adaptive control with safe switching. *International Journal of Adaptive Control and Signal Processing*, 15(5):445–470, 2001. 12

[4] B. D. O. Anderson, T. S. Brinsmead, F. D. Bruyne, J. Hespanha, D. Liberzon, and A. S. Morse. Multiple model adaptive control. part 1: Finite controller coverings. *International Journal of Robust and Nonlinear Control*, 10(11-12):909–929, 2000. 12

[5] S. Baldi, G. Battistelli, E. Mosca, and P. Tesi. Multi-model unfalsified adaptive switching supervisory control. *Automatica*, 46(2):249–259, 2010. 12

[6] B. R. Barmish. *New tools for robustness of linear systems*. Macmilllan, New York, 1994. 42, 85

[7] J. Bernat, J. Kolota, and D. Cieslak. Reset strategy for output feedback multiple models mrac applied to deap. *IEEE Access*, 8:120905–120915, 2020. 16

[8] F. D. Bianchi, Hernan. D. Battista, and R. J. Mantz. *Wind turbine control systems: principles, modelling and gain scheduling design*. Advances in industrial control. Springer, London, 1st ed. 2007. edition, 2007. 10

[9] F. Blanchini, D. Casagrande, S. Miani, and U. Viaro. Stable lpv realization of parametric transfer functions and its application to gain-scheduling control design. *IEEE Transactions on Automatic Control*, 55(10):2271–2281, 2010. 10

[10] S. P. Boyd and L. Vandenberghe. *Convex Optimization*. Cambridge University Press, Cambridge, UK, second edition, 2006. 54

[11] K. Büyükkabasakal, B. Fidan, and A. Savran. Mixing adaptive fault tolerant control of quadrotor UAV. *Asian Journal of Control*, 19(4):1441–1454, July 2017. 15

[12] M. C. Campi, J. P. Hespanha, and M. Prandini. Cautious hierarchical switching control of stochastic linear systems. *International Journal of Adaptive Control and Signal Processing*, 18(4):319–333, 2004. 13

[13] M. H. Chang and E. J. Davison. Adaptive switching control of lti mimo systems using a family of controllers approach. *Automatica (Oxford)*, 35(3):453–465, 1999. 13

[14] S. Dasgupta and B. Fidan. Uniform asymptotic convergence of an adaptive algorithm with diminishing persistent excitation. *IFAC Proceedings Volumes*, 45(16):1514–1516, 2012. 16th IFAC Symposium on System Identification. 99

[15] L. Dutta and D. D. Kumar. Adaptive model predictive control design using multiple model second level adaptation for parameter estimation of two-degree freedom of helicopter model. *International Journal of Robust and Nonlinear Control*, 31(8):3248–3278, 2021. 15

[16] B. Fidan, S. Dasgupta, and B. D. O. Anderson. Adaptive range-measurement-based target pursuit. *International Journal of Adaptive Control and Signal Processing*, 27(1-2):66–81, 2013. 99

[17] Z. Han and K. S. Narendra. New concepts in adaptive control using multiple models. *IEEE Transactions on Automatic Control*, 57(1):78–89, January 2012. 15, 16

[18] M. Harrer and P. E. Pfeffer. *Steering handbook*. Springer, Cham, Switzerland, 2017. 71

[19] J. P. Hespanha. Uniform Stability of Switched Linear Systems: Extensions of LaSalle's Invariance Principle. *IEEE Transactions on Automatic Control*, 49(4):470–482, April 2004. 11, 15

[20] J. P. Hespanha, D. Liberzon, and A. S. Morse. Hysteresis-based switching algorithms for supervisory control of uncertain systems. *Automatica (Oxford)*, 39(2):263–272, 2003. 12

[21] J. P. Hespanha, D. Liberzon, and A. S. Morse. Overcoming the limitations of adaptive control by means of logic-based switching. *Systems & Control Letters*, 49(1):49–65, May 2003. 11, 12

[22] J. P. Hespanha, D. Liberzon, A. S. Morse, B. D. O. Anderson, T. S. Brinsmead, and F. D. Bruyne. Multiple model adaptive control. Part 2: switching. *International Journal of Robust and Nonlinear Control*, 11(5):479–496, April 2001. 11, 12

[23] J. P. Hespanha and A. S. Morse. Switching between stabilizing controllers. *Automatica*, 38(11):1905–1917, November 2002. 11

[24] Jun Huang, Xiang Ma, Haochi Che, and Zhengzhi Han. Further result on interval observer design for discrete-time switched systems and application to circuit systems. *IEEE Transactions on Circuits and Systems II: Express Briefs*, 67(11):2542–2546, 2020. 13

[25] R. A. Hyde and K. Glover. The application of scheduled H_∞ controllers to a VSTOL aircraft. *IEEE Transactions on Automatic Control*, 38(7):1021–1039, July 1993. 10

[26] M. Imani and U. Braga-Neto. Multiple Model Adaptive controller for Partially-Observed Boolean Dynamical Systems. In *American Control Conference*, pages 1103–1108, May 2017. 16

[27] P. A. Ioannou and B. Fidan. *Adaptive Control Tutorial*. SIAM, 2006. 8, 18, 19, 29, 32, 43, 82, 86, 87

[28] P. A. Ioannou and J. Sun. *Robust Adaptive Control*. Prentice-Hall, 1996. 10

[29] W. P. Jan. A state space approach to the problem of adaptive pole assignment. *Mathematics of Control, Signals, and Systems*, 2(1):71–94, 1989. 11, 22

[30] R. E. Kalman. A new approach to linear filtering and prediction problems. *Journal of Fluids Engineering*, 82:35–45, 1960. 11

[31] J. Kelly and J. Evers. An interpolation strategy for scheduling dynamic compensators. In *Guidance, Navigation, and Control Conference*, New Orleans, LA, USA, August 1997. American Institute of Aeronautics and Astronautics. 10

[32] S. Kersting and M. Buss. Direct and indirect model reference adaptive control for multivariable piecewise affine systems. *IEEE Transactions on Automatic Control*, 62(11):5634–5649, 2017. 13

[33] B. Kolodziejczak and T. Szulc. Convex combinations of matrices — full rank characterization. *Linear Algebra and its Applications*, 287(1-3):215–222, 1999. 52, 55, 78

[34] M. Kuipers and P. A. Ioannou. Multiple model adaptive control with mixing. *IEEE Transactions on Automatic Control*, 55(8):1822–1836, August 2010. 14, 15

[35] H. Kwakernaak and R. Sivan. *Linear optimal control systems*. Wiley Interscience, New York, 1972. 11

[36] D. Liberzon. *Switching in systems and control*. Systems & Control. Birkhäuser, Boston, 2003. 12, 13, 15

[37] D. Liberzon, J. P. Hespanha, and A. S. Morse. Stability of switched systems: a Lie-algebraic condition. *Systems & Control Letters*, 37(3):117–122, July 1999. 15

[38] S. Liu, A. Russo, D. Liberzon, and A. Cavallo. Integral-input-to-state stability of switched nonlinear systems under slow switching. *IEEE Transactions on Automatic Control*, 67(11):5841–5855, 2022. 13

[39] A. Lovi, B. Fidan, and C. Nielsen. Multiple model reference adaptive tracking control of multivariable systems with blending. In *IEEE Conference on Decision and Control*, pages 1362–1367, 2022. 32

[40] A. Lovi, B. Fidan, and C. Nielsen. A blending based multiple model reference adaptive approach to lateral vehicle motion control. In *IEEE Conference on Decision and Control*, pages 7220–7225, 2024. 16, 70

[41] A. Lovi, B. Fidan, and C. Nielsen. Blending based multiple model pole placement adaptive control of multivariable systems. In *European Control Conference*, pages 120–125, 2025. 16

[42] A. Lovi, B. Fidan, and C. Nielsen. Multiple model reference adaptive control with blending for non-square multivariable systems. *IEEE Transactions on Automatic Control*, pages 1–12, 2025. 15, 16, 51

[43] D. Luenberger. An introduction to observers. *IEEE Transactions on Automatic Control*, 16(6):596–602, 1971. 11, 21, 42

[44] J. L. Mancilla-Aguilar and R. A. Garcia. Uniform asymptotic stability of switched nonlinear time-varying systems and detectability of reduced limiting control systems. *IEEE Transactions on Automatic Control*, 64(7):2782–2797, 2019. 13

[45] I. M. Y. Mareels, B. D. O. Anderson, R. R. Bitmead, M. Bodson, and S. S. Sastry. Revisiting the mit rule for adaptive control. *IFAC Proceedings Volumes*, 20(2):161–166, 1987. 2nd IFAC Workshop on Adaptive Systems in Control and Signal Processing 1986, Lund, Sweden, 30 June-2 July 1986. 9

[46] R. Mekel, Raymond C. M., and S. Nachmias. Learning control system studies for the f-8 dfbw aircraft. In *1976 IEEE Conference on Decision and Control including the 15th Symposium on Adaptive Processes*, pages 24–28. IEEE, 1976. 10

[47] R. Mekel and S. Nachmias. *An adaptive learning control system for aircraft*. NASA, Legacy CDMS, 1976. 10

[48] R. H. Middleton, G. C. Goodwin, D. J. Hill, and D. Q. Mayne. Design issues in adaptive control. *IEEE Transactions on Automatic Control*, 33(1):50–58, 1988. 12

[49] K. Moffat and C. Tomlin. The Multiple Model Adaptive Power System State Estimator. In *IEEE Conference on Decision and Control*, pages 3525–3530, December 2021. 16

[50] A. S. Morse. Supervisory control of families of linear set-point controllers - Part I. Exact matching. *IEEE Transactions on Automatic Control*, 41(10):1413–1431, October 1996. 12, 13, 15

[51] A. S. Morse. Supervisory control of families of linear set-point controllers. 2. Robustness. *IEEE Transactions on Automatic Control*, 42(11):1500–1515, November 1997. 12, 13

[52] A. S. Morse. A simple example of an adaptive control system. *Communications in Information and Systems*, 11(2):105–118, 2011. 13

[53] A. S. Morse, D. Q. Mayne, and G. C. Goodwin. Applications of hysteresis switching in parameter adaptive control. *IEEE Transactions on Automatic Control*, 37(9):1343–1354, September 1992. 12

[54] S. D. Moxley. Control concepts of the an/gsn-11 terminal air traffic control system. *I.R.E. Transactions on Aerospace and Navigational Electronics*, ANE-8(2):51–59, 1961. 10

[55] K. S. Narendra and J. Balakrishnan. Improving transient response of adaptive control systems using multiple models and switching. *IEEE Transactions on Automatic Control*, 39(9):1861–1866, 1994. 12, 13

[56] K. S. Narendra and J. Balakrishnan. Adaptive control using multiple models. *IEEE Transactions on Automatic Control*, 42(2):171–187, 1997. 12

[57] K. S. Narendra, O. A. Driollet, M. Feiler, and K. George. Adaptive control using multiple models, switching and tuning. *International Journal of Adaptive Control and Signal Processing*, 17(2):87–102, 2003. 12

[58] K. S. Narendra and K. Esfandiari. Adaptive identification and control of linear periodic systems using second-level adaptation. *International Journal of Adaptive Control and Signal Processing*, 33(6):956–971, June 2019. 16

[59] K. S. Narendra and Z. Han. The changing face of adaptive control: The use of multiple models. *Annual Reviews in Control*, 35(1):1–12, 2011. 13, 14

[60] K. S. Narendra and Z. Han. A new approach to adaptive control using multiple models. *International Journal of Adaptive Control and Signal Processing*, 26(8):778–799, August 2012. 15, 16

[61] K. S. Narendra, W. Yu, and C. Wei. Stability, robustness, and performance issues in second level adaptation. In *American Control Conference*, pages 2377–2382, 2014. 3, 69

[62] R. A. Nichols, R. T. Reichert, and W. J. Rugh. Gain scheduling for H_∞ controllers: a flight control example. *IEEE Transactions on Control Systems Technology*, 1(2):69–79, 1993. 10

[63] V. K. Pandey, I. Kar, and C. Mahanta. Controller design for a class of nonlinear mimo coupled system using multiple models and second level adaptation. *ISA Transactions*, 69:256–272, 2017. 15

[64] R. Rajamani. *Vehicle dynamics and control*. Mechanical engineering series. Springer, New York, 2nd ed. edition, 2012. 70

[65] J. G. Romero and R. Ortega. Adaptive state observation of linear time-varying systems with switching unknown parameters: Application to gain scheduling and event-triggered control. *International Journal of Adaptive Control and Signal Processing*, 37(11):2915–2933, 2023. 10

[66] H. H. Rosenbrock and G. E. Hayton. The general problem of pole assignment. *International Journal of Control*, 27(6):837–852, 1978. 11

[67] Yuan G. S., L. Wang, Guangming X., and Mei Y. Improved overshoot estimation in pole placements and its application in observer-based stabilization for switched systems. *IEEE Transactions on Automatic Control*, 51(12):1962–1966, 2006. 13

[68] S. M. Shahruz and S. Behtash. Design of controllers for linear parameter-varying systems by the gain scheduling technique. *Journal of Mathematical Analysis and Applications*, 168(1):195–217, July 1992. 10

[69] J. S. Shamma. *An Overview of LPV Systems*, pages 3–26. Springer US, Boston, MA, 2012. 10

[70] J. S. Shamma and M. Athans. Analysis of gain scheduled control for nonlinear plants. *IEEE Transactions on Automatic Control*, 35(8):898–907, August 1990. 10

[71] J. S. Shamma and M. Athans. Gain scheduling: potential hazards and possible remedies. *IEEE Control Systems Magazine*, 12(3):101–107, 1992. 10

[72] J. D. Simard, C. Nielsen, and D. E. Miller. Periodic adaptive stabilization of rapidly time-varying linear systems. *Mathematics of Control, Signals, and Systems*, 31(2):1–42, June 2019. 10

[73] D. J. Stilwell and W. J. Rugh. Interpolation of observer state feedback controllers for gain scheduling. *IEEE Transactions on Automatic Control*, 44(6):1225–1229, 1999. 10

[74] D. J. Stilwell and W. J. Rugh. Stability preserving interpolation methods for the synthesis of gain scheduled controllers. *Automatica*, 36(5):665–671, May 2000. 10

[75] C. Tan, G. Tao, and R. Qi. An adaptive control scheme using multiple reference models. *International Journal of Adaptive Control and Signal Processing*, 28(11):1290–1298, 2014. 16

[76] C. Tan, G. Tao, R. Qi, and H. Yang. A direct mrac based multivariable multiple-model switching control scheme. *Automatica*, 84:190–198, 2017. 13

[77] G. Tao. *Adaptive Control Design and Analysis*. Wiley, 2003. 8, 9, 21, 52

[78] G. Tao. Adaptive output tracking control with reference model system uncertainties: Extensions. *arXiv*, 2024. 99

[79] G. Tao. Discrete-time adaptive state tracking control schemes using gradient algorithms. *Automatica (Oxford)*, 169:111849–, 2024. 99

[80] K. S. Tsakalis. The sigma -modification in the adaptive control of linear time-varying plants. In *IEEE Conference on Decision and Control*, pages 694–698 vol.1, 1992. 10

[81] L. Vu and D. Liberzon. Supervisory control of uncertain linear time-varying systems. *IEEE Transactions on Automatic Control*, 56(1):27–42, 2011. 12

[82] S. Wang, W. Ren, and J. Chen. Fully distributed state estimation with multiple model approach. In *IEEE Conference on Decision and Control*, pages 2920–2925, December 2016. 16

[83] S. R. Weller and G. C. Goodwin. Hysteresis switching adaptive control of linear multivariable systems. *IEEE Transactions on Automatic Control*, 39(7):1360–1375, 1994. 12

[84] G. Wen and W. X. Zheng. On constructing multiple lyapunov functions for tracking control of multiple agents with switching topologies. *IEEE Transactions on Automatic Control*, 64(9):3796–3803, 2019. 13

[85] E. Weyer, I. M. Y. Mareels, and J. W. Poldermann. Limitations of robust adaptive pole placement control. *IEEE Transactions on Automatic Control*, 39(8):1665–1671, 1994. 11

[86] W. Wonham. On pole assignment in multi-input controllable linear systems. *IEEE Transactions on Automatic Control*, 12(6):660–665, 1967. 11, 86

[87] W. M. Wonham. *Linear multivariable control: a geometric approach*. Applications of Mathematics. Springer-Verlag, New York, 2nd edition, 1979. 78

[88] J. Xie, S. Li, H. Yan, and D. Yang. Model reference adaptive control for switched linear systems using switched multiple models control strategy. *Journal of the Franklin Institute*, 356(5):2645–2667, 2019. 16

[89] L. Xing, C. Wen, Z. Liu, H. Su, and J. Cai. Event-triggered adaptive control for a class of uncertain nonlinear systems. *IEEE Transactions on Automatic Control*, 62(4):2071–2076, 2017. 13

[90] C. Yang and Y. Jia. Adaptive Multiple-Model Control of A Class of Nonlinear Systems. *Journal of Robotics, Networking and Artificial Life*, 2(2):69, 2015. 15

[91] H. Zengin, N. Zengin, B. Fidan, and A. Khajepour. Blending based multiple-model adaptive control of multivariable systems with application to lateral vehicle motion control. *European Journal of Control*, 58:1–10, March 2021. 16

[92] H. Zhang, J. Huang, H. Che, and Z. Han. Optimal interval observer for discrete-time switched systems. *IEEE Transactions on Circuits and Systems II: Express Briefs*, 69(3):1233–1237, 2022. 13

[93] K. Zhang, B. Zhou, H. Jiang, and G. Duan. Event-triggered and self-triggered gain scheduling control of input constrained systems with applications to the spacecraft rendezvous. *International Journal of Robust and Nonlinear Control*, 31(10):4629–4646, 2021. 10

[94] Y. Zhang, X. Wang, and Z. Wang. Adaptive multiple model control for a class of nonlinear discrete time systems: second-level adaption design approach. *International Journal of Control*, 96(2):497–507, 2023. 15, 100